

American University in Cairo

## AUC Knowledge Fountain

---

Theses and Dissertations

---

2-1-2017

### Encapsulation of essential oils in chitosan nanoparticle formulations and Investigation on their antioxidant and antibacterial properties.

Amro Abdel Azeem Shetta

Follow this and additional works at: <https://fount.aucegypt.edu/etds>

---

#### Recommended Citation

##### APA Citation

Shetta, A. (2017). *Encapsulation of essential oils in chitosan nanoparticle formulations and Investigation on their antioxidant and antibacterial properties*. [Master's thesis, the American University in Cairo]. AUC Knowledge Fountain.

<https://fount.aucegypt.edu/etds/40>

##### MLA Citation

Shetta, Amro Abdel Azeem. *Encapsulation of essential oils in chitosan nanoparticle formulations and Investigation on their antioxidant and antibacterial properties*. 2017. American University in Cairo, Master's thesis. *AUC Knowledge Fountain*.

<https://fount.aucegypt.edu/etds/40>

This Thesis is brought to you for free and open access by AUC Knowledge Fountain. It has been accepted for inclusion in Theses and Dissertations by an authorized administrator of AUC Knowledge Fountain. For more information, please contact [mark.muehlhaeusler@aucegypt.edu](mailto:mark.muehlhaeusler@aucegypt.edu).

School of Sciences and Engineering

**Encapsulation of Essential Oils in Chitosan  
Nanoparticle formulations and Investigation on their  
Antioxidant and Antibacterial Properties**

A Thesis Submitted to  
The Nanotechnology Master's Program  
In partial fulfilment of the requirements for  
The degree of Master of Science

By:

**Amro Abdel Azeem Hassan Shetta**

Under the supervision of:

**Dr. Wael Mamdouh** (Advisor)  
Assistant Professor, Department of Chemistry,  
The American University in Cairo (AUC)

November 9, 2017

The American University in Cairo

**Encapsulation of Essential Oils in Chitosan Nanoparticle formulations and Investigation  
on their Antioxidant and Antibacterial Properties**

A Thesis Submitted by

**Amro Abdel Azeem Hassan Shetta**

To the Nanotechnology Graduate Program

November 9, 2017

In partial fulfillment of the requirements for

The degree of Master of Science

Has been approved by

Thesis Committee Supervisor/Chair

**Dr. Wael Mamdouh**

Affiliation **Assistant Professor, Department of Chemistry, AUC**

Thesis Committee Reader/Examiner

**Dr. Mayyada Elsayed**

Affiliation **Associate Professor, Department of Chemistry, AUC**

Thesis Committee Reader/External Examiner

**Dr. Aliaa El-Meshad**

Affiliation: **Professor, Faculty of Pharmacy, Department of Pharmaceutics and  
Industrial Pharmacy, Cairo University**

Thesis Committee Moderator

**Dr. Hatem Tallima**

Affiliation **Assistant Professor, Department of Chemistry, AUC**

---

Dept. Chair/Director

Date

Dean

Date

## Table of Contents

Acknowledgments .....	vi
Abstract.....	vii
List of Abbreviations .....	ix
List of Figure .....	xi
List of Tables .....	xiv
List of Equations .....	xv
<b>Chapter 1: General Introduction &amp; Literature review .....</b>	<b>2</b>
<b>1.1. Bacterial Infectious diseases in the twentieth century .....</b>	<b>2</b>
<b>1.2. Traditional solutions for combating bacterial infections.....</b>	<b>4</b>
<b>1.3. Mechanisms of antibiotic resistance .....</b>	<b>6</b>
<b>1.4. Reactive oxygen species and oxidative stress.....</b>	<b>8</b>
<b>1.5. Essential oil .....</b>	<b>11</b>
1.5.A. Essential oil extraction.....	12
1.5.B. Essential oil chemical composition.....	14
1.5.C. Essential oils as natural antimicrobial and antioxidant agents.....	16
1.5.D. Essential oil antibacterial mode of action .....	17
1.5.E. Essential oil antioxidant mode of action .....	18
1.5.F. EOs limits and challenges.....	18
<b>1.6. Nanotechnology .....</b>	<b>19</b>
<b>1.7. Nanoparticles mechanisms for combating microbial resistance.....</b>	<b>20</b>
1.7.A. Nitric oxide-releasing nanoparticles (NO NPs) .....	20
1.7.B. Chitosan nanoparticles .....	22
1.7.C. Silver nanoparticles .....	23
1.7.D. Copper nanoparticles.....	23
1.7.E. Magnesium nanoparticles.....	24
<b>1.8. EOs loaded in nanosystems .....</b>	<b>24</b>
1.8.A. Polymer-Based Nanocarriers.....	25
<b>1.8.B. Lipid-Based Nanocarriers.....</b>	<b>28</b>
1.8.B.1 Nanoemulsions .....	28
1.8.B.2. Solid Lipid Nanoparticles.....	29

1.8.B.3. Liposomes .....	29
<b>Thesis Scope and Objectives .....</b>	<b>33</b>
<b>Chapter 2: Materials &amp; Methods .....</b>	<b>36</b>
<b>2.1. Materials: .....</b>	<b>36</b>
<b>2.2. Compositional analysis of PO and GTO .....</b>	<b>36</b>
<b>2.3. Preparation of EOs loaded CS NPs .....</b>	<b>36</b>
2.3.A. Oil in water (O/W) emulsion preparation .....	39
2.3.B. Ionic gelation process and separation of the prepared NPs.....	39
<b>2.4. Characterization of the prepared NPs .....</b>	<b>40</b>
2.4.A. Particle size and zeta potential of the prepared NPs .....	40
2.4.B. Morphology of the prepared NPs .....	41
2.4.C. Fourier transform InfraRed (FTIR) Spectroscopy analysis.....	41
2.4.D. Thermogravimetric analysis (TGA) analysis.....	41
2.4.E. Powder X-ray diffraction (XRD) analysis.....	41
<b>2.5. Determination of encapsulation efficiency (EE%) and loading capacity (LC%) .....</b>	<b>42</b>
<b>2.6. In-vitro release studies .....</b>	<b>42</b>
<b>2.7. Estimation of Total phenolic contents (TPC) .....</b>	<b>43</b>
<b>2.8. Investigation of the antioxidant activities of NPs .....</b>	<b>44</b>
<b>2.9. Investigation of the antibacterial activities of the NPs.....</b>	<b>44</b>
<b>2.10. Theoretical background.....</b>	<b>45</b>
2.10.A. Rotor-Stator homogenizer.....	45
2.10.B. Probe sonicator .....	46
2.10.C. Lypholizer (freeze dryer) .....	47
2.10.D. Dynamic light scattering (DLS, Zetasizer) .....	48
2.12.E. Transmission electron microscopy (TEM).....	50
2.12.F. Fourier transform infrared spectroscopy (FTIR) .....	52
2.12.G. X-ray diffraction analysis (XRD) .....	53
2.12.H. Thermal gravimetric analysis (TGA).....	54
2.12.I. Folin–Ciocalteu (FC) method.....	55
2.12.J. Ultraviolet/Visible spectroscopy (UV-Vis spectroscopy).....	56

2.12.K. Antibacterial Assessment by Agar dilution and colony counting method.....	58
<b>Chapter 3: Results and Discussion– Chitosan/ (Peppermint and Green Tea Oil) Nanoparticle Formulations, Characterization and in-vitro Release.....</b>	<b>61</b>
<b>3.1. Compositional Analysis of PO and GTO by GC/MS/MS.....</b>	<b>61</b>
3.3.A. Impact of homogenization parameters on the average size and zeta potential of CS/PO NPs.....	63
3.3.B. Impact of TPP concentration on the average size and zeta potential of CS/PO NPs.....	65
<b>3.4. Characterization of nanoparticles formulations of EOs.....</b>	<b>68</b>
3.4.A. Nanoparticles hydrodynamic size .....	68
3.4.B. Zeta potential of nanoparticles.....	70
3.4.C. Morphology of nanoparticles.....	72
3.4.D. Fourier transform infra-red (FT-IR) spectroscopy analysis of CS, EOs and NPs .....	75
3.4.E. Thermal gravimetric analysis (TGA) of CS, EOs and NPs.....	77
3.4.F. Powder X-ray Diffraction (XRD) analysis of CS, and NPs .....	80
<b>3.5. Determination of the Encapsulation Efficiency (EE%) and loading capacity     (LC%) of NPs.....</b>	<b>81</b>
<b>3.6. In-vitro release studies of NPs.....</b>	<b>84</b>
<b>3.7. Stability of phenolic contents in CS NPs .....</b>	<b>88</b>
<b>Chapter 4: Antioxidant and antibacterial activities of Chitosan/ (Peppermint and Green Tea Oil) Nanoparticle .....</b>	<b>91</b>
<b>4.1. Evaluation of antioxidant activity of EOs NPs .....</b>	<b>91</b>
<b>5.2. Evaluation of the antibacterial activity of EOs NPs.....</b>	<b>95</b>
<b>Chapter 5: Conclusion and Future perspectives.....</b>	<b>102</b>
<b>Chapter 6: Appendices .....</b>	<b>105</b>
<b>Appendix I: GC/MS/MS analysis of PO.....</b>	<b>105</b>
<b>Appendix II: GC/MS/MS analysis of GTO.....</b>	<b>106</b>
<b>Appendix III: Polydispersity of nanoparticles .....</b>	<b>107</b>
<b>References .....</b>	<b>109</b>

## **Acknowledgments**

First and foremost, I would like to express my sincere gratitude to my supervisor, **Dr. Wael Mamdouh**, for giving me the opportunity to work under his supervision and also for his valuable guidance and continuous support and encouragement throughout this research work. He provided me with unlimited support and gave me his precious time and advice whenever I needed it.

I am also thankful to all my professors at AUC chemistry department whom I have learnt a lot from throughout the course of my studies.

I also feel grateful to every one of my colleagues in my research group for their support, help and the time I spent with them.

Special thanks to the researchers and colleagues here at AUC who participated in teaching me some research skills and provided me with continuous guidance during my work; for their care and guidance during my research work, **Ahmed Nour** for helping me in the SEM imaging, **Mr. Mahmoud Abdel Moez** and **Ahmed Omaia** for the FTIR experiments, **Mr Emad Rafaat** for the XRD experiments.

I would like to acknowledge my family for their support; without them in my life I couldn't have achieved this study. I would like to acknowledge my father, **Abdel Azeem Shetta**, for his continual support and his full presence. He has been great role model for me and he will always be my hero. Also, I would like to express my sincere appreciation to my mother, **Eman**, whom her prayers have been always with me and always being with me to face the difficulties through this study.

I wish to express my heartfelt thanks to my wife, **Rana**, my daughter; **Lara** whom have played crucial role in this research. Thanks, **Rony** for your advice, warm support, and strength throughout the Masters. I would also like to thank my dear brother **Ahmed** for his love, care and encouragement. Finally, I would like to express my endless thanks to my friends at AUC **Omar Hamed, James Kegrere, Sara Hassan** and **Ahmed Emad**

**Last, but by no means least, I thank God.**

## Abstract

Peppermint oil (PO) and Green Tea oil (GTO) are two essential oils (EOs) were encapsulated in chitosan nanoparticles (CS NPs) via two-steps method (emulsification followed by ionic gelation). Encapsulation of GTO and PO in CS NPs were investigated through different characterization techniques such as; Fourier transform infrared (FT-IR) spectroscopy, powder X-ray diffraction (XRD). Both NPs (CS/PO NPs and CS/GTO NPs) showed a spherical shape with 20-90 nm size range as detected by Transmission electron microscopy (TEM). Thermogravimetric analysis (TGA) was used to study the thermal stability of both bulk and encapsulated EOs that showed an enhancement in the thermal stability of both encapsulated EOs by about 2.18 and 1.75 folds for PO and GTO, respectively. Through UV-vis spectroscopy, both encapsulation efficiency (EE%), loading capacity (LC%) and in-vitro release were estimated. EE% of CS/PO NPs and CS/GTO NPs were about 82-78% and 22-81%, respectively, when the initial EO amount was 0.25–1 w/w CS. Whereas, the loading capacity (LC%) of CS/PO NPs and CS/GTO NPs were about 8-22% and 2.2-23%, respectively for the initial EO amount was 0.25–1 w/w CS. The *in-vitro* release studies of both EOs showed an initial rapid release profile followed by a slow release at two different pH conditions: acidic pH (acetate buffer) and neutral pH (phosphate buffer saline). Furthermore, the stability of the total phenolic contents (TPC) of both EOs in CS NPs was studied using Folin–Ciocalteu reagent. The antioxidant activity of both pure and encapsulated PO and GTO was evaluated by 2,2-diphenyl-1-picrylhydrazyl radical (DPPH). The antioxidant activities of CS/PO NPs and CS/GTO NPs were improved by about 2 and 2.4 folds, respectively. Finally, agar dilution and colony counting method were used to study the antibacterial activity of pure and encapsulated PO and GTO against Gram positive (*Staphylococcus aureus*) and Gram

negative (*Escherichia coli*) bacteria. In case of Gram positive bacteria, encapsulated PO showed an enhanced antibacterial activity by about 39.63%, while encapsulated GTO showed an improvement in antibacterial activity by about 57.5% on the other hand, against Gram negative bacteria, encapsulated PO showed an enhanced antibacterial activity by about 3%, while encapsulated GTO showed an improvement in antibacterial activity by about 1.8%.

## **List of Abbreviations**

**AD:** Alzheimer's disease

**Ag NPs:** Silver nanoparticles

**AMD:** Age-related macular degeneration

**ATP:** Adenosine triphosphate

**CS NPs:** Chitosan nanoparticles

**CS:** Chitosan

**Cu NPs:** Copper nanoparticles

**DPPH:** 2,2-diphenyl-1-picrylhydrazyl radical

**DTG:** Derivative thermogravimetry

**E.coli:** Escherichia coli

**EE:** Encapsulation efficiency

**EO:** Essential oil

**EP:** European pharmacopeia

**FTIR:** Fourier Transform Infrared spectroscopy

**GC/MS/MS:** Gas chromatography/Mass spectroscopy/ Mass spectroscopy

**GC/MS:** Gas chromatography/Mass spectroscopy

**GC:** Gas chromatography

**GTO:** Green Tea oil

**hr:** Hour

**ISO:** International Organization for Standardization

**LB:** Luria broth

**LC:** Loading capacity

**MLV:** Multilamellar vesicles

**MRSA:** Methicillin resistant Staphylococcus aureus

**MS:** Mass spectroscopy

**NLC:** nanostructures lipid capsule

**nm:** Nanometer

**NO NPs:** Nitric oxide nanoparticles

**NP:** Nanoparticles

**PBS:** Phosphate buffer saline  
**PC:** Phosphatidylcholine  
**PDI:** Polydispersity index  
**PEG:** Polyethylene glycol  
**PLGA:** Polylactic glycolic acid  
**PO:** Peppermint oil  
**RNOS:** reactive nitric oxide species  
**ROS:** Reactive oxygen species  
**S. aureus:** Staphylococcus aureus  
**SCF:** Supercritical fluid  
**SDS:** Sodium dodecyl sulfate  
**SEM:** Transmission electron microscopy  
**SFE:** Supercritical fluid extraction  
**SLN:** Solid lipid nanoparticles  
**SOD:** Superoxide dismutase  
**Tc:** Critical temperature  
**Td:** degradation temperature  
**TGA:** Thermogravimetric analysis  
**TPC:** Total phenolic content  
**TPP:** Sodium tripolyphosphate  
**ULV:** Unilamellar vesicle  
**UV-Visible spectroscopy:** UV-Vis spectroscopy  
**WHO:** World health organization  
**XRD:** powder X-ray diffraction  
**ZP:** Zeta potential

## List of Figure

Figure 1: Main causes of deaths at the beginning of the twentieth century <sup>1</sup> . -----	2
Figure 2: Leading infectious disease Killer, 1998 <sup>5</sup> -----	3
Figure 3: Bacterial Biofilm formation <sup>8</sup> . -----	4
Figure 4: Classes of antibiotics/antibacterial agents and their modes of action on bacteria <sup>13</sup> . -	5
Figure 5: Resistance strategies in bacteria <sup>18</sup> . -----	7
Figure 6: Reactive oxygen species <sup>19</sup> . -----	8
Figure 7: Imbalance between antioxidant and free radicals levels <sup>20</sup> . -----	9
Figure 8: Oxidative stress complications <sup>21</sup> . -----	10
Figure 9: Steam distillation for EOs extraction <sup>23</sup> . -----	12
Figure 10: Supercritical fluid extraction (SFE) for EOs extraction <sup>31</sup> . -----	14
Figure 11: EOs representative chemical structures <sup>32</sup> . -----	15
Figure 12: Mechanism of action and target sites of the essential oils on microbial cells <sup>37</sup> . ----	17
Figure 13: Types of nanomaterials <sup>44</sup> . -----	20
Figure 14: Nanoparticles multiple antibacterial mechanisms <sup>16</sup> . -----	21
Figure 15: Chitin and chitosan chemical structures <sup>47</sup> . -----	23
Figure 16: Nanosystem platforms for EOs <sup>24</sup> . -----	25
Figure 17: Schematic Representation of nanoparticle and nanocapsules with adsorbed or encapsulated EOs <sup>52</sup> . -----	26
Figure 18: Illustrative diagram of nanoemulsion <sup>24</sup> . -----	28
Figure 19: Illustrative diagram of SLN <sup>65</sup> . -----	29
Figure 20: Illustrative diagram of liposome <sup>65</sup> . -----	30
Figure 21: Schematic illustrations of EO encapsulation two-step process. -----	37
Figure 22: (A) chemical structure of chitosan ionically crosslinked with TPP <sup>76</sup> , (B) Parameters that affect the size, PDI and ZP of formulated NPs. -----	38
Figure 23: Rotor-stator type homogenizer <sup>80</sup> . -----	46
Figure 24: A typical probe sonicator (a), The phenomena of cavitation (b) <sup>81</sup> . -----	47
Figure 25: A typical benchtop freeze dryer (a), the lyophilization cycle (b) <sup>82</sup> . -----	48
Figure 26: A typical Dynamic light scattering system (a), DLS principle (b) <sup>83</sup> . -----	50
Figure 27: A typical TEM components <sup>85</sup> . -----	51
Figure 28: Schematic diagram of Michelson interferometer <sup>87</sup> . -----	53
Figure 29: Bragg's hypothesis (a), Schematic diagram of a typical XRD system (b) <sup>88</sup> . -----	54
Figure 30: Schematic diagram of TGA <sup>89</sup> . -----	55
Figure 31: UV-Vis spectrophotometer <sup>95</sup> -----	57
Figure 32: Agar dilution and colony count method <sup>96</sup> -----	59
Figure 33: DPPH assay principle <sup>98</sup> -----	60
Figure 34: Chemical structures of PO and GTO phytochemicals <sup>32</sup> . -----	62
Figure 35: Impact of homogenization parameters on (a) the average NPs diameter and (b) size distribution of CS/PO NPs. -----	65

Figure 36: Impact of TPP concentrations on (a) the NPs size and size distribution (b) the zeta potential of CS/PO NPs.-----	67
Figure 37:Z-average diameter of nanoparticles as a function of initial PO and GTO content. 70	
Figure 38:Zeta potential of CS NPs as a function of initial PO and GTO content. -----	72
Figure 39: TEM of spherical nanoparticle, CS NP (a), CS/PO NP (1:1) (b) and CS/GTO NP (1:1) (c). -----	73
Figure 40: Size distribution histograms of the prepared nanoparticles, CS NP (a), CS/PO NP (1:1) (b) and CS/GTO NP (1:1) (c). -----	73
Figure 41:TEM of aggregated nanoparticle, CS NP (a), CS/PO NP (1:1) (b) and CS/GTO NP (1:1) (c). -----	74
Figure 42:TEM of aggregated CS/ Carvacrol nanoparticle <sup>76</sup> . -----	74
Figure 43: FT-IR of CS NP(a), pure PO (b) and CS/PO NP (c-f) with different ratios of CS: PO 1:0.25 (c), 1:0.50 (d), 1:0.75 (e) and 1:1.00 w/w (f). -----	76
Figure 44:FT-IR of CS NP(a), pure GTO (b) and CS/GTO NP (c-f) with different ratios of CS: GTO: 1:0.25 (c), 1:0.50 (d), 1:0.75 (e) and 1:1.00 w/w (f). -----	77
Figure 45:TGA thermogram of CS/PO NP (A) and CS/GTO NP (B): pure EO (a), CS NP (b) and CS/EO NP (c-f) with different ratios of CS: EO 1:0.25 (c), 1:0.50 (d), 1:0.75 (e) ---	78
Figure 46:DTG thermogram of CS/PO NP (A) and CS/GTO NP (B): pure EO (a), CS NP (b) and CS/EO NP (c-f) with different ratios of CS: EO 1:0.25 (c), 1:0.50 (d), 1:0.75 (e) ---	79
Figure 47: XRD pattern of CS powder (a), CS NPs (b), CS/GTO NPs (1:1 w/w) (c) and CS/PO NPs (1:1 w/w) (d). -----	81
Figure 48:UV–Vis spectra of CS/PO NP (A) and CS/GTO NP (B): CS NPs (a) and CS/EO NPs (b-e) with different ratios of CS: EO 1:0.25 (c), 1:0.50 (d), 1:0.75 (e) -----	82
Figure 49:Calibration curve of (A) PO in ethanol and (B) GTO in ethanol. -----	82
Figure 50: EE% and LC% of (A) CS/PO as a function of initial PO content and (B) CS/GTO as a function of initial GTO content -----	83
Figure 51: <i>In-vitro</i> release profiles of PO from CS/PO NPs (1:1) in different pH media: pH 3 and pH 7.4. -----	85
Figure 52: <i>In-vitro</i> release profiles of GTO from CS/GTO NPs (1:1.00) in different pH media: pH 3 and pH 7.4. -----	86
Figure 53:Impact of pH of the release media on CS-TPP system <sup>76</sup> .-----	87
Figure 54:TPC of CS NPs, PO, GTO, CS/GTO NPs and CS/PO NPs expressed in (mg GAE/g oil). -----	89
Figure 55: Mechanism of DPPH oxidation <sup>120</sup> .-----	91
Figure 56: DPPH inhibition (%) of pure PO, CS NPs and CS/PO NPs. -----	92
Figure 57:DPPH inhibition (%) of pure GTO, CS NPs and CS/GTO NPs. -----	93
Figure 58:(A) % Inhibition of <i>S. aureus</i> and, (B) representative photographs of the bactericidal activity toward <i>S. aureus</i> by PO, GTO, CS NPs, CS/PO NPs, CS/GTO NPs, negative and positive control. -----	97

Figure 59: (A) % Inhibition of *E.coli* and, (B) representative photographs of the bactericidal activity toward *E.coli* by PO, GTO, CS NPs, CS/PO NPs, CS/GTO NPs, negative and positive control.----- 99

Figure 60: GC/MS/MS chromatogram of PO. ----- 105

Figure 61: GC/MS/MS chromatogram of GTO. ----- 106

Figure 62:PDI values of nanoparticles as a function of initial PO and GTO content. ----- 107

## List of Tables

Table 1:Parts of plant material containing essential oils <sup>23</sup> . -----	11
Table 2:Examples of EOs extracted by steam distillation and SFE. -----	13
Table 3: list of EOs against bacterial species. -----	16
Table 4:List of EOs loaded into polymeric nanocarriers. -----	26
Table 5:List of EOs loaded into CS NPs, and their biomedical application using two steps encapsulation method. -----	27
Table 6:List of EOs loaded into lipid-based nanocarriers-----	31
Table 7: List of CS NPs samples with their CS:EOs weight ratios. -----	40
Table 8: IC <sub>50</sub> of antioxidant activities of PO, GTO, CS NPs, CS/PO NPs and CS/GTO NPs.	93
Table 9: Chemical composition of PO.-----	105
Table 10:Chemical composition of GTO. -----	106

## List of Equations

<b>Equation 1:</b> SOD reaction .....	10
<b>Equation 2:</b> Peroxisomes reaction .....	10
<b>Equation 3:</b> Loading capacity.....	41
<b>Equation 4:</b> Encapsulation efficiency .....	41
<b>Equation 5:</b> Cumulative release percentage.....	42
<b>Equation 6:</b> Gallic acid equivalent equation .....	42
<b>Equation 7:</b> DPPH scavenging activity.....	43
<b>Equation 8:</b> Inhibition of bacterial growth.....	44
<b>Equation 9:</b> Stock Einstein equation.....	48
<b>Equation 10:</b> Abbe's equation.....	49
<b>Equation 11:</b> Bragg's law.....	52
<b>Equation 12:</b> Energy of radiation.....	55
<b>Equation 13:</b> Beer Lambert law.....	55

# **Chapter 1**

## **General Introduction & Literature Review**

## Chapter 1: General Introduction & Literature review

### 1.1. Bacterial Infectious diseases in the twentieth century

Bacterial infectious diseases such as tuberculosis, pneumonia and diarrhea were the main reasons of mortality worldwide at the beginning of the twentieth century as represented in **Figure (1)**. Bacterial infections represent about 30 percent of mortality percentage that led to reduction in life expectancy to 47 years with high mortality in infant and childhood . Pneumonia and diarrhea were enough to kill 10% of children between the age of 1 to 4 years old<sup>1</sup>.

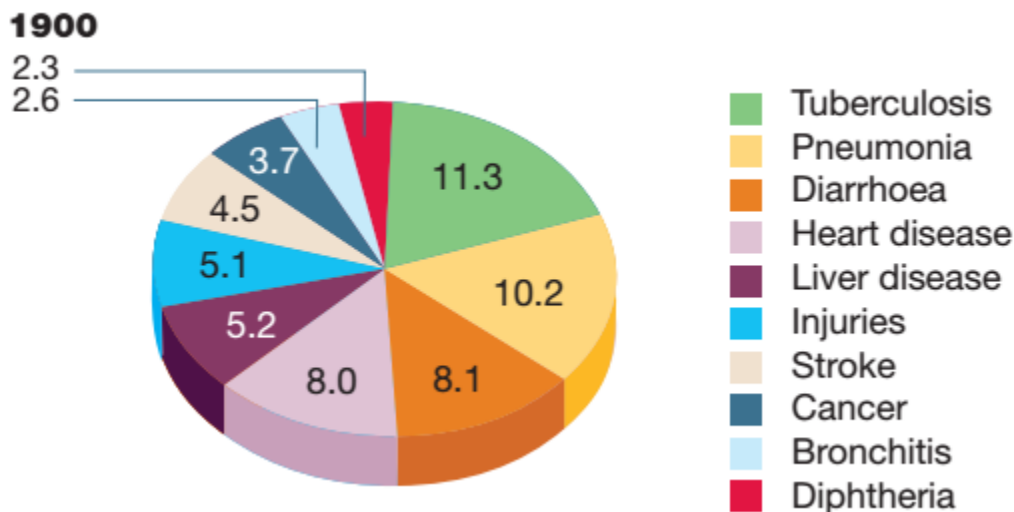


**Figure 1:** Main causes of deaths at the beginning of the twentieth century<sup>1</sup>.

By the mid of the twentieth century, the rate of mortality due to bacterial infectious diseases declined after the introduction of antimicrobial agents<sup>2</sup>. About 50% reduction in childhood fever mortalities caused by *Streptococcus pyogenes* due to the introduction of sulfa antibiotics as Sulphadiazine. Between 1938 and 1952, the annual rate of deaths from bacterial infectious diseases, especially tuberculosis and pneumonia, was reduced by 8.2% with the beginning of the antibiotic era<sup>3</sup>. Despite of the success of antimicrobial agents to minimize the bacterial diseases

mortalities, the World Health Organization (WHO) estimated, in 1998, that bacterial infectious diseases such as pneumonia, diarrhea and tuberculosis cause about 25% of mortalities worldwide especially in children that represented in **Figure (2)**. The reason behind that was due to the development of antimicrobial resistance that becomes a serious worldwide danger<sup>4</sup>. For instance, bacterial diseases mortalities in USA were increased at a rate of 4.8% between 1981 to 1995 due to drug-resistant infection. One of the main reasons behind developing antimicrobial resistance is owing to bacterial biofilm formation that provides a protection for bacterial community against antibacterial drugs<sup>4</sup>.

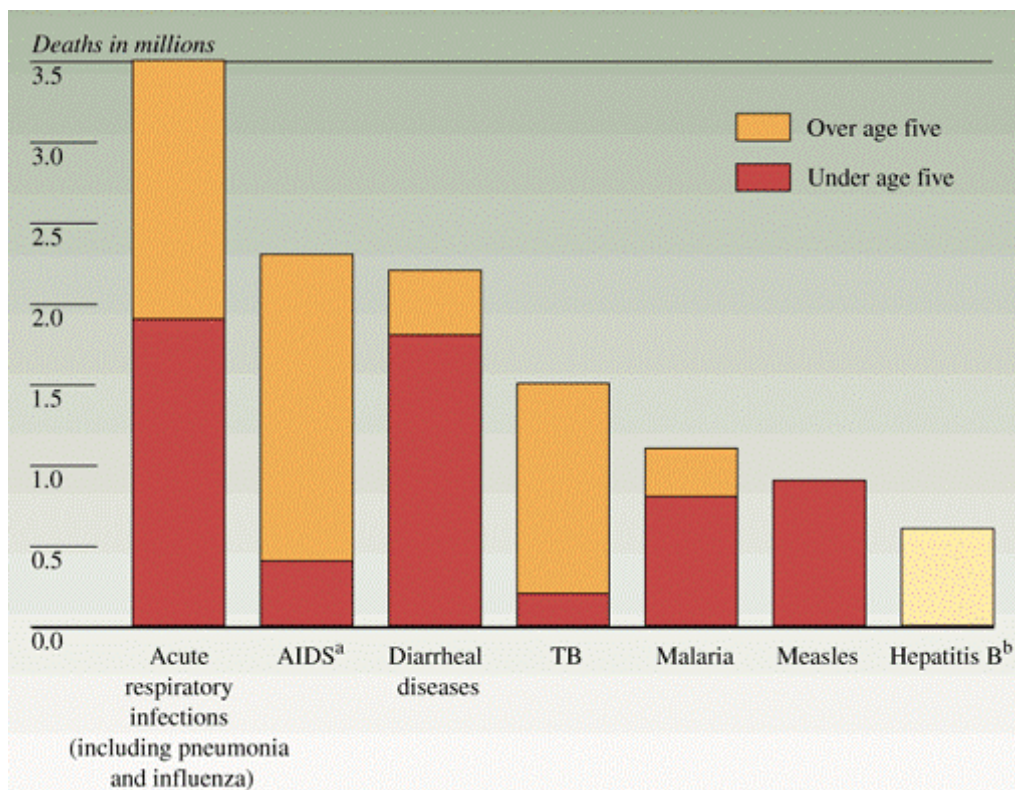


**Figure 2:** Leading infectious disease Killer, 1998<sup>5</sup>

Bacteria live in communities that are composed of different species interacting with each other and with the environment too. They grow in association with surfaces with a higher capabilities to adhere, persist and colonize, forming bacterial biofilm as shown in **Figures (3)**<sup>6</sup>. Bacterial

biofilm formation is based on three main stages; (i) first is the irreversible attachment of bacteria through their secretion of adhesion for binding protein. Then, (ii) bacteria are able to proliferate and colonize inside an envelope made of peptidoglycan and finally, (iii) the development of biofilm maturation. Matured biofilm provides not only a protection of bacteria from antimicrobial agents and immune system, but also a bacterial reservoir that ready to rupture for further bacterial dispersion to infect new surfaces<sup>7</sup>. About 80% of microbial infections is owing to bacterial biofilm resulting in higher potential of morbidity and mortality in addition to increase in medical expenses<sup>8,9</sup>.

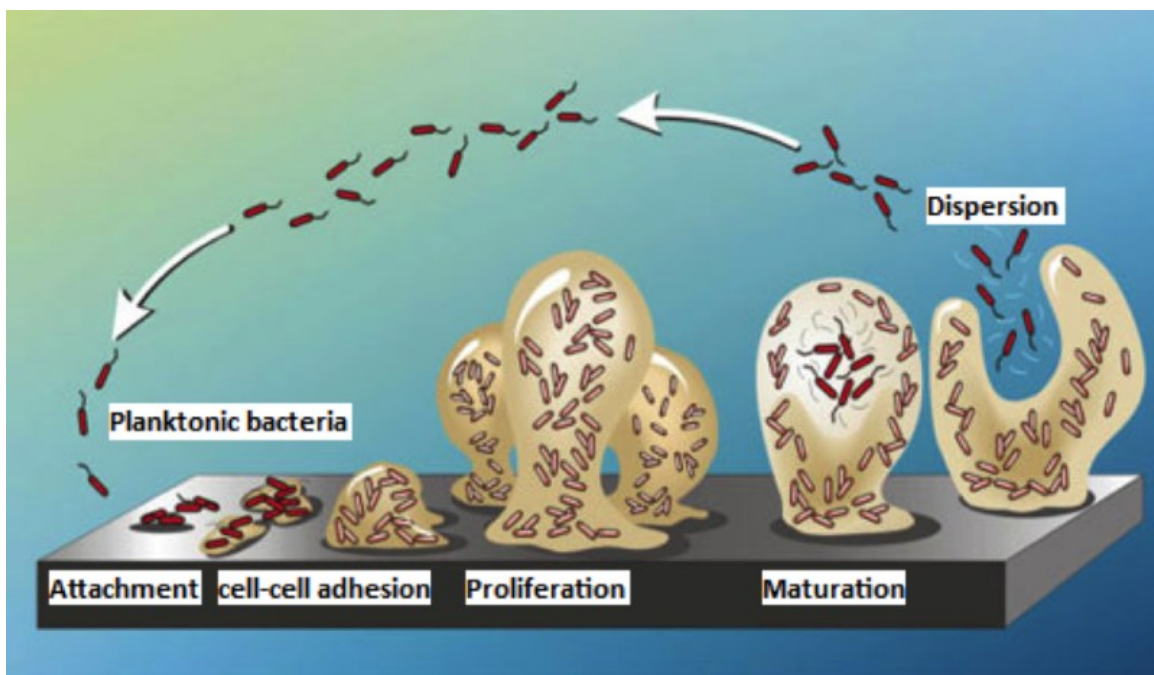


**Figure 3:** Bacterial Biofilm formation<sup>8</sup>.

## 1.2.Traditional solutions for combating bacterial infections

The most commonly used solution that revolutionized the treatment of bacterial infections worldwide was the use of antibiotic and antibacterial agents for more than 50 years for both human and animal health especially during antibiotic golden age<sup>10</sup>. They have several targets on

the bacteria including; cell wall and cell membranes, ribosomes, nucleic acids, cellular metabolism and enzymes as shown in **Figure (4)**. The selective toxicity of antibiotics depends on the structural and metabolic differences between bacteria and mammalian cells<sup>11</sup>. Combating biofilm infections requires using antimicrobial agent with a higher penetration power to ensure delivery of a sufficient concentration of antimicrobial agent to kill bacteria. For instance, well known antimicrobial agents with efficient penetration power such as rifamycins, sulfonamides, quinolones, macrolides, lincosamides, tetracyclines, fusidic acid and oxazolidinones, are commonly used to combat bacterial biofilm than other antimicrobials with higher molecular weight and poor penetration power such as aminoglycosides, polymyxin and beta-lactam antibiotics (penicillins, cephalosporins and carbapenems)<sup>12</sup>. However, many parameters should be considered to fight microbial biofilm such as, tissue pH, therapy protocol and duration of treatment.

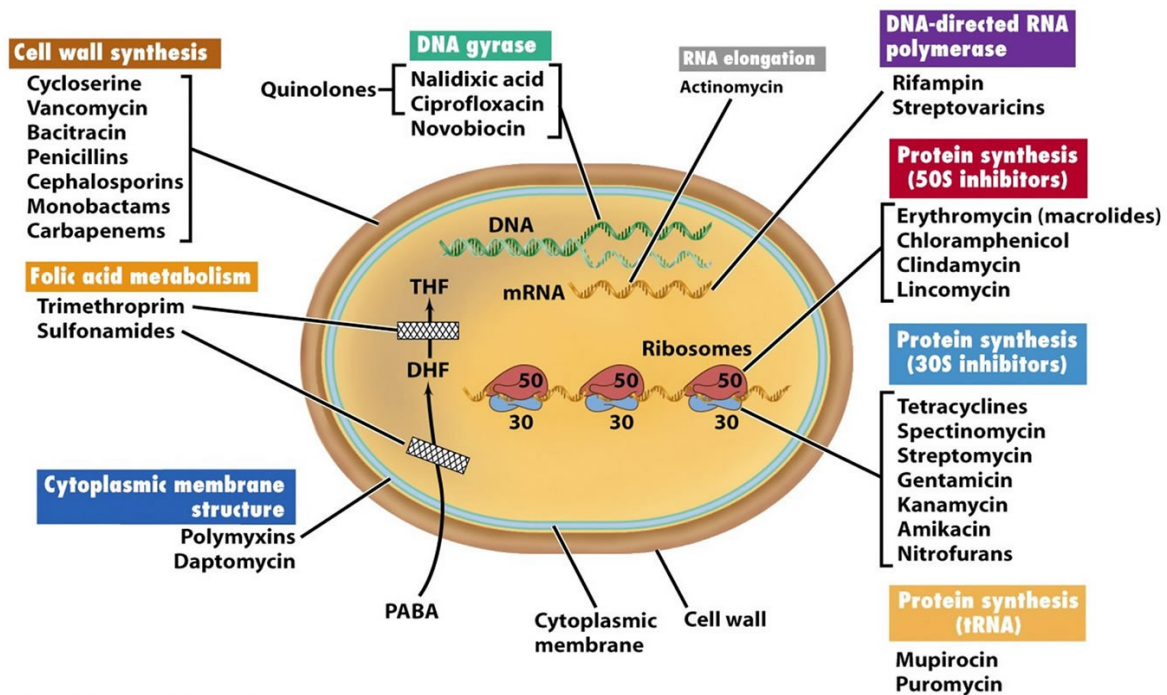


**Figure 4:** Classes of antibiotics/antibacterial agents and their modes of action on bacteria<sup>13</sup>.

It is well known that tissue pH can control the efficiency of antibiotics towards biofilms. Inflammation that comes from bacterial infection results in a reduction in tissue oxygen level due to faster metabolism rate which in turn leads to activation of cellular glycolysis process that minimizes the tissue pH (tissue acidosis). For instance, lower pH value to less than 5.2 can result in reduction in efficiency of  $\beta$ -lactam antibiotics while increasing efficiency rifamycin<sup>14</sup>. On the other hand, protocol therapy to eradicate bacterial biofilm could also affect the biofilm combating efficacy. For example, tobramycin-colistin combination therapy is significantly efficient than monotherapy against *P. aeruginosa* biofilm infection<sup>15</sup>.

### **1.3. Mechanisms of antibiotic resistance**

Antibiotic resistance in bacterial infection has negative effects upon medicine and society. Drug resistance leads to usage of higher doses of antibiotics with a higher potential of toxicity as well as longer hospital stays and higher mortality rate. For example, Methicillin-resistant *Staphylococcus aureus* (MRSA) is associated with higher deaths percentage that added \$20 billion to the total health care costs in addition to \$35 billion in costs to the American society<sup>16</sup>. Antibacterial drug resistance is based on two main mechanisms: (i) preventing the antibiotic from reaching their targets in bacterial cell and, (ii) modifying the bacterial targets that the antibiotic work on as represented in Figure (5)<sup>17</sup>.

Bacteria can prevent the antibiotic from reaching its targets by different mechanisms. Pumping the antibiotic molecule out of bacterial cell through bacterial efflux pump is one of antibiotic resistance mechanism that lowers the antibiotic concentration inside the bacterial cell. Furthermore, bacteria can reduce the permeability of the membrane that surrounds the bacterial cell as it makes it more difficult to pass through. On the other hand, bacterial enzymes can inactivate the antibiotics. For instance,  $\beta$ -lactamase enzyme can inactivate the component  $\beta$ -

lactam antibiotic such as penicillins. Finally, Bacteria can modify the chemical structure of the antibiotic that prevent the binding interaction between antibiotic and bacterial cell<sup>17</sup>.

Bacterial target modification is the second strategy for antibacterial drug resistance that depends on different mechanisms. Mutations in the bacterial DNA can induce a change in the structure of the target in the bacteria inhibiting the interaction of antibiotic with the bacterial cell target. Furthermore, bacteria can express other proteins that replace the inhibited ones by the antibiotic. For instance, *S. aureus* bacteria can express a new penicillin-binding protein that resists the  $\beta$ -lactam antibiotics antibacterial action which is the basis in appearance of MRSA strains<sup>17</sup>.

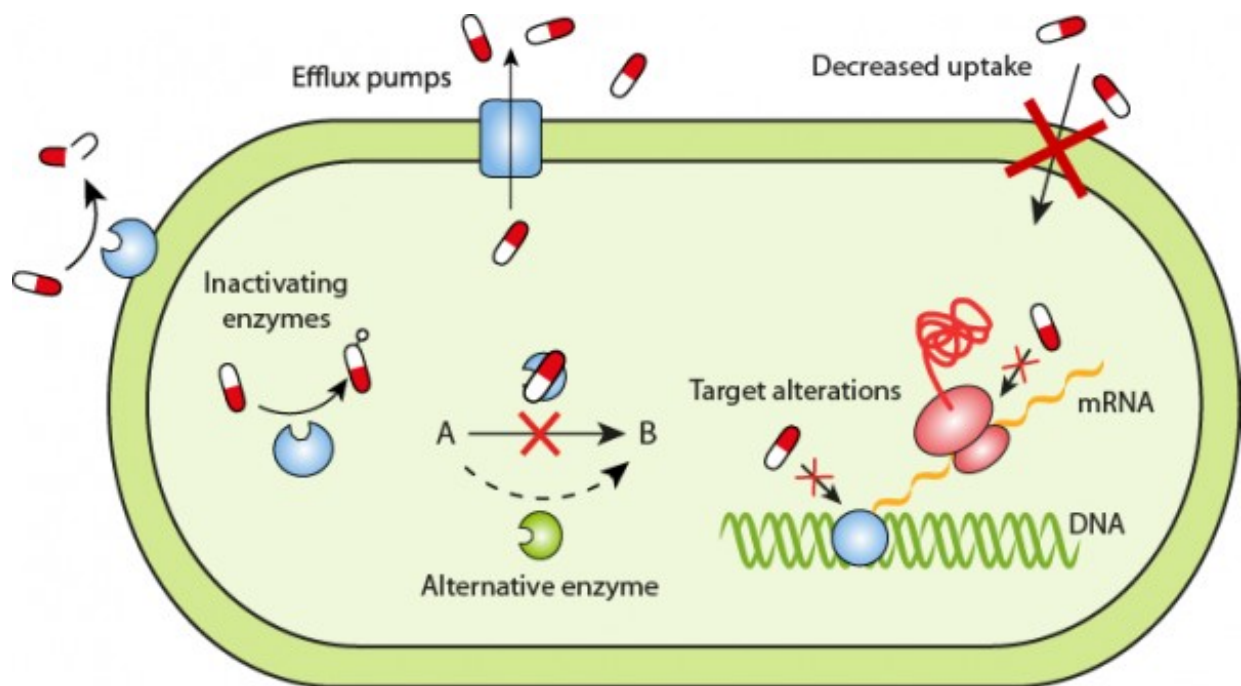


**Figure 5:**Resistance strategies in bacteria<sup>18</sup>.

#### 1.4. Reactive oxygen species and oxidative stress

Reactive Oxygen Species (ROS) are reactive molecules that come from molecular oxygen as shown in Figure (6). Mitochondrial aerobic respiration is one of the ROS source formation as well as oxidoreductase enzymes. ROS can induce cellular apoptosis which in turn activates the cellular signaling cascades as they serve as both intra- and intercellular messengers. Furthermore, ROS can damage DNA, protein, lipids and carbohydrates and is related to pathogenesis of different diseases<sup>19</sup>.

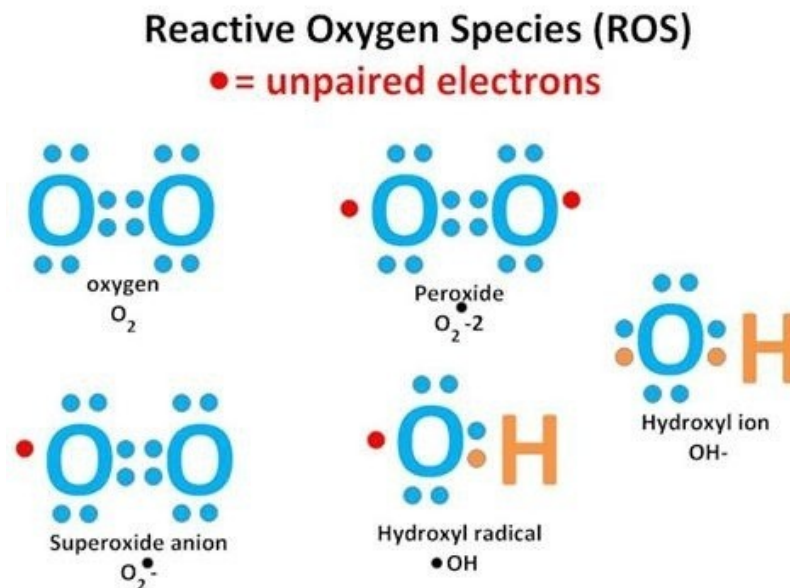


**Figure 6:** Reactive oxygen species<sup>19</sup>.

Survival of the cell is based on detoxification of ROS. There is normal balance between production and removal of ROS as represented in Figure (7)<sup>20</sup>. Elevation of ROS levels results in a condition that is called “oxidative stress”.

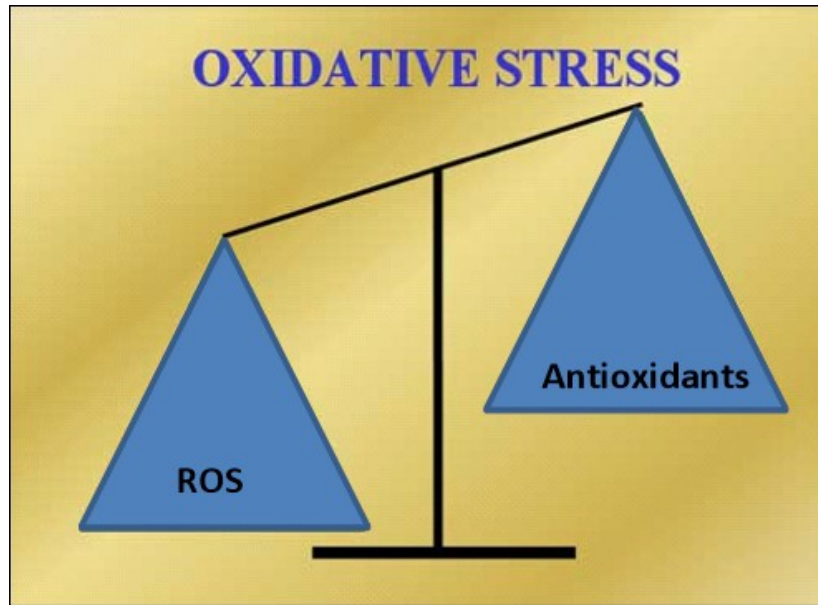


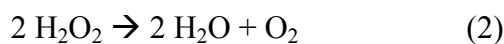
**Figure 7:** Imbalance between antioxidant and free radicals levels<sup>20</sup>.

As represented in **Figure (8)**, oxidative stress has a key role in age-related diseases such as renal nephritis, atherosclerosis, retinal degenerations, cancer, arthritis, obesity, type 2 diabetes and Alzheimer's disease (AD)<sup>21</sup>.



**Figure 8:** Oxidative stress complications<sup>21</sup>.

Antioxidant enzymes such as superoxide dismutase (SOD) helps in conversion of superoxide into hydrogen peroxide ( $\text{H}_2\text{O}_2$ ) (equation 1)<sup>20</sup> that is converted into water molecule through the help of peroxisomes of eukaryotic cells (equation 2)<sup>20</sup>. On the other hand, Glutathione peroxidase is a group of enzymes support conversion of hydrogen peroxide into alcohols<sup>20</sup>.



The challenges that face the conventional antibiotics in fighting bacterial infections and the search for antioxidants that prevent the diseases related oxidative stresses have made many scientists investigating a natural alternative that provides antibacterial and antioxidant activities with minimal side effects. Aromatic plants and their EOs have been widely applied for a variety of purposes for thousands of years. Therefore, essential oils (EOs) were one of the natural compounds that have been investigated for their biomedical activities.

## 1.5. Essential oil

According to the International Organization for Standardization (ISO), EOs are defined as: “colorless, highly volatile hydrophobic liquids containing complex mixtures of organic compounds”. EOs are secondary plant metabolites that are stored in plant secretory cells and cavities after synthesis in flowers, stems, seeds and leaves that are summarized in **Table (1)**. They are characterized by their lower density (less than water), lower mass (less than 300 molecular weight) in addition to their higher dissolution in organic solvents such as ethanol, hexane and chloroform<sup>22</sup>.

**Table 1:**Parts of plant material containing essential oils<sup>23</sup>.

<b>Parts</b>	<b>Plants</b>
<b>Leaves</b>	Basil, bay leaf, cinnamon, common sage, eucalyptus, lemon grass, citronella, melaleuca, mint, oregano, patchouli, peppermint, pine, rosemary, spearmint, tea tree, thyme, wintergreen, kaffir lime, laurel, savory, tarragon, cajuput, lantana, lemon myrtle, lemon teatree, niaouli, may chang, petitgrain, laurel, cypress
<b>Seeds</b>	Almond, anise, cardamom, caraway, carrot celery, coriander, cumin, nutmeg, parsley, fennel, Camilla sinensis
<b>Wood</b>	Amyris, atlas cedarwood, himalayan cedarwood, camphor, rosewood, sandalwood, myrtle, guaiac wood
<b>Bark</b>	Cassia, cinnamon, sassafras, katrafay
<b>Berries</b>	Allspice, juniper
<b>Resin</b>	Frankincense, myrrh
<b>Flowers</b>	Blue tansy, chamomile, clary sage, clove, cumin, geranium, helichrysum hyssop, jasmine, lavender, manuka, marjoram, orange, rose, baccharises, palmarosa, patchouli, rhododendron, anthopogon, rosalina, ajowan, ylang-ylang, marjoram sylvestris, tarragon, immortelle, neroli
<b>Peel</b>	Bergamot, grapefruit, kaffir lime, lemon, lime, orange, tangerine, mandarin
<b>Root</b>	Ginger, plai, turmeric, valerian, vetiver, spikenard, angelica
<b>Fruits</b>	Xanthoxylum, nutmeg, black pepper

### 1.5.A. Essential oil extraction

EOs are extracted from vegetables by steam distillation as well as by supercritical fluid carbon dioxide<sup>24</sup>. Steam distillation is the most common technique used for EOs extraction. Basically, as shown in **Figure (9)**, the required part of a plant is subjected to minimum amount of heated steam with enough temperature (without soaking the plant in boiling water) that cause plant cell rupture and EOs are released with steam and condensed through a cooling condenser and finally the EOs are separated by an oil separator. The extraction yield (93%) and the antioxidant activity of EOs extracted by steam distillation were found to be higher than EOs extracted by hydro distillation (soaking of plant cells in boiling water) which makes steam distillation the most favourable technique to be used for EOs extraction<sup>25,26</sup>. Examples of some EOs that were extracted by steam distillation are listed below in **Table (2)**.

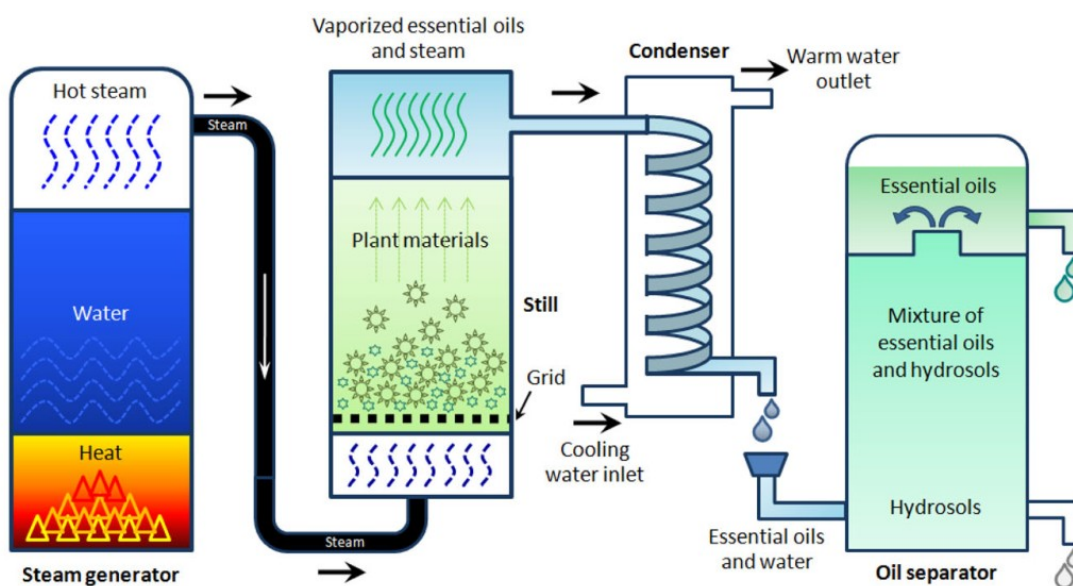


**Figure 9:** Steam distillation for EOs extraction<sup>23</sup>.

**Table 2:** Examples of EOs extracted by steam distillation and SFE.

Extraction methods	Plants	References
Steam Distillation	rose-scented geranium ( <i>Pelargonium</i> sp.)	[27]
	thyme ( <i>Thymus kotschyanus</i> )	[28]
	germander ( <i>Teucrium orientale</i> )	[29]
	rosemary ( <i>Rosmarinus officinalis</i> )	[30]
	fennel ( <i>Foeniculum vulgare</i> )	[30]
	anise( <i>Pimpinella anisum</i> )	[30]
	eucalyptus ( <i>Eucalyptus citriodora</i> ),	[31]
	Peppermint oil ( <i>Mentha piperita</i> )	[32]
Super critical fluid extraction (SFE)	cumin seed ( <i>Cuminum cyminum</i> )	[33]
	sage ( <i>Salvia officinalis</i> )	[34]
	lemon ( <i>Citrus x limon</i> )	[35]
	carrot fruit ( <i>Daucus carota</i> L.)	[36]
	marjoram ( <i>Majorana hortensis</i> Moench)	[37]
	Baccharises ( <i>Baccharis uncinella</i> )	[38]
	Green tea ( <i>Camellia sinensis</i> )	[39]

However, due to prolonged extraction time as well as degradation of unsaturated fatty compounds that are present in EOs, supercritical fluid extraction (SFE) using carbon dioxide (CO<sub>2</sub>) have been considered as an alternative medium for EOs extraction<sup>27,28</sup>. The most common super critical fluid (SCF) in extraction is CO<sub>2</sub> due to its lower critical temperature (T<sub>c</sub>) (which is the temperature needed to convert a material state into SCF state) that preserve thermal stability of EOs during extraction. Furthermore, SCF CO<sub>2</sub> can be evaporated easily by subjecting it to atmospheric pressure which gives an advantage of removing any CO<sub>2</sub> residue in EOs<sup>27,29,30</sup>. However, pure CO<sub>2</sub> has low extraction rate (80% extraction after 90 min) therefore, methylene chloride is used as a modifier that enhances the extraction efficacy<sup>29</sup>. According to **Figure** (10), liquid CO<sub>2</sub> is compressed through a compressor and heated up to achieve a critical pressure (P<sub>c</sub>) as well as a critical temperature (T<sub>c</sub>) that are required to achieve SCF state as shown in **Figure**

(10). Then, SCF CO<sub>2</sub> starts to extract the EOs from plant cells that are placed in an extractor due to higher penetration, diffusion and solubilizing powers of SCF. The EOs are dissolved in SCF then pass through a separator that is adjusted with atmospheric pressure to evaporate CO<sub>2</sub> and separate EOs<sup>31</sup>. Escaped CO<sub>2</sub> is then condensed to liquified CO<sub>2</sub> for the next run. Examples of some EOs that were extracted by SFE are listed in **Table (2)**.

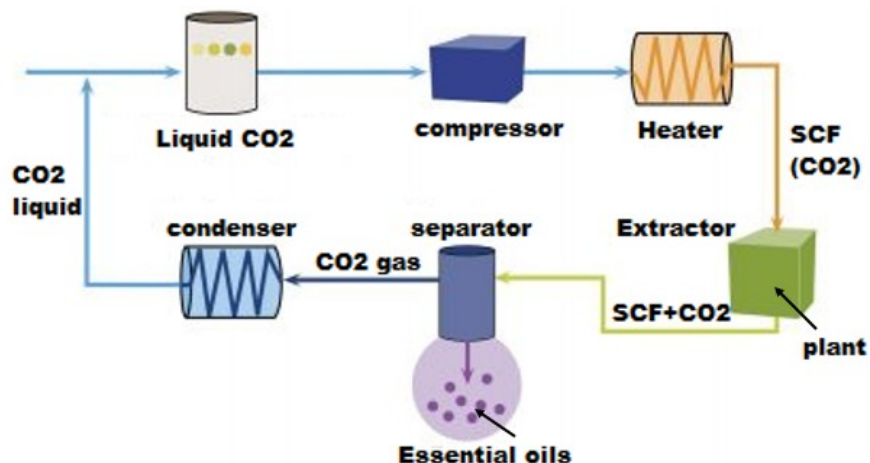


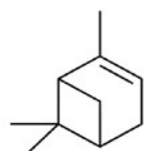
**Figure 10:**Supercritical fluid extraction (SFE) for EOs extraction<sup>31</sup>.

### 1.5.B. Essential oil chemical composition.

The chemical compositions of EOs are classified into two main categories; (i) oxygenated compounds and (ii) hydrocarbons. The former are organic compounds that contain oxygen atoms in their structures such as aldehydes, lactones, ethers, alcohols, esters, ketones and phenols while the later contains hydrogen and carbon atoms such as terpenes and sesquiterpenes<sup>32</sup>. In addition, phytochemicals can also be classified into; monoterpenoids, sesquiterpenoids, phenylpropanoids, short-chain aliphatic hydrocarbon derivatives, glucosinolates and isothiocyanate derivatives as shown in **Figure (11)**<sup>33</sup>.

## Terpenes

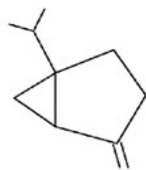
### Monoterpenes



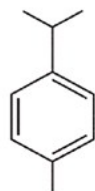
$\alpha$ -Pinene



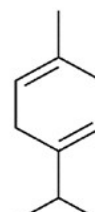
Limonene



Sabinene

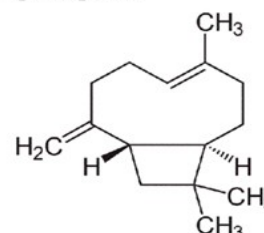


p-Cymene



$\gamma$ -Terpinene

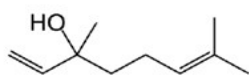
### Sesquiterpenes



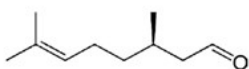
$\beta$ -Caryophyllene

## Terpenoids

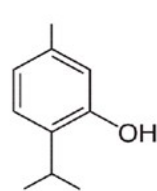
### Monoterpenoids



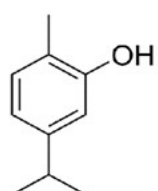
Linalool



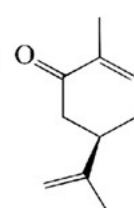
Citronellal



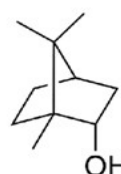
Thymol



Carvacrol

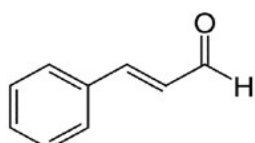


Carvone

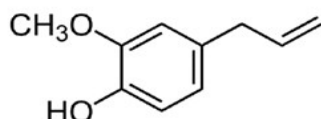


Borneol

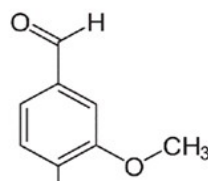
## Phenylpropanoids



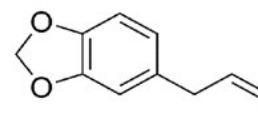
Cinnamaldehyde



Eugenol

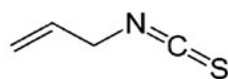


Vanillin

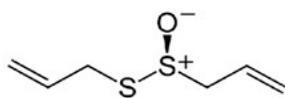


Safrole

## Others



Allyl-isothiocyanate



Allicin

**Figure 11:**EOs representative chemical structures<sup>32</sup>.

The variation in the chemical composition of EOs is related to the difference in molecules' types, quantity and stereochemical structures. Furthermore, other factors can affect the chemical compositions of EOs such as extraction methods, environmental conditions and plant organ<sup>32</sup>. Accordingly, European Pharmacopoeia (EP) and WHO Analytical monographs have been issued

to confirm the quality and quantity of EOs utilizing advanced analytical techniques such as Gas chromatography (GC) and Mass spectrometry (MS)<sup>33</sup>. Generally, about 20-100 single components are present in EOs in different concentrations. Nearly 2-3 components are considered as main constituents with relative high proportions (20–70%) that determine the biological activities of EOs while others are considered as trace constituents. For instance, in *Origanum* species EOs, both carvacrol (30%) and thymol (27%) are the main constituents<sup>33</sup>.

### 1.5.C. Essential oils as natural antimicrobial and antioxidant agents

Aromatic plants and their EOs have been applied for many purposes for thousands of years. They were used by Ancient Egyptians in embalming to inhibit the growth of bacteria. Their lipophilic liquids, that are composed of a mixture of chemical components with a higher antibacterial property, therefore they were used as preservative for fooda, as well as in pharmaceutical<sup>34</sup>. Different EOs with their antibacterial activities are listed below in **Table (3)**.

**Table 3:** list of EOs against bacterial species.

<b>Essential oil</b>	<b>Bacterial species</b>	<b>References</b>
Thyme	<i>Salmonella choleraesuis</i> and <i>Salmonella typhimurium</i>	[35]
Carvacrol	<i>Escherichia coli</i> and <i>Listeria monocytogenes</i>	[36]
Oregano	<i>Escherichia coli</i> and <i>Salmonella enteritidis</i>	[35]
Eugenol	<i>Escherichia coli</i> and <i>Listeria monocytogenes</i>	[36]
Peppermint	<i>Escherichia coli</i> and <i>Staphylococcus aureus</i>	[37]
Green tea	<i>M. luteus</i> and <i>bacillus. Cereus</i>	[38]
Rosemary	<i>Escherichia coli</i> and <i>Staphylococcus aureus</i>	[39]
Lemongrass	<i>Escherichia coli</i> and <i>Staphylococcus aureus</i>	[40]
Sage	<i>Escherichia coli</i> and <i>S. typhimurium</i>	[40]
Clove	<i>Listeria monocytogenes</i>	[41]
Turmeric	<i>Escherichia coli</i>	[42]

### 1.5.D. Essential oil antibacterial mode of action

EOs have complex chemical nature as they are composed of several components as mentioned earlier, therefore they have different antimicrobial mechanisms as shown in Figure (12). Phenolic components of EOs play a role in enhancing the penetration and disruption of bacterial membranes that cause inhibition effect on cell functional properties and eventually causing leakage of the internal contents of the bacterial cell. The reason behind that is owing to the presence of phenolic components that are found in thymol, carvacrol, eugenol, peppermint (PO) and green tea (GTO) can enrich the amount of saturated fatty acids ( $C_{16}$ - $C_{18}$ ) while decreasing the amount of unsaturated fatty acids ( $C_{18}$ ) in bacterial cell membrane<sup>35</sup>. Furthermore, EOs lipophilicity can detach the lipids of bacterial cell membrane making bacterial cell more permeable. On the other hand, oregano EO can interfere with cellular energy (ATP) generation system that reduce significantly *S. aureus* intracellular ATP levels. Moreover, EOs such as p-cymene can disrupt the proton motive force of bacterial cell membrane that required for flagellar movement which result in cell death<sup>36</sup>.

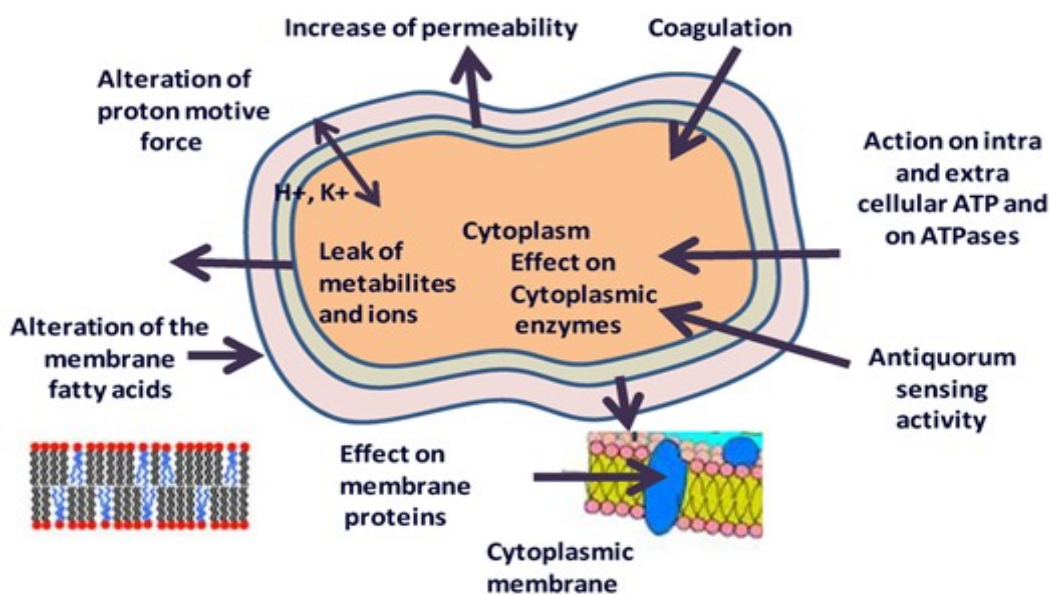


Figure 12: Mechanism of action and target sites of the essential oils on microbial cells<sup>37</sup>.

### **1.5.E. Essential oil antioxidant mode of action**

EOs exhibit their antioxidant role due to their behaviour as physical barrier to stop ROS generation. Furthermore, they may act as chemical trap for electrons such as carotenoids, and anthocyanidins. They may also act as chain-breaker to destroy ROS such as tocopherols and flavonoids components<sup>32</sup>.

Generally, antioxidant agent is classified into: (i) primary and (ii) secondary antioxidants. The former one act as a hydrogen ion doner to a radical to convert it into a new stable radical. Secondary antioxidants can reduce the oxygen level (scavenging of oxygen or chelating metal) to prevent initiation of ROS generation<sup>38</sup>.

### **1.5.F. EOs limits and challenges**

All EOs antibacterial mechanisms can induce growth inhibition of some gram-positive such as, *S. aureus*, *Listeria monocytogenes* and *Bacillus cereus*, less than gram-negative bacteria such as *E. coli* and *Salmonella Enteritidis* due to the direct interaction between EOs components and bacterial cell membrane. Hydrophilic nature of gram-positive bacterial cell wall explains the high resistance toward plant EOs<sup>39</sup>.

Some EOs components have some degree of toxicity as shown in case of eugenol at a concentration of 0.1 Mm that can cause rat hepatocytes membrane lysis due to the reduction of the surface tension of the membrane. Furthermore, carvacrol can inhibit the proliferation of purified porcine lymphocytes<sup>39</sup>.

Beside EOs' higher volatility, the direct exposure of EOs to heat, light, moisture and oxygen can trigger chemical and/or enzymatic reactions such as dehydrogenation, oxidation, cyclization and

isomerization reactions that in turn lead to the decomposition of their chemical constituents and changing in their viscosity and organoleptic properties<sup>40</sup>. For instance, oxygenated terpenoids such as menthol and menthone that are present in PO were converted into ketones, acids, and aldehydes upon exposure to atmospheric conditions, and consequently, these new products result in skin hypersensitivity reaction and allergic dermatitis<sup>41</sup>. On the other hand, polyphenols such as epigallocatechin gallate that were found in GTO are exposed to epimerization and oxidation reactions leading to its degradation into catechin monomers and gallic acid<sup>42</sup>.

The above drawbacks of using EOs in bulk form in different biomedical application have made many scientists looking for a magical solutions to overcome these limitations and improve EOs properties. Nanotechnology opened new avenues towards preparing novel materials at much smaller scale – nanoscale - than their bulk counterparts, and exhibit promising improvement in material properties.

## **1.6. Nanotechnology**

Nanoscience is a multidisciplinary science that connect chemistry, physics, engineering, pharmacy medicine and other sciences together. Therefore, nanoscience is considered a real convergence among distant knowledge areas. Nanoscience impact is very strong on many fields connected to life and health. Nanotechnology (applied nanoscience) may provide new track for combating both microbial disease as well as oxidation stresses. Nanoscience is the study behavior of materials that has one dimension between 1 to 100 nm as represented in **Figure (13)**<sup>43</sup>.

Nanomaterials are classified into four classes; (i) zero dimensional nanomaterials (all three dimensions are less than 100 nm) such as nanoparticles and quantum dots. (ii) one dimensional

nanomaterials have two dimensions less than 100 nm such as nanotubes (iii) two dimensional nanomaterials (with one dimension less than 100 nm) such as thin films. And (iv) finally, three dimensional nanomaterials which are composed of assembled nanomaterials such as nanocrystalline grains. Dealing with material in the nanoscale offers higher innovation potential in many fields, particularly in the fields of antibacterial and antioxidant agents<sup>43</sup>.

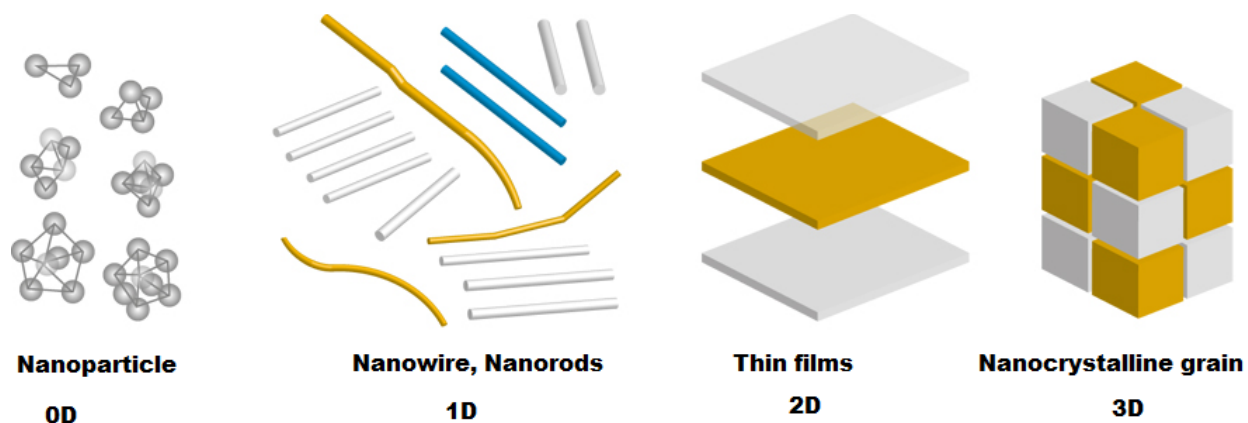


**Figure 13:**Types of nanomaterials<sup>44</sup>.

## 1.7. Nanoparticles mechanisms for combating microbial resistance

### 1.7.A. Nitric oxide-releasing nanoparticles (NO NPs)

Nitric oxide-releasing nanoparticles (NO NPs) have a strong antibacterial activity due to the formation of reactive nitrogen oxide species (RNOS) as a result of NO-superoxide interaction inside bacterial cell especially when NO level exceeds 1nM as represented in **Figure** (14). Furthermore, NO has the ability to bind with bacterial membrane protein as well as its efficiency to break DNA strands. Moreover, NO enhances the generation of hydrogen peroxide that causes a damage of DNA as well as their ability to simulate human innate immunity response. For instance, NO NPs shows a good antibacterial activity against spores of *Bacillus cereus*<sup>45</sup>.

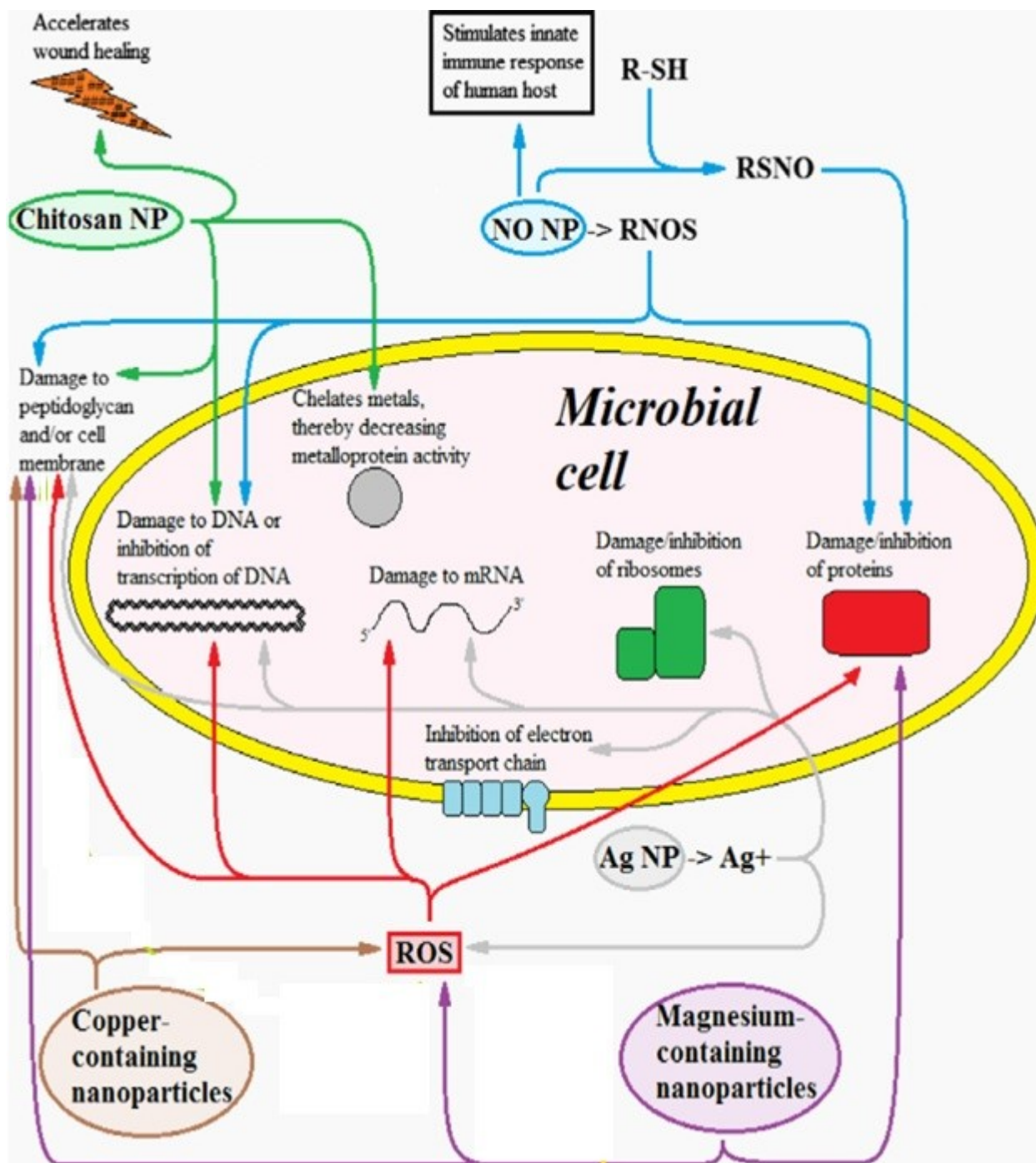
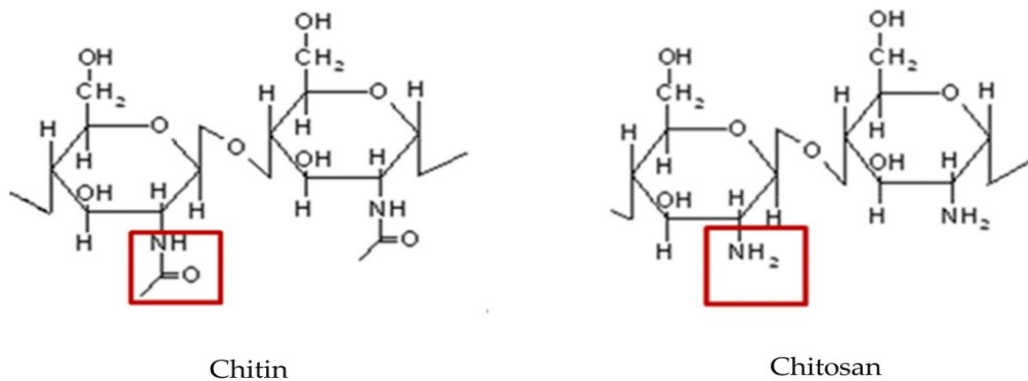


Figure 14: Nanoparticles multiple antibacterial mechanisms<sup>16</sup>.

### 1.7.B. Chitosan nanoparticles

Chitosan nanoparticles (CS NPs) can combat microbes with different mechanisms. CS is derived from chitin (polymer of N-acetyl-glucosamine residues) after deacetylation at random monomer residues as shown in **Figure** (15) with a pKa of 6.5. At a pH below 6.5 (as in bacterial biofilm), all CS amino groups become protonated and bind with bacterial cell walls and plasma membranes (which are negatively charged) that increases the permeability of the microbial cell wall. As represented in **Figure** (14), CS NPs are also able to bind to bacterial DNA and inhibiting both transcription and translation processes<sup>46</sup>. Furthermore, CS NPs can reduce the activity of metalloprotein through their chelation power with bacterial cytoplasmic metals. Encapsulation of CS into nanoparticles increase the surface area per volume that results in intense positive charges on CS NPs surface as well as enhancing their solubility in physiological environment. It was previously reported that CS NPs have strong antibacterial activity against *S. aureus* and *E. coli* than CS polymer. It was found that the molecular weight of CS could affect the antibacterial activity of CS NPs, so, NPs containing CS with lower molecular weight have higher bactericidal activity against gram negative bacteria while those containing higher molecular weight showed higher bactericidal activity towards gram positive bacteria<sup>47</sup>.



**Figure 15:**Chitin and chitosan chemical structures<sup>47</sup>.

### 1.7.C. Silver nanoparticles

As represented in **Figure (14)**, silver nanoparticles (Ag NPs) can reduce biofilm resistance through different mechanisms. Like CS, when silver is dissolved in water, it carries positive charge that interacts with cell wall protein containing sulfur and phosphorus groups and thus creating holes in bacterial cell membrane that allows the flow of cellular contents out of the cell and causes death of bacteria<sup>48</sup>. Efficiency of Ag NPs against gram negative bacteria was found to be higher than gram positive bacteria because of thinner gram negative bacterial cell wall. However, it has also been argued that silver penetration power through gram negative bacterial membrane is low due to interaction between the positive charge of silver and the negative charge of lipopolysaccharide of the outer bacterial membrane<sup>49</sup>.

### 1.7.D. Copper nanoparticles.

The antibacterial activity of Copper nanoparticles such as copper oxide nanoparticles (CuO NPs) and copper nanoparticle-loaded polymer rely on two mechanisms. First, copper ion has an ability to bind with the carboxyl and amine groups that are located on the microbial cell surface such as *B. subtilis*. ROS formation is the second mechanism<sup>50</sup>. Higher concentration of copper ion induces the formation of ROS that inhibits DNA replication as well as protein synthesis as

represented in **Figure (14)**. It has been reported that copper nanoparticles have strong antibacterial effect against *E. coli*, *S. aureus*, and *Listeria monocytogenes* that showed a dose dependent activity<sup>50</sup>.

#### **1.7.E. Magnesium nanoparticles.**

Magnesium nanoparticles have bactericidal effect based on different mechanisms. Like copper nanoparticles, they induce formation of ROS resulting in lipid peroxidation and pore formation through bacterial cell membrane. Furthermore, they adsorb halogen molecules from bacterial cytoplasm on their surfaces as represented in Figure (14). It has been reported that magnesium nanoparticles could inhibit the growth and biofilm formation of *E. coli* and *S. aureus*<sup>51</sup>.

#### **1.8. EOs loaded in nanosystems**

Nanoencapsulation of EOs provides an efficient approach to enhance the stability, controlled release, reduced EOs volatility, improved patient compliance and minimized the interaction with external environment conditions (light, pH, oxygen and moisture). Furthermore, unique smaller size could enhance cellular penetration and uptake. Different polymeric and lipid based nanocarriers are structured with a characteristic biodegradability and biocompatibility as shown in **Figure (16)**<sup>24</sup>.

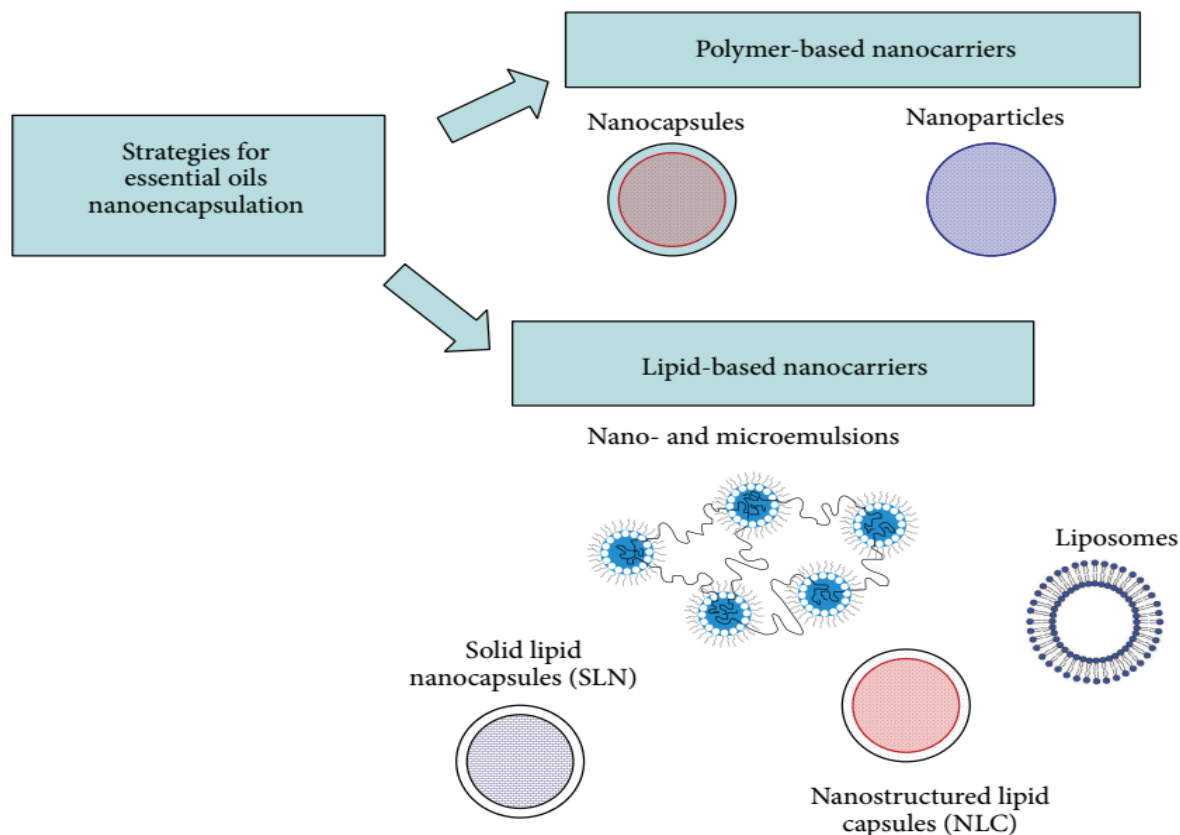


**Figure 16:** Nanosystem platforms for EOs<sup>24</sup>.

### 1.8.A. Polymer-Based Nanocarriers.

Polymeric nanocarriers are divided into nanocapsules and nanoparticles (nanospheres). Nanocapsules are composed of outer polymeric membrane encapsulating material in inner core or to be adsorbed on the outer surface while nanoparticles (nanosphere) composed of matrix system. EOs might be incorporated within the polymeric membrane or encapsulated in the core that are illustrated in Figure (17)<sup>52</sup>. Different EOs were loaded into polymeric nanocarriers as listed below in **Table (4)** with their average size, zeta potential loading capacity and biological activities. In case of encapsulation of EOs in chitosan nanoparticles, two-steps method (emulsification followed by ionic gelation) are used. **Table (5)** lists previous published studies

specifically for essential oils that encapsulated in chitosan with the surfactants used, organic solvent as well as their targeted biomedical application.

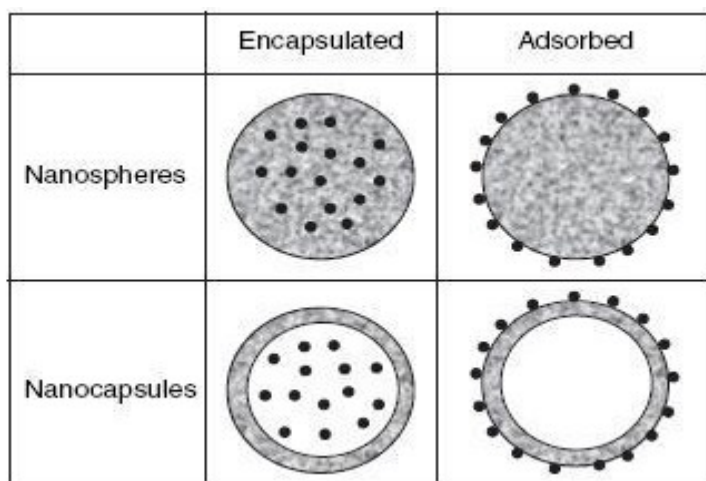


**Figure 17:** Schematic Representation of nanoparticle and nanocapsules with adsorbed or encapsulated EOs<sup>52</sup>.

**Table 4:** List of EOs loaded into polymeric nanocarriers.

EO	Polymer	Preparation method	Size (nm)	LC and EE%	Formula/benefits	References
Eugenol	Chitosan	Emulsification and ionic gelation	< 100	LC= 12%	- nanoparticles - thermally stable - higher antioxidant activity	[ <sup>53</sup> ]
Oregano	Chitosan	Emulsification and ionic gelation	40–80	LC = 3 – 8%	- nanoparticles - thermally stable - higher antioxidant activity - higher antimicrobial activity	[ <sup>54</sup> ]
Lippia sidoides	Alginate/ cashew	spray-drying	223–399	LC= 1.9 -4.4	- nanoparticles - fungicide	[ <sup>55</sup> ]

	gum				- bactericide activities	
Jasmine	gelatin/ arabic gum	complex coacervation	600	----- -	- nanocapsules - heat-resistant flavour	[ <sup>56</sup> ]
Thymol	Zein	liquid–liquid dispersion method	200	EE= 80	- nanoparticles - suppress Gram- +ve bacterium	[ <sup>57</sup> ]
Eugenol	PLGA	Emulsion evaporation method	173 - 225	EE = 98	- nanoparticles - inhibiting growth of Salmonella	[ <sup>58</sup> ]
Carvacrol	PLGA	solvent displacement process	209.8	LC = 21	- nanocapsules - antimicrobial activity	[ <sup>59</sup> ]
Thymol	Methyl cellulose ethyl cellulose	displacing the ethanol solvent with water	420	EE= 43.53%	- nanocapsules - reduce E. coli	[ <sup>60</sup> ]

LC = loading capacity      EE = encapsulation efficiency      PLGA = polylactic glycolic acid

**Table 5:**List of EOs loaded into CS NPs, and their biomedical application using two steps encapsulation method.

<b>Essential oil</b>	<b>Surfactant</b>	<b>Organic solvent</b>	<b>Application</b>	<b>Reference</b>
<b>Carum copticum</b>	Tween 80	Dichloromethane	Antioxidant	[ <sup>61</sup> ]
<b>Carvacrol</b>	Tween 60	Ethanol	Model system	[ <sup>62</sup> ]
<b>Eugenol</b>	Tween 60	Ethanol	Antioxidant	[ <sup>63</sup> ]
<b>Oregano</b>	Tween 80	Dichloromethane	Antifungal	[ <sup>64</sup> ]
<b>Satureja hortensis</b>	Tween 80	Ethanol	Antioxidant	[ <sup>65</sup> ]
<b>Zataria multiflora</b>	without surfactant	Ethanol	Antifungal	[ <sup>64</sup> ]

### 1.8.B. Lipid-Based Nanocarriers.

Lipid-based nanocarriers are classified into: nanoemulsion, liposomes, solid lipid nanoparticles (SLN), and nanostructured lipid carriers (NLC). Liposomes are bilayer vesicle composed of association of phospholipids (amphiphilic nature) that can carry both hydrophobic (EOs) and hydrophilic drugs. SLN and NLC are solid particles with lipid core for encapsulation of EOs. They have a capacity of dissolution in aqueous media and maintain or enhance EOs biological activity.

#### 1.8.B.1 Nanoemulsions

Nanoemulsions are stable homogenous system that composed of two immiscible liquids with a droplet size less than 500nm as shown in **Figure** (18). They are prepared with lower surfactant concentration, in contrast to microemulsion (droplet size more than 500 nm), therefore, irritation that comes from surfactant is not likely to happen. Nanoemulsions have a higher kinetic stability owing to their smaller size and steric effect. The antimicrobial feature of EOs nanoemulsion is due their higher surface tension that enhance penetration power of EOs through bacterial cell membranes. Different EOs were loaded into nanoemulsion that are listed below in **Table** (6) with their average size, composition and biological activities<sup>24</sup>.

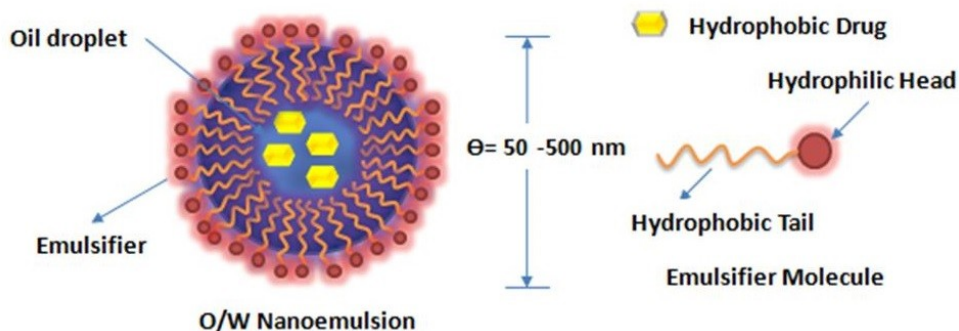


**Figure 18:** Illustrative diagram of nanoemulsion<sup>24</sup>.

### 1.8.B.2. Solid Lipid Nanoparticles.

Solid lipid nanoparticles (SLN) are nanoparticles with a diameter ranging from 50 nm to 1  $\mu\text{m}$  and composed of different lipids such as triglycerides and waxes. EOs are immobilized in the core or in the outside part of SLN which provide a protection from external environment and provide a sustained release for EOs as shown in Figure (19)<sup>24</sup>. Different EOs were loaded into SLN that are listed below in **Table (6)**, with their average size, composition and biological activities.

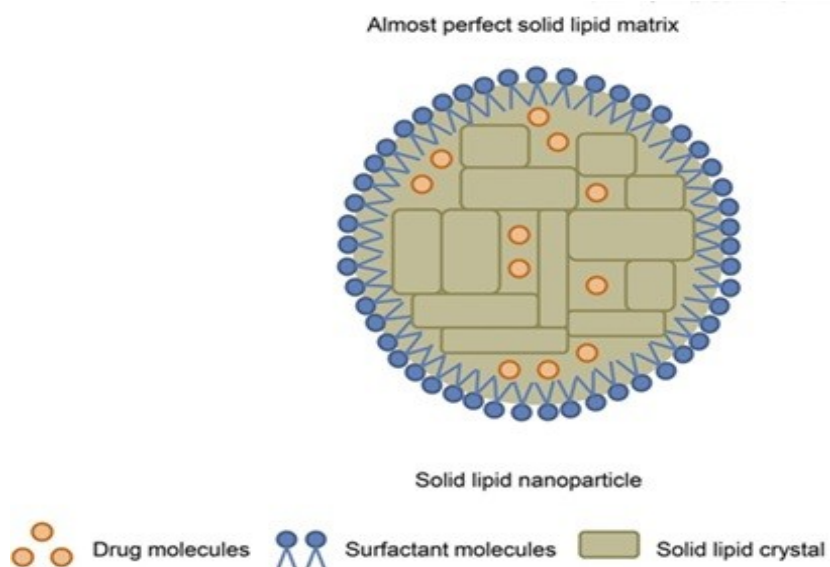


**Figure 19:** Illustrative diagram of SLN<sup>65</sup>.

### 1.8.B.3. Liposomes

Liposomes are type of colloidal delivery systems for both hydrophilic and lipophilic (EOs) drugs. They consist of phospholipids that are assembled in one or more layered vesicular form. They may be unilamellar vesicles (ULV) of one bilayer with diameter ranging from 25 nm (small ULV) to more than 100 nm (large ULV). Multilamellar vesicular vesicles (MLV) are other type of liposomes that composed of multilayers with a diameter exceeding 1  $\mu\text{m}$  that are represented in Figure (20). They provide a protection against environmental degradation of EOs

and enhance the aqueous solubility as well<sup>24</sup>. Different EOs were loaded into liposomes that are listed in **Table (6)**, with their average size, composition and biological activities.

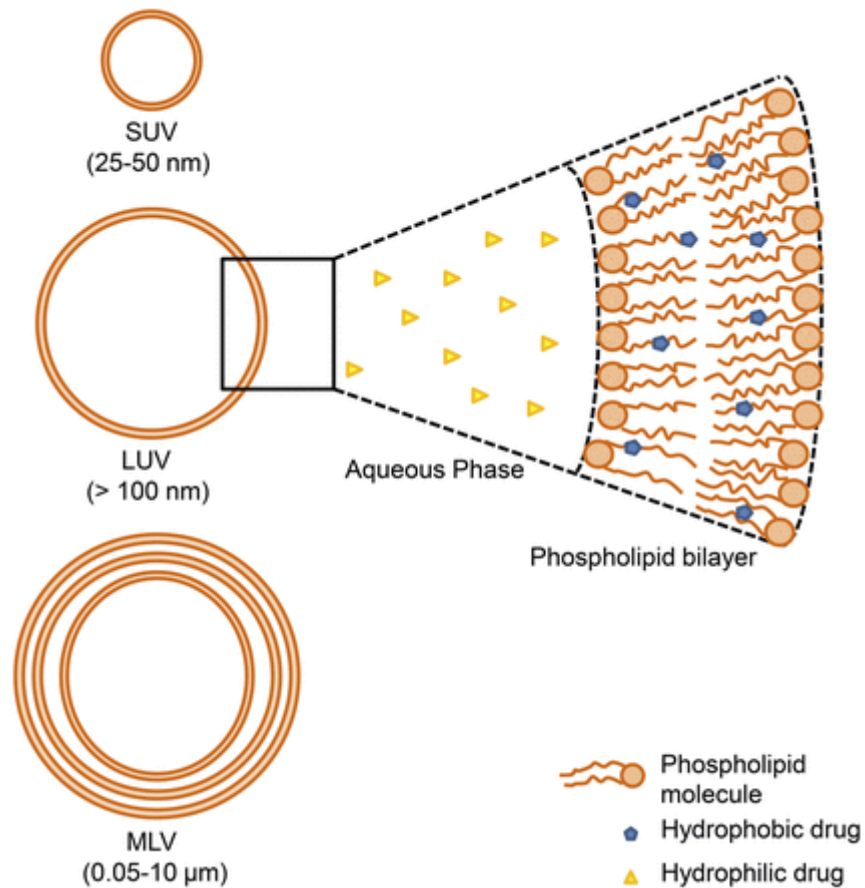


**Figure 20:** Illustrative diagram of liposome<sup>65</sup>.

**Table 6:**List of EOs loaded into lipid-based nanocarriers

EO	Nano Carriers	Composition	Size (nm)	LC & EE%	Properties and activities	References
Melaleuca alternifolia	Nano-emulsion	lecithin, Tween 20 and glycerol monooleate	74-365	----- -----	enhance antimicrobial activity	[ <sup>66</sup> ]
Zedoary turmeric	Nano-emulsion	ethyl oleate, Tween 80 Transcutol P	68.3	LC = 30%	enhancement of both AUC and Cmax of turmeric oil	[ <sup>67</sup> ]
Artemisia arborescens	SLN	compritol 888 ATO and Poloxamer 188	223	EE = 87%	antiviral activity (HSV-1)	[ <sup>68</sup> ]
Nigella sativa	SLN	Palm oil Sofisan 154, sorbitol, and water	-----	----- --	-antimicrobial activities -antioxidant activities	[ <sup>69</sup> ]
Zataria multiflora	SLN	SDS, PEG and cetyl alcohol	650	EE= 38.66 %	-antimicrobial activities	[ <sup>70</sup> ]
Santolina insularis	Liposome	hydrogenated soya PC and cholesterol	-----	----- -	-antiviral activity (HSV-1)	[ <sup>71</sup> ]
Artemisia arborescens	Liposome (MLV)	hydrogenated (P90H) and soy PC	252-408	EE = 60-74%	-antiviral activity (HSV-1)	[ <sup>72</sup> ]
Atractylode macrocephala	Liposome	PC and cholesterol	173	LC = 5.18% EE = 82.18 %	- enhanced EE -increase dissolutin rate	[ <sup>73</sup> ]
Origanum dictamnus	Liposome (MLV)	PC and cholesterol	----- -	LC = 4.16%	Antioxidant activites and antimicrobial activites	[ <sup>74</sup> ]

PEG = polyethylene glycol    SDS = sodium dodecyl sulfata    PC = phosphatidyl choline

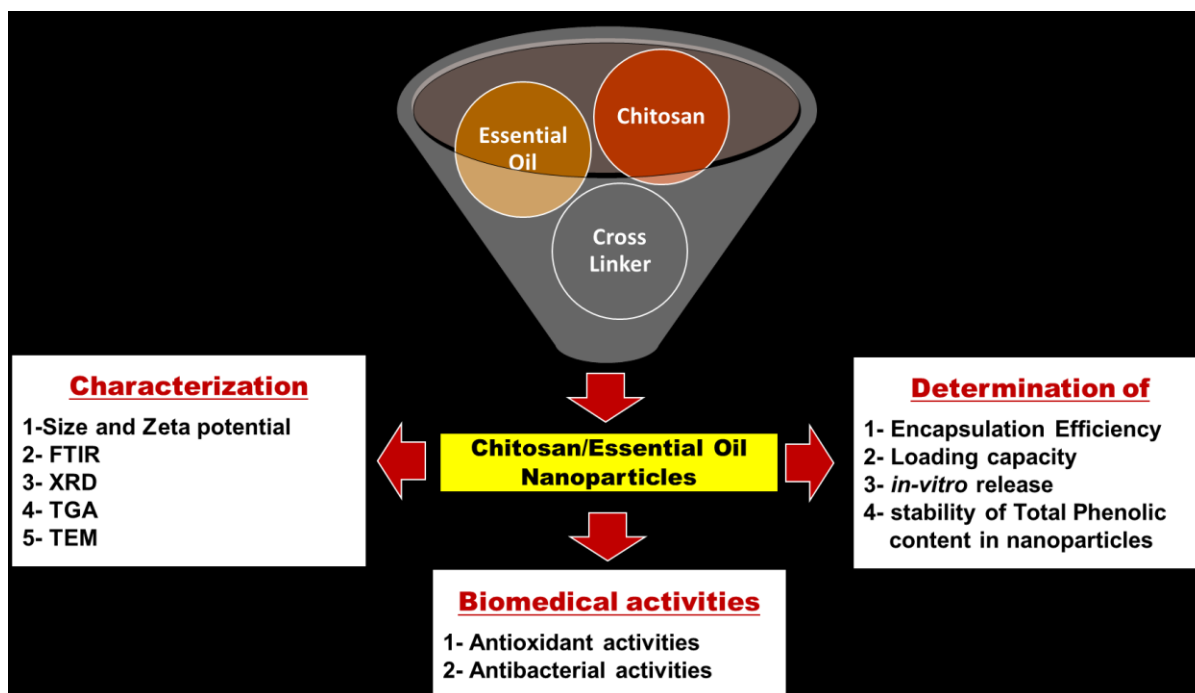
# **Thesis Scope and Objectives**

### **Thesis Scope and Objectives**

The scope of the study as shown in **Scheme** (1) was to encapsulate natural EOs such as “GTO” and “PO” in natural biodegradable polymeric nanocarrier as CS. The aim of the encapsulation is to enhance the thermal stability of the EOs, protect their phenolic contents, reach sustained release profile, improve their antioxidant activity and to improve their antibacterial activities.

The novelty in this work relies on converting these EOs specifically into nanoform that are not found in previous published literature. The selection of PO and GTO was mainly based on the clear difference and variation in their chemical composition, phenolic contents, phytochemical components and their well-established biomedical activities.

The preparation of encapsulated EOs NPs was followed by examination of these NPs via different characterization techniques. Furthermore, Different studies were used to estimate the EE%, LC% of the EOs, thermal stability, *in-vitro* release at different pH media, and finally the ability of CS NPs to preserve the phenolic contents. After optimization of the NP formulas, they had been investigated on their antioxidant activity and antibacterial activities against both Gram-positive and Gram-negative bacteria.



Scheme 1: Study scope diagram.

# **Chapter 2**

## **Materials & Methods**

## **Chapter 2: Materials & Methods**

### **2.1. Materials:**

Sodium tripolyphosphate (TPP), Tween 80, (2,2-DiPhenyl-1-Picryl Hydrazyl) (DPPH) and Dichloromethane were purchased from Sigma Aldrich Co. (USA). Chitosan of medium molecular weight (84,8 % degree of dealkylation) was purchased from (Primex ehf, Chitoclear, Iceland). Green tea as well as peppermint essential oils were obtained from Nefertari Natural Body Care Line (Cairo, Egypt). Folin–Ciocalteu reagents and Gallic acid were supplied by Merck Chemicals Co. (Germany). Glacial acetic acid and sodium carbonate were obtained from Adwek Co. (Egypt). All materials were consumed as received without further treatment.

### **2.2. Compositional analysis of PO and GTO**

The Gas Chromatography (GC) coupled to Tandem Mass Spectrometry (GC/MS/MS) technique was used to assure the identity and to identify the components of both PO and GTO<sup>75</sup>. The analysis was carried out using a GC (Agilent Technologies 7890A) with capillary column (30 m × 0.25 mm i. d. and 0.25 µm film thickness to separate the component of EOs that were carried by helium gas (linear velocity of 1mL/min) to mass-selective detector (MSD, Agilent 7000)) where they are identified. The identification of components relying on the comparison of the chemical components mass spectra and retention time with standard compounds and by computer matching with NIST (National Institute of Standards and Technology) library<sup>75</sup>.

### **2.3. Preparation of EOs loaded CS NPs**

Preparation of EOs loaded CS NPs was performed at two steps based on the method described by (Hosseini et al., 2013)<sup>54</sup> and (Woranuch et at.,2013)<sup>53</sup> with slight modifications. The process of EO encapsulation in CS NPs relied on two steps (as shown in **Figure** (21)); Step 1: a process

involves oil in water (O/W) emulsification in which an aqueous phase, composed of CS and Tween 80 dissolved in acidic solution, was emulsified with an organic phase containing EO through rotor stator homogenizer with adjustable speed (rpm) and duration (min). As a result, O/W nanoemulsion was formed. Step 2 is a process known as ionic gelation that is commonly used in order to formulate composite nanoparticles, and involves a negatively-charged cross-linker such as sodium tripolyphosphate (TPP) was added to the nanoemulsion obtained in step 1 to interconnect the positively charged CS polymer chains as represented in **Figure (22A)**<sup>56,61,76</sup>.

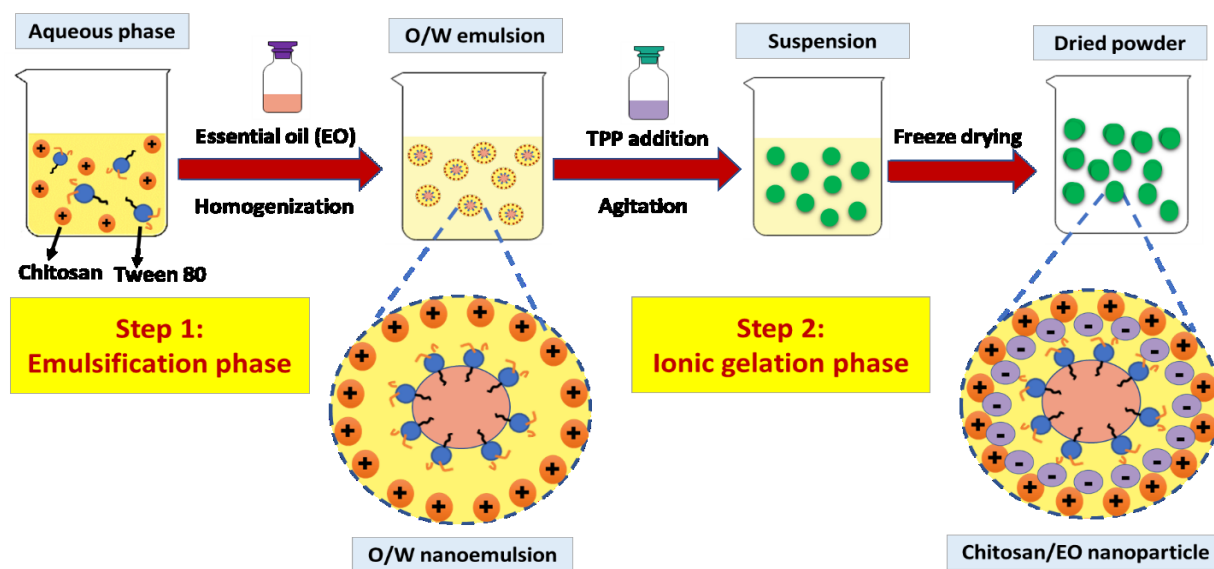


**Figure 21:** Schematic illustrations of EO encapsulation two-step process.

There were mainly two factors that thoroughly examined and were found to greatly affect the size of the formulated NPs, their polydispersity index (PDI) and zeta potential (ZP) during the preparation of CS/PO NPs and CS/GTO NPs; (i) the homogenization parameters (speed and time) and (ii) the concentrations of the components (such as TPP, and CS/EO ratio) as represented in **Figure (22B)**. The CS concentration and tween 80/CS ratio were kept constant during all experiments.

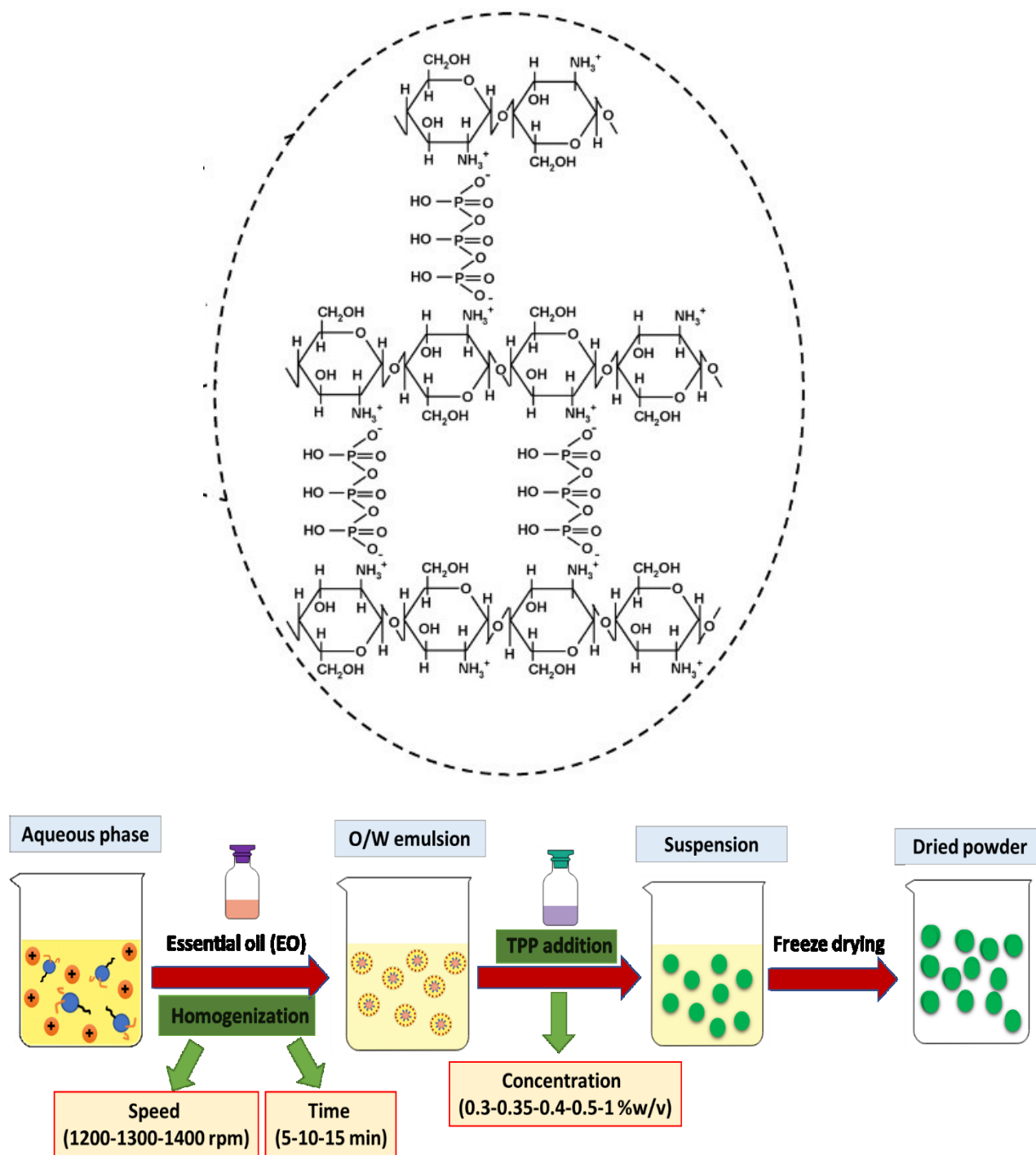


**Figure 22:** (A) chemical structure of chitosan ionic crosslinked with TPP<sup>76</sup>, (B) Parameters that affect the size, PDI and ZP of formulated NPs.

### **2.3.A. Oil in water (O/W) emulsion preparation**

In the preparation of O/W emulsion, the aqueous phase was prepared by dissolution of CS powder in 1% (v/v) glacial acetic acid to get a solution of 1% CS solution after overnight shaking. To 50 mL CS solution, tween 80 (CS: Tween 80 was 1:1.12 w/w) with HLB (hydrophilic lipophilic balance) of 15.9 was added and stirred for two hours at 45 °C to form an aqueous phase of the emulsion. On the other hand, the oily phase was prepared by dissolving PO (0.12, 0.24, 0.36 and 0.48 g) in 5mL dichloromethane to get concentrations of (CS: PO) of 1:0.25, 1:0.5, 1:0.75 and 1:1.00 w/w). Then, the oily phase was added drop-wise into the aqueous phase during homogenization at 14000 rpm for 10 min under an ice bath condition to get an O/W emulsion. GTO was treated as PO. It should be pointed out that the homogenization speed and duration are chosen based on the preliminary studies that are illustrated in chapter 3 of the result and discussion.

### **2.3.B. Ionic gelation process and separation of the prepared NPs**

In order to finally form the NPs, 50 mL of 0.4% (w/v) aqueous TPP solution was gradually added to 50 mL emulsion under 400 rpm stirring via magnetic stirrer (Phoenix, RSM-01SH, Germany) for 40 min at a room temperature to allow the cross-linking of CS polymer and to facilitate the formation of NPs. The formed NPs were collected by 10000 rpm centrifugation for 30 min at 4°C, and followed by washing several times by deionized water. The formed wet pellets were dispersed in distilled water to get a homogeneous suspension via probe sonicator (Qsonica 500, Qsonica, LLC, USA), for 4 min. with a sequence of 2 seconds sonication and 1 second rest in an ice bath. Finally, trehalose dihydrate which acts as a cryoprotectant was mixed via magnetic stirrer (Phoenix, RSM-01SH, Germany) with the nano-suspensions (NPs: Trehalose ratio of 1:1) and subsequently freeze dried at -65°C for 72 hrs. It should be pointed out that the

TPP concentration is chosen based on the preliminary studies that are illustrated in chapter 3 of the result and discussion. CS NPs were stored at the refrigerator until further analysis. CS: EOs weight ratios that were used for the present study are listed in **Table (8)**.

**Table 7:** List of CS NPs samples with their CS:EOs weight ratios.

sample No	Weight ratios (w/w)
1	CS NP (1:0)
2	CS/GTO (1:0.25)
3	CS/GTO (1:0.50)
4	CS/ GTO (1:0.75)
5	CS/GTO (1:1.00)
6	CS/PO (1:0.25)
7	CS/PO (1:0.50)
8	CS/PO (1:0.75)
9	CS/PO (1:1.00)

## 2.4. Characterization of the prepared NPs

### 2.4.A. Particle size and zeta potential of the prepared NPs

To study the nanoparticle hydrodynamic size and zeta potential Malvern nano-series Zetasizer (UK), with a helium-neon laser operating at 90° scattering angle with a power of mW and wavelength of 633 nm at 25 °C, was used. Freshly prepared nano-suspension were diluted with distilled water to a concentration of (1 mg/mL), according to Zetasizer manual specification, before measurement. Triplicate samples were analyzed and mean value was reported.

#### **2.4.B. Morphology of the prepared NPs**

To study the morphology of the prepared NPs, Hitachi H-7650 (Japan) transmission electron microscopy (TEM) analysis was carried out using a voltage of 200 kV. Before lyophilization process, 1mL of nano-suspension in the concentration (1mg/mL) was diluted with 50 mL deionized water and spread onto a copper grid and left to dry at a room temperature before TEM analysis.

#### **2.4.C. Fourier transform InfraRed (FTIR) Spectroscopy analysis**

Fourier transform InfraRed (FTIR) Spectroscopy (Thermo Scientific Nicolet 8700, USA) was used to study the chemical characteristics of the NPs. Pure EOs, CS NPs, CS/PO NPs and CS/GTO NPs were analyzed via 16 scans at a resolution of 4  $\text{cm}^{-1}$  at a range of 400–4000  $\text{cm}^{-1}$ . Lyophilized NPs were triturated with potassium bromide and compressed in form of pellets.

#### **2.4.D. Thermogravimetric analysis (TGA) analysis**

To estimate the thermal stability of nanoparticles and EOs, Q50 TGA Thermogravimetric Analyzer (TGA) was performed. Each 4-10 mg of lyophilized powder were placed in the platinum pan and heated up by TGA furnace with heating rate of 10  $^{\circ}\text{C}/\text{min}$  under nitrogen atmosphere and from 25 to 600  $^{\circ}\text{C}$ .

#### **2.4.E. Powder X-ray diffraction (XRD) analysis**

To study the material packing characteristics and crystallinity, X-ray diffraction (XRD) via a (Bruker AXS D8, Germany) diffractometer was used in operation conditions of 40 mA current, a power of 40 kV and radiation with  $\text{Cu K}\alpha$  ( $\lambda = 1.5 \text{ \AA}$ ). Lyophilized samples were scanned over a  $2\theta$  range of  $5^{\circ}$  to  $50^{\circ}$  at a speed of  $0.03^{\circ}$  per second.

## 2.5. Determination of encapsulation efficiency (EE%) and loading capacity (LC%)

EO amount that was encapsulated in CS NPs was determined by UV–Vis spectrophotometry<sup>54,62</sup>. Each of 30 mg of GTO loaded CS NPs and 80 mg of PO loaded CS NPs were dropped into 10 mL dehydrated ethanol and centrifuged at 12000 rpm for 20 min at 25 °C as reported by (Deka et al., 2016)<sup>77</sup>. The EO content in the supernatant was analyzed using UV–Vis spectrophotometry at a wavelength of 274nm and 227nm for GTO and PO, respectively. The amount of GTO and PO was calculated by suitable calibration curve of pure GTO as well as PO in ethanol with R<sup>2</sup> of 0.996 and 0.999, respectively. CS NPs was used as a blank, however it was treated likewise as CS/PO NPs and CS/GTO NPs. Triplicate samples for each batch were recorded.

The loading capacity (LC) along with encapsulation efficiency (EE) were estimated from Equations (3) and (4) respectively<sup>54</sup>:

$$LC (\%) = \frac{\text{Total amount of loaded EO}}{\text{weight of nanoparticles after freeze drying}} \times 100 \quad (3)$$

$$EE (\%) = \frac{\text{Total amount of loaded EO}}{\text{intial amount of EO}} \times 100 \quad (4)$$

## 2.6. *In-vitro* release studies

40 mg of dried NPs (samples 5 and 9 that are in **Table** (8)) were placed in a dialysis bag (12000-14000 KDa), containing 2 mL of release media (40% ethanol and 60% phosphate buffer saline with a pH of 7.4) or (40% ethanol and 60% acetate buffer with a pH of 3), and incubated in 13 mL of the same release media at room temperature under gentle shaking. The reason behind choosing acetate buffer and phosphate buffer saline, is to mimic the stomach and blood pH in the human body and to understand the release behavior if these formulas were taken via oral or parenteral routs. Specific volume of release media at specific sampling time intervals was taken

for analysis, with addition of an equal volume of fresh release media. Total cumulative amount of GTO and PO (g) in volume of the release medium (mL) that were encapsulated in NPs, was estimated through UV–vis spectrophotometer at 274 nm and 227 nm for GTO and PO respectively<sup>54,56,61,63</sup>. The percentage of cumulative EO released represented by the ratio of the cumulative amount of EO released at each time interval (Mt) to the initial amount of the EO encapsulated in the NPs (M0) are illustrated in equation (5)<sup>54</sup>.

$$\text{Cumulative release percentage} = \sum_{t=0}^t \frac{M_t}{M_0} \times 100 \quad (5)$$

## 2.7. Estimation of Total phenolic contents (TPC)

Folin–Ciocalteu method was used to estimate the contents of total phenolic contents of pure EOs as well as in their encapsulations<sup>61</sup>. Pre-determined amount of CS NPs, PO, GTO, CS/PO NPs and CS/GTO NPs were mixed with dehydrated ethanol to get a final concentration (3% w/v) and (8% w/v) for GTO and PO, respectively. On 0.5 mL of each sample, 2.5 mL of (10% v/v) aqueous Folin–Ciocalteu reagent and left for 4 min. Then, 2 mL aqueous solution of 7.5% (w/v) sodium carbonate was dropped to the mixture and left in the dark for 6 hrs at room temperature. Finally, all the samples were centrifuged for 3 min at a speed of 10000 rpm and the supernatant was sucked out for measuring the absorbance at 765 nm using a spectrophotometer. To estimate the TPC, different concentrations of gallic acid (0.01 – 0.1 mg. mL<sup>-1</sup>) in ethanol were treated like the samples, and a standard calibration curve was built (R<sup>2</sup>= 0.99) and EOs TPC was expressed in mg gallic acid that is equivalent to 1 gram of each EO as represented in equation (6)<sup>61</sup>.

$$\text{mg GAE/ g oil} = \frac{1000 \times A}{B} \quad (6)$$

where, (A) is the amount of gallic acid that gives the same absorbance as the sample (calculated from the calibration curve), and (B) the amount of sample that was used.

## 2.8. Investigation of the antioxidant activities of NPs

The antioxidant activity of EOs loaded CS NPs was examined using DPPH free radical scavenging assay as illustrated by (Chen et al., 2009)<sup>78</sup> with slight modification. First, predetermined amounts of pure PO, pure GTO, CS/PO NPs and CS/GTO NPs (samples 5 and 9 that are in **Table (8)**) were dispersed in 2 mL of (ethanolic DPPH solution (0.05 mM) and left for 2 hours in the dark at ambient temperature. The samples containing encapsulated EO were centrifuged for 3 min to take the supernatant for analysis. Spectrophotometer at 517 nm was used to measure the absorbance of samples considering dehydrated ethanol as a blank. The percent inhibition of DPPH was calculated using equation (7)<sup>61</sup>:

$$\text{DPPH inhibition (\%)} = \frac{A_{\text{control}} - A_{\text{sample}}}{A_{\text{control}}} \times 100 \quad (7)$$

where  $A_{\text{control}}$  is the DPPH absorbance and  $A_{\text{sample}}$  is the sample absorbance.

## 2.9. Investigation of the antibacterial activities of the NPs

Agar dilution and colony counting methods were used to investigate the impact of encapsulation of PO and GTO on the antibacterial activity against both *Staphylococcus aureus* (*S. aureus*) and *Escherichia coli* (*E.coli*) as examples for Gram positive and Gram negative bacteria, respectively (Wei et al., 2009)<sup>79</sup>. *E. coli* and *S. aureus* were cultivated in Luria broth (LB) medium (10 g peptone, 5 g yeast extract, and 10 g sodium chloride per liter) aerobically for 24 hours at 37 °C. Tubes turbidity was noted visually before and after incubation. All EOs and NPs were previously kept under UV light for 2 hours for sterilization. After overnight growth, 2.5 mL of the bacterial culture were taken in falcon tubes containing 5 mg of CS NPs, CS/PO NPs,

CS/GTO NPs, and the corresponding amounts of pure PO (1.11 mg) and pure GTO (1.15 mg) for an overnight incubation at 37 °C on shaking platform at 250 rpm. Serial dilutions were prepared from the falcon tubes by addition of sterile LB agar and the 7<sup>th</sup> fold dilutions were spread on nutrient agar and cultured at 37 °C for 24 hrs then the colonies were quantified. Additionally, a positive control was prepared (LB broth with incubated bacteria) to check the growth of incubated bacteria, and a negative control shows the sterility of the LB agar medium, and a negative control was prepared (only LB broth) to check for sterility of the media used in the experiment. The antibacterial activity was estimated through the reduction in numbers of the bacterial colonies after introducing the sample compared to the positive control. Percent inhibition of bacterial growth was calculated using equation (8)<sup>79</sup>:

$$\text{Inhibition of bacterial growth (\%)} = \frac{C - A}{C} \times 100 \quad (8)$$

C and A are the bacterial colonies of positive control and treated plated respectively.

## **2.10. Theoretical background**

### **2.10.A. Rotor-Stator homogenizer**

Rotor-stator homogenizer is a type of cutting blade mixers that belongs to mechanical homogenizers<sup>80</sup>. The homogenization action relies on the movement of a rotor at a very high rpm that creates extremely powerful shear force occurring within the narrow gap between the rotor and the stator. In other word, the close proximity of the inner revolving rotor and outer fixed stator creates a circumferential force that expels material between the spaces of the rotor-stator generating cavitation and extreme turbulence and converting a bulk sized material into nano-sized material in a very short period of time as illustrated in **Figure (23)**. The main application of a rotor-stator generator type homogenizer is to make dispersions and emulsions in

a nano-sized form<sup>81</sup>. To optimize the rotor stator homogenizer, many variables should be controlled such as; design and size of the rotor-stator probe, tip speed, duration of homogenization, vessel shape and positioning of rotor-stator as well. On the other hand, sample condition affecting the homogenization efficiency for example are; the sample initial size, medium viscosity, sample volume and concentration<sup>81</sup>.

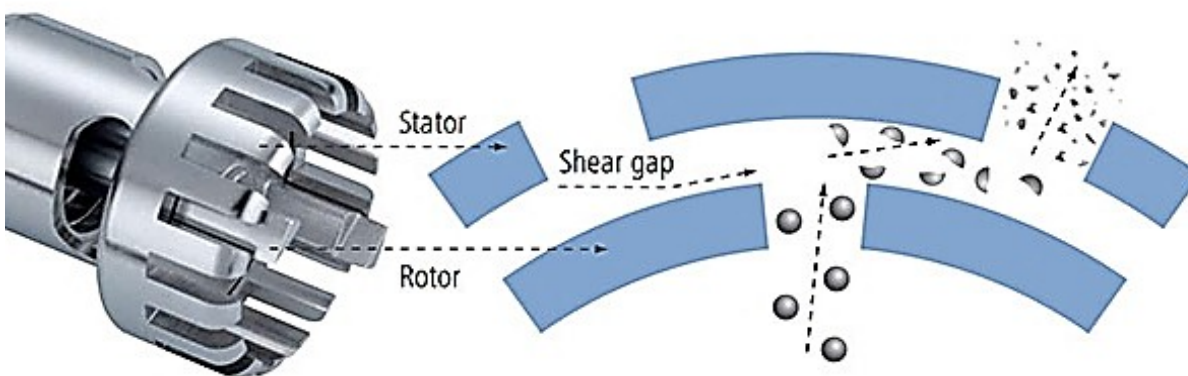


**Figure 23:** Rotor-stator type homogenizer<sup>80</sup>.

### **2.10.B. Probe sonicator**

Probe sonication or ultrasonicator as represented in **Figure (24a)**, is a device exerts its action by generating powerful ultrasonic waves in a liquid medium causing cavitation phenomenon. According to cavitation, ultrasonic waves have a pressure that causes liquid streaming that results in an immediate development of micro-sized bubbles which grow and merge until they reach their critical size. Subsequently, large sized bubbles vibrate aggressively, and finally collapse generating a shock wave with an enough power to disrupt covalent bonds in a dispersed material triggering deagglomeration as shown in **Figure (24b)**. To optimize the efficiency of probe sonicator, many variables should be controlled such as tip amplitude and intensity, temperature, material concentration, vessel capacity and shape<sup>81</sup>. Regarding of specifications of probe sonicator, piezoelectric horn produces vibrations of 15- 25 kHz with a power vary from 10

to 375 Watts. It should be pointed out that the probe sonicator is considered a direct sonication technique where the probe is immersed directly into the suspension which is more powerful than the indirect sonication technique that relies on immersing the container in the liquid that is propagated by ultrasound waves.<sup>81</sup>

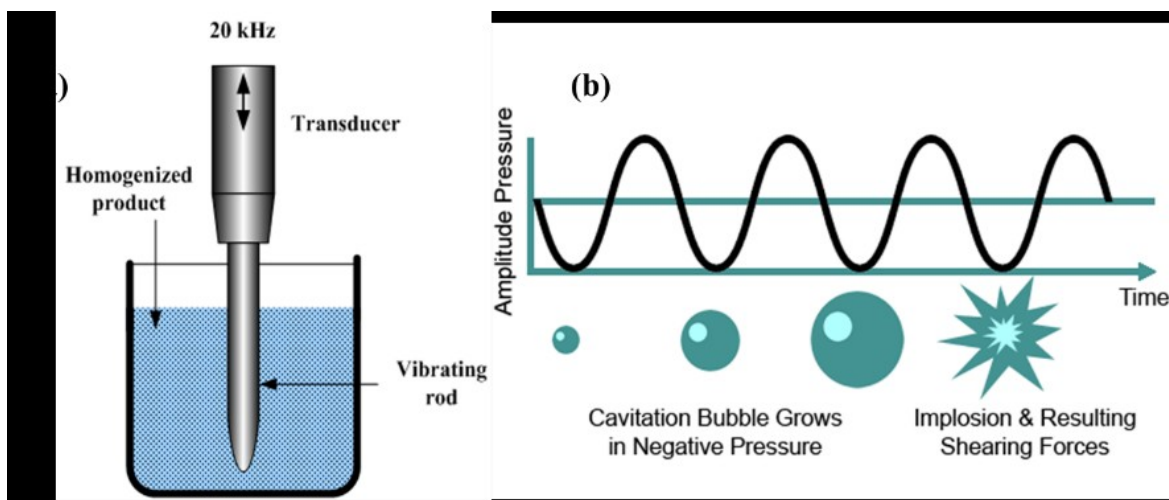


**Figure 24:** A typical probe sonicator (a), The phenomena of cavitation (b)<sup>81</sup>.

### 2.10.C. Lypholizer (freeze dryer)

Freeze-drying or lypholization is an extensively used process for drying of colloidal carriers including liposomes, nanoemulsions and nanoparticles in order to enhance the stability of these carriers. A typical lypholizer is composed of a drying chamber including temperature-controlled shelves that are connected to a condenser chamber and vacuum pumps **Figure** (25a). Lyophilized product is characterized by intact characteristics of the product such as; nanoparticle size distribution, intact activity of encapsulated drug and long-term shelf life. Lypholization cycle is divided into three stages: (i) solidification, (ii) ice sublimation and (iii) desorption of unfrozen water that are represented in **Figure** (25b).

First, in solidification phase pure water in colloidal suspension is converted into ice crystal resulting in an increase in the suspension concentration and viscosity that inhibits further

crystallization. Second, applying vacuum which leads to depression of the boiling point that in turn induces ice sublimation stage. At the end of the second stage, porous pellet is formed due to sublimation of ice crystals. Finally, desorption of unfrozen water stage is characterized by removal of water that did not come out during the first and second stages. However, lyophilization may generate freezing and dehydration stresses as well as phase separation during freezing that could destabilize and induce irreversible fusion of nanoparticles in colloidal suspension. Therefore, cryoprotectant (excipient that protect nanoparticles during freezing phase through immobilization of nanoparticles within a glassy matrix) including; trehalose, sucrose, glucose and mannitol should be incorporated.

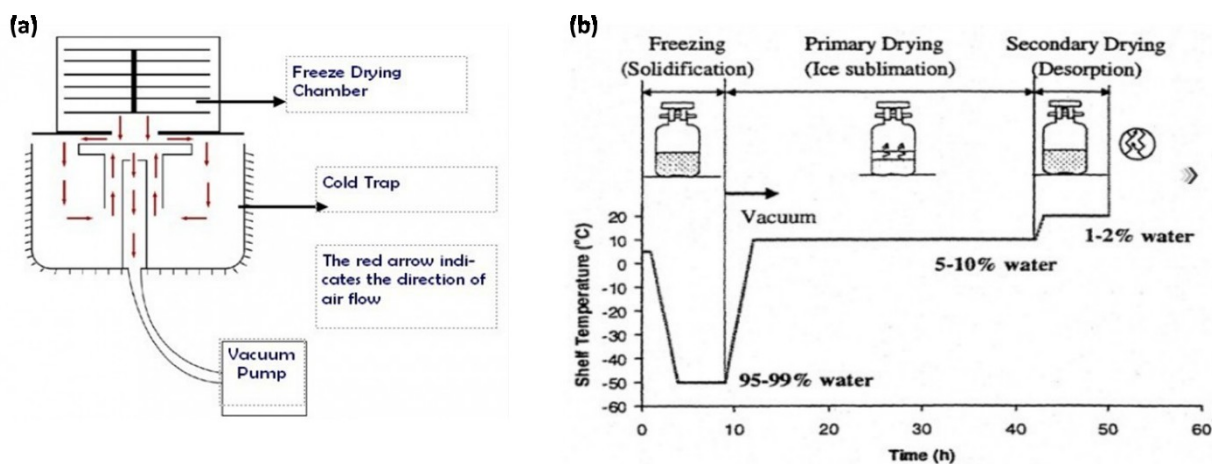


**Figure 25:** A typical benchtop freeze dryer (a), the lyophilization cycle (b) <sup>82</sup>.

#### 2.10.D. Dynamic light scattering (DLS, Zetasizer)

Dynamic Light Scattering (DLS) is a system that shines suspended particles with a laser beam and investigating the intensity fluctuations in the scattered light. The DLS system consists of six components as shown in **Figure (26a)**; (i) a laser light source for sample illumination, (ii) the sample that is placed in plastic cuvette, (iii) two avalanche photodiode detectors (positioned at certain angles) for detecting the scattered light that comes out from the sample, (iv) an attenuator

to reduce intensity of scattering if it is outside detector range, (v) a collector and finally (vi) display software.

DLS system measures particle size depending on the measurement of Brownian motion (random collision) between nanoparticles and solvent molecules that is based on Stokes-Einstein equation (9)<sup>83</sup>.

$$d(H) = \frac{k T}{3\pi\eta D} \quad (9)$$

According to Stokes-Einstein equation,  $d(H)$  is the hydrodynamic radius,  $k$  is Boltzmann's constant,  $T$  is the absolute temperature,  $\eta$  is the medium viscosity and  $D$  is the velocity of Brownian Motion. Therefore, through measuring Brownian motion velocity, hydrodynamic size can be measured<sup>83</sup>. It should be noted that, the hydrodynamic size is related to a thin, electric dipole layer of liquid medium that adheres to the surface of nanoparticle, influencing the Brownian motion of the nanoparticle. Smaller particles size exhibits much easier random collision with solvent molecules than larger particles. Velocity of Brownian motion is measured by detecting the rate of scattered light fluctuation. Therefore, the smaller particle size, the more rapid fluctuation in scatter light occurs as represented in **Figure (26b)**. DLS could be quite advantageous if compared to other techniques, as it is a non-invasive technique that requires minimal sample preparation and no calibration is required for it. In addition, DLS instruments are quite much more compact and affordable and they offer user friendly interfaces that allows users to perform comprehensive data analysis<sup>84</sup>

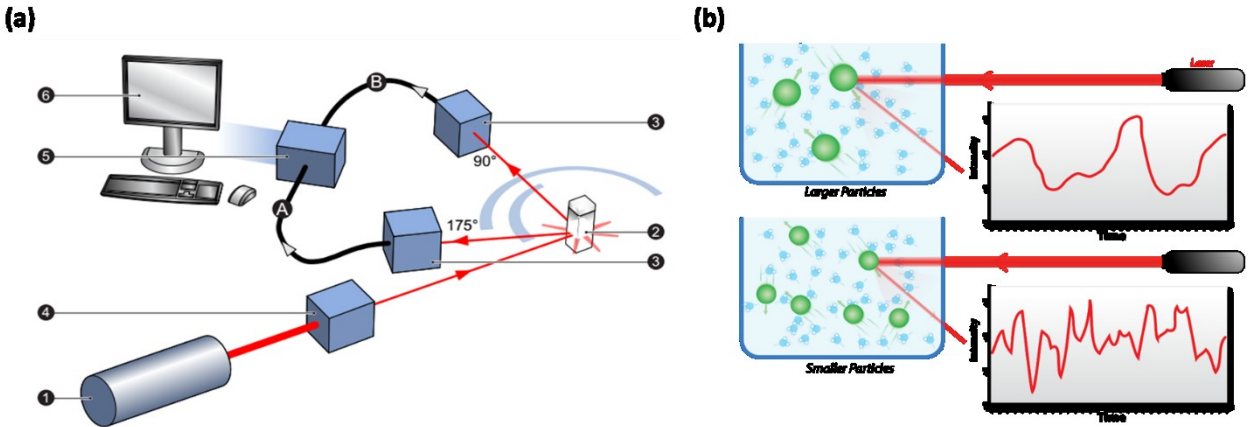


**Figure 26:** A typical Dynamic light scattering system (a) , DLS principle (b) <sup>83</sup>.

### 2.12.E. Transmission electron microscopy (TEM)

Transmission electron microscopy (TEM) is a microscopy technique that depends on the interaction of a sample deposited on the surface of copper grid with a beam of electrons that is transmitted through it. A typical TEM, it composed of; (i) high voltage (100-400 kV), (ii) Electron source of 0.1-1 $\mu$ A (electron gun), (iii) condenser system of lenses and apertures that controls the illumination on specimen, (iv) objective lens for imaging, (v) projector lens that magnifies

image as represented in **Figure (27)**<sup>85</sup>. The image that results from high-energy (>100 kV) electron interaction with the sample is magnified and focused onto a fluorescent screen. In the TEM image, the regions where electrons do not pass through the sample results in a dark image. Image resolution of the microscope relies on the wavelength of radiation according to Abbe's equation (10)<sup>85</sup>:

$$d = \frac{0.61 \lambda}{n \sin \alpha} \quad (10)$$

Where,  $(d)$  is the image resolution,  $(\lambda)$  wavelength of imaging radiation,  $(n)$  refraction index of medium between source and lens and  $(\alpha)$  is the half angle of the cone of light from specimen plane. Image resolution  $(d)$  is the shortest distance between two points that can be distinguished by the camera system. Based on Abbe's equation 7, TEM images are characterized with a significantly higher resolution (0.2 nm) due to small electron wavelength (de Broglie wavelength). TEM image contrast is due to the thickness and composition of the material as well as absorption of electrons in the material<sup>85</sup>.

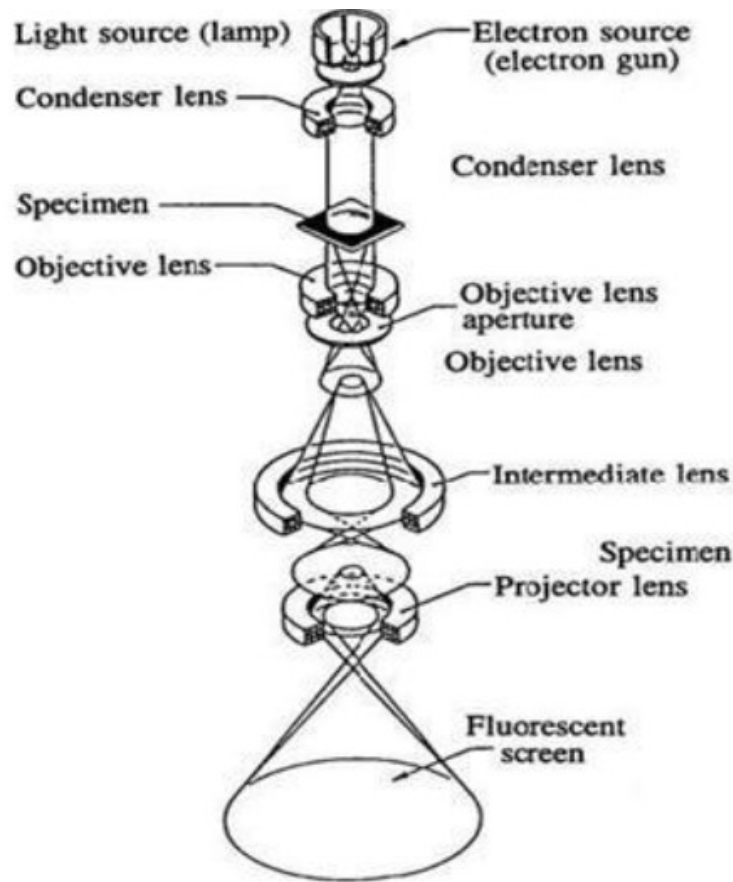


**Figure 27:**A typical TEM components<sup>85</sup>.

#### 2.12.F. Fourier transform infrared spectroscopy (FTIR)

Fourier transform infrared spectroscopy (FTIR) is a spectroscopic technique that measures the vibrational oscillation of molecular bonds in forms of molecular stretching and bending of chemical bonds when they are subjected to a matched light wavelength (mid IR wavelength of 2.5  $\mu\text{m}$  and 25  $\mu\text{m}$ ), that generates absorption peaks in the IR spectrum. FTIR is a rapid a technique that estimate the chemical composition of the system (qualitative analysis) as well as identification of characteristic functional groups in the formula. FTIR depends on Michelson interferometer as represented in **Figure** (28). In Michelson interferometer, He-Ne laser beam are splitting into two halves, the first half of the light hits a fixed mirror while the second part hits the moving mirror. Then, the two halves are recombined with different traveling distances that generates interference pattern due to the difference in the path lengths. The resulted interferogram shows variable transmitted intensities versus time that are converted into a frequency spectrum using a Fourier transform mathematical function. Light with interference pattern passes through the sample and the detector can collect the interfering signals and generates a plot of the response<sup>86</sup>.

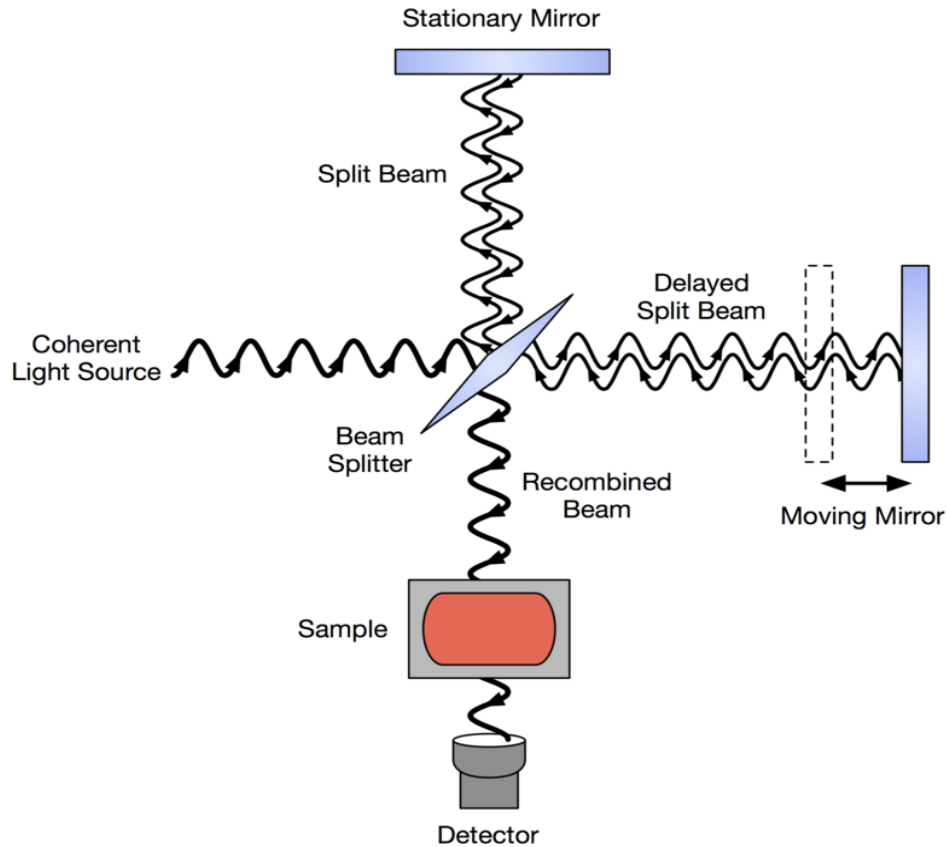


**Figure 28:** Schematic diagram of Michelson interferometer<sup>87</sup>.

### 2.12.G. X-ray diffraction analysis (XRD)

X-Ray Diffraction (XRD) analysis provides a valuable information about material packing character as well as material crystallinity through interpretation of diffraction peaks (shape, intensity and position). XRD relies on Bragg's law (equation 11) that studies the conditions needed for light diffraction. According to Bragg's law,  $\lambda$  is the wavelength, while  $d$  is the spacing between the planes and  $\theta$  is a diffraction angle.

$$\lambda = 2d \sin \theta \quad (11)$$

According to **Figure** (29 a, b), when a fixed wavelength of X-ray ( $\lambda$ ) is applied with an incident angle ( $\omega$ ) on planes of atoms having a space ( $d$ ), diffraction peak will simultaneously be generated at a specific angle ( $\theta$ ). The angle between incident beam and the detector angle is called diffracted angle ( $2\theta$ ). Therefore, according to the peak position (at a specific angle  $\theta$ ), the spacing between the planes ( $d$ ) can be estimated. On the other hand, the types of atoms in diffracting plane can easily be determined by peak intensity<sup>88</sup>.

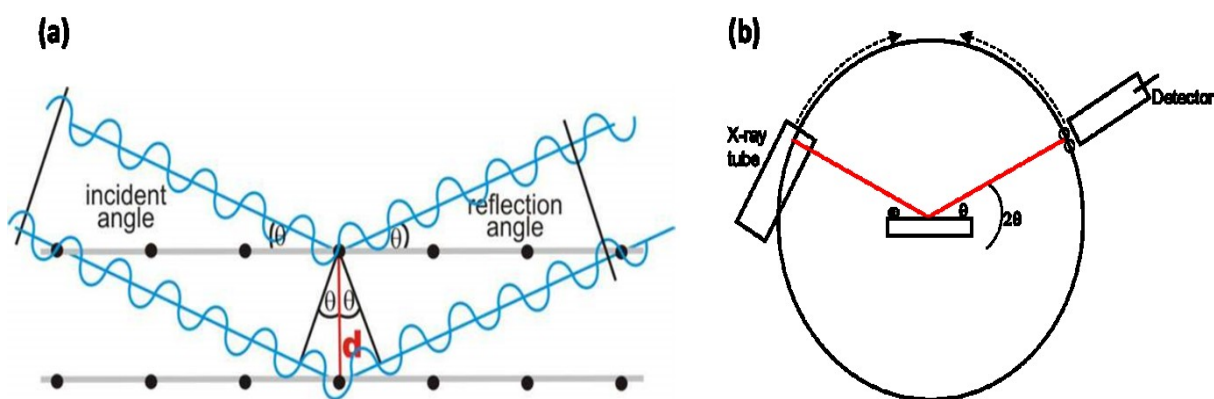


**Figure 29:** Bragg's hypothesis (a), Schematic diagram of a typical XRD system (b)<sup>88</sup>.

#### 2.12.H. Thermal gravimetric analysis (TGA)

Thermal gravimetric analysis (TGA) provides useful information about the behavior of a material during heating conditions. TGA can estimate the impact of temperature on the material's weight change that helps in understanding the thermal properties of a material. The sample is heated in a controlled way in an oven with an environment of different gases. The weight difference is measured as a function of temperature. The plot that come out of TGA is called thermogram. A typical TGA consists of an oven with a platinum thermocouple and a microgram balance as represented in **Figure** (30). A thermocouple that is made of platinum is used to measure the temperature. The change in weight is recorded from the beam deflection.<sup>89</sup>

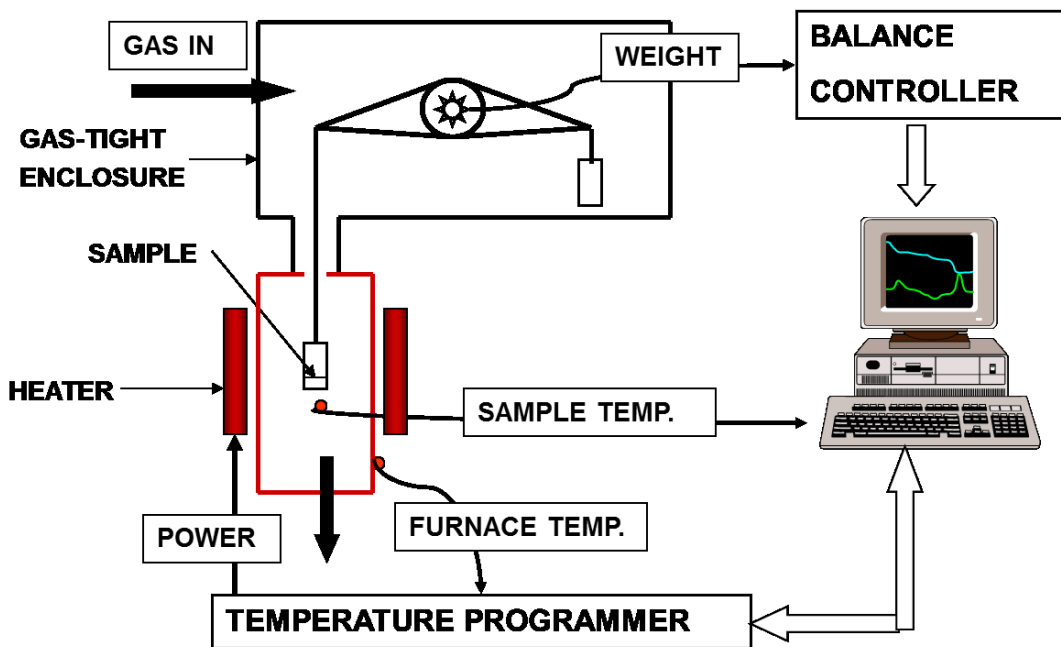


Figure 30: Schematic diagram of TGA<sup>89</sup>.

### 2.12.I. Folin–Ciocalteu (FC) method

The Folin Ciocalteu method is a simple spectroscopic method for determination of phenolic contents in herbal extracts and EOs<sup>61</sup>. Folin Ciocalteu reagent is typically composed of 100 g of sodium tungstate (VI) dihydrate and 25g of sodium molybdate (VI) dihydrate dissolved in 700mL distilled water. Then, the formed solution is added to 100mL concentrated hydrochloric acid and 50mL of 85% phosphoric acid added to it 150g of lithium sulphate hydrate<sup>90</sup>. The net results of the previous addition is the formation of phosphomolybdic and phosphotungstic acids (oxidation states of molybdenum and tungsten are 6+). The mechanism of FC reagent in determining the amount of phenolic contents depends on the chemical reaction between FC reagent with a reductant such as phenolic compound that forms molybdenum blue and tungsten blue that are measured through UV-Vis spectroscopy at a wavelength of 765 nm. The reaction is accelerated by increasing the pH of the medium by the addition of sodium carbonate<sup>91</sup>. The F-C method was found to be beneficial in estimating the total phenolic content (TPC) rather than

High Performance Liquid Chromatography(HPLC), owing to its equivalent response to different phenolic substances<sup>92</sup>. For instance, HPLC estimated only 10% of the TPC in Eucalyptus leaf that is estimated by FC reagent<sup>93</sup>. However, the F-C method has an ability to react with non-phenolic compounds such as with tertiary aliphatic amines, sugars and inorganic reducing agents<sup>94</sup>.

#### **2.12.J. Ultraviolet/Visible spectroscopy (UV-Vis spectroscopy)**

UV-Vis spectroscopy is a technique that is used mainly for quantitative as well as qualitative analysis. It depends on the absorbance of a molecule to UV and Visible radiations that are part of the electromagnetic spectrum. These radiations have energy that ranges from 36 to 143 kcal/mol which are enough for electrons transition from the ground state to an excite state. The energy of the UV and visible electromagnetic radiations can be calculated using equation (12)<sup>95</sup>:

$$E = h \cdot \nu \quad (12)$$

Where, (E) is the radiation energy, (h) is Plank's constant and ( $\nu$ ) is the radiation frequency.

The wavelength at which maximum absorbance occurred which is called  $\lambda_{\max}$  is characteristic for different chemical species that makes UV-Vis spectroscopy a reliable qualitative method of analysis. Furthermore, UV/Vis spectroscopy can be used for quantitative analysis based on Beer Lambert law shown in equation (13)<sup>95</sup>:

$$A = \epsilon bc \quad (13)$$

Where, (A) is the absorbance, ( $\epsilon$ ) is the absorptivity coefficient which is characteristic for each substance, (b) is the path length of radiation that passes through a cuvette containing the sample

and finally (c) is the sample concentration. Accordingly, through instrumental measurement of the sample absorbance, sample concentration can be estimated<sup>95</sup>.

A typical UV/Vis spectrophotometer as represented in **Figure (31)** consists of; (i) a radiation source either a deuterium lamp (for UV radiation wavelength that ranges between 200-400 nm) or a tungsten-halogen lamp (for Vis radiation wavelength that ranges between 400-800 nm), (ii) monochromator either grating or a prism to select only part of the electromagnetic radiation to reach the sample, (iii) a sample holder either plastic cuvettes (for Visible radiation range) or quartz cuvettes (for UV and Visible radiation range) and finally (iv) a detector either photomultiplier tube detector or photodiode are used to convert the transmitted light beam into an electrical signal<sup>95</sup>.

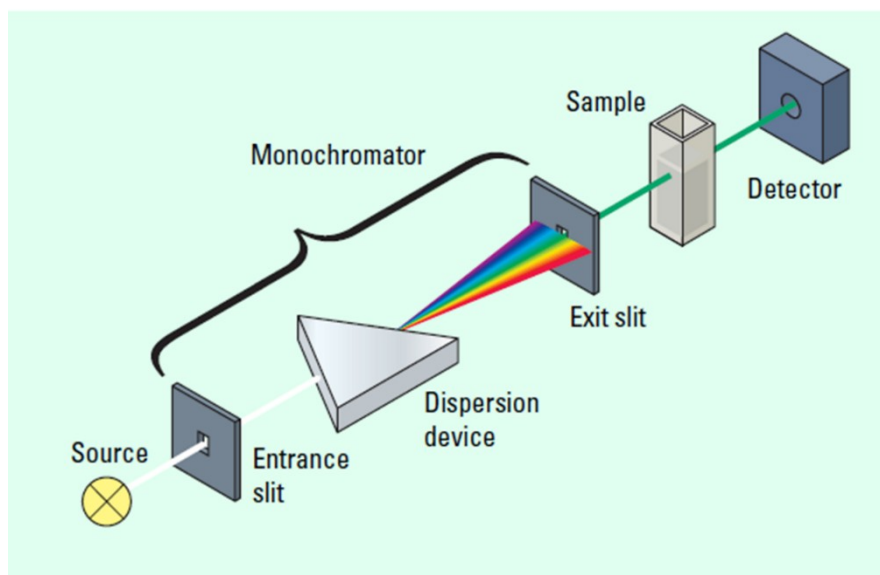


**Figure 31:**UV-Vis spectrophotometer<sup>95</sup>

### **2.12.K. Antibacterial Assessment by Agar dilution and colony counting method**

The agar dilution method is one of the methods that uses an antibiotic sensitivity test. In brief, an antimicrobial agent is incorporated into a molten agar medium that contains the incubated bacteria. The mixture is incubated while shaking under specific conditions of temperature, speed and duration. Serial dilutions are prepared from the incubated mixture and the desired dilution is spread on nutrient agar. Agar plate is cultured and the colonies are quantified as represented in **Figure** (32). This method is commonly used for antibacterial testing against both Gram-positive and Gram-negative bacteria<sup>96</sup>. The agar dilution method is considered a gold standard technique of antimicrobial susceptibility testing that is characterized by its accuracy in determination of the minimum inhibitory concentrations (MICs), and the ability to extend the antimicrobial concentration as far as required. On the other hand, agar dilution method is an expensive method as it requires large amount of manual handling that needs extensive training of personnel<sup>97</sup>.

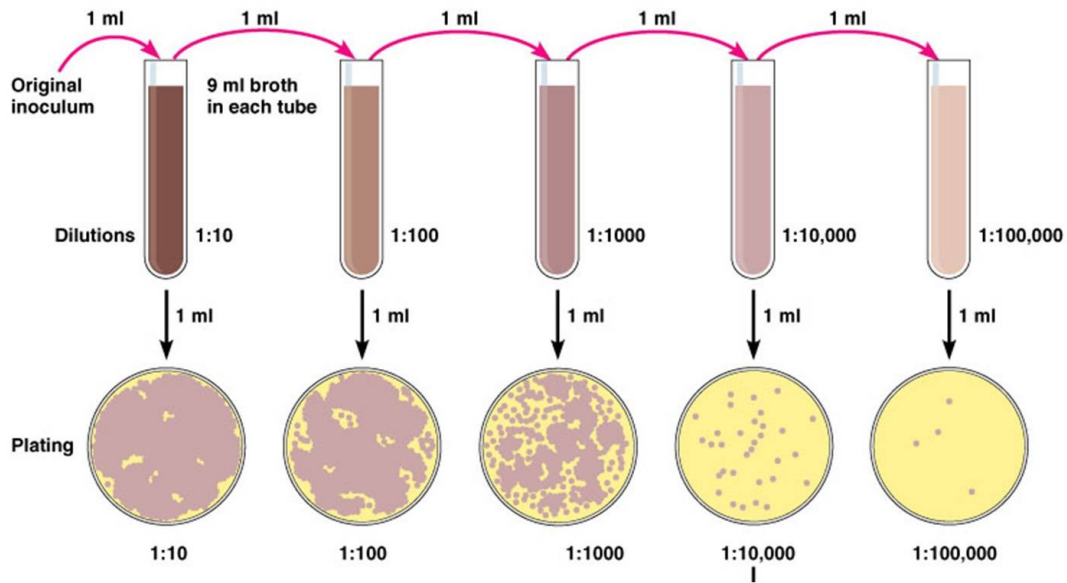


**Figure 32:** Agar dilution and colony count method<sup>96</sup>

### 2.12.L. DPPH test

DPPH is a stable radical and has a violet color with a maximum absorbance at a wavelength of 517 nm in ethanolic solution. When DPPH comes in contact with another radical (an antioxidant) it gets reduced. The reduced form of DPPH loses its properties as a free radical and accordingly changes its color to yellow as represented in **Figure (33)**. DPPH assay is easy and rapid way for investigating the antioxidant properties. However, DPPH is not a peroxy-radicals (physiological radical), therefore Light, O<sub>2</sub>, and pH can influence the DPPH absorbance. Furthermore, compounds as carotenoids with absorption wavelength of 517 nm can interfere with the absorption maximum of DPPH.

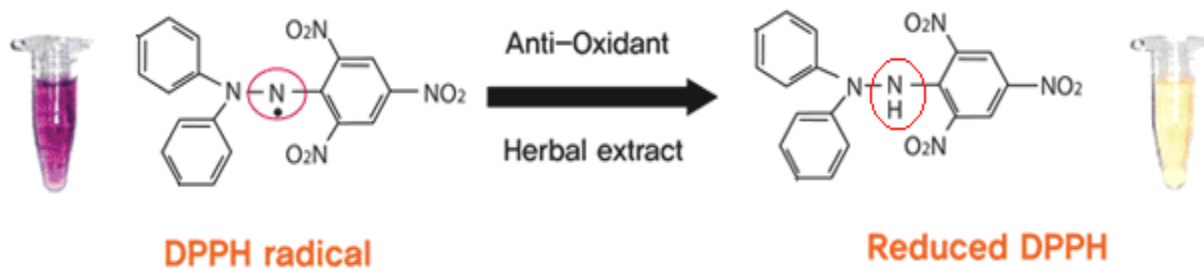


Figure 33:DPPH assay principle<sup>98</sup>

## Chapter 3

### Results and Discussion:

### **Chapter 3: Results and Discussion– Chitosan/ (Peppermint and Green Tea Oil) Nanoparticle Formulations, Characterization and *in-vitro* Release.**

#### **3.1. Compositional Analysis of PO and GTO by GC/MS/MS.**

PO is a pale-yellow liquid obtained by steam distillation of leaves that comes from *Labiatae* herbs family such as *Mentha piperita* L. and *M. arvensis* var. *piperascens*<sup>99</sup>. GTO on the other hand is a yellow liquid obtained by steam distillation of leaves that comes from *Theaceae* herbs family such as *Camellia sinensis*<sup>100</sup>. Both liquids are freely soluble in ethanol.

The Gas Chromatography coupled to Tandem Mass Spectrometry (GC/MS/MS) technique was used to assure the identity and to identify the components of both PO and GTO<sup>75</sup>. GC/MS/MS chromatogram obtained from PO is illustrated in **appendix I**. Based on the results of GC/MS/MS chromatogram, Citronellol is the most abundant compound in PO which is characteristic oxygenated monoterpene phytochemical in Labiatae herbs family<sup>101</sup>. Furthermore, other oxygenated monoterpenes were identified such as menthone, tetrahydrocarvone, menthol, levomenthol,  $\alpha$ -terpineol and pulegone which are characteristic for peppermint herbs<sup>102</sup>. Based on the results revealed by GC/MS/MS chromatogram of PO, it was found that about 70.32% of PO components are non-phenolic oxygenated monoterpenes phytochemicals as shown in **Figure (34)**. These results are agreed to (Gharib et al., 2013)<sup>103</sup> findings who found about 62.2% of PO composition was non-phenolic oxygenated monoterpenes phytochemicals.

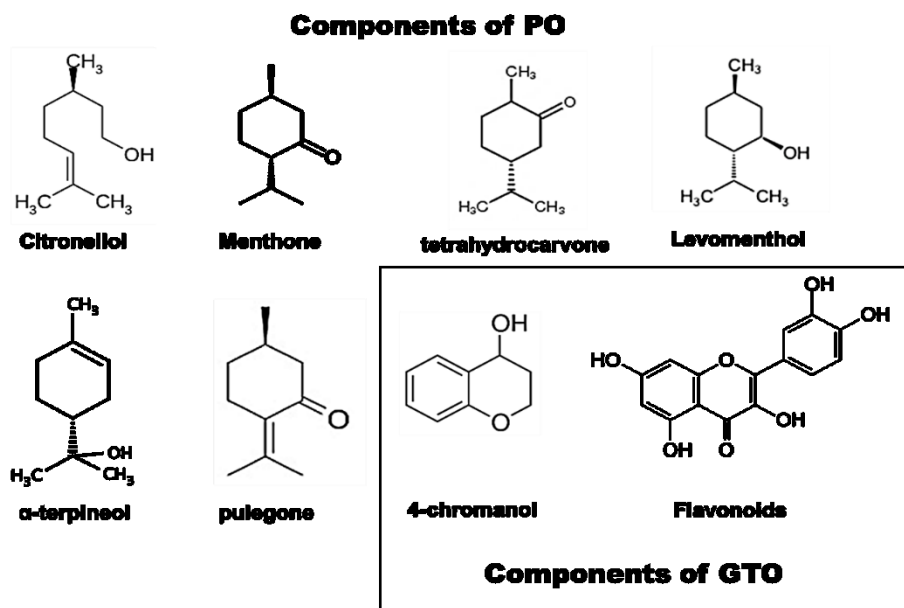


**Figure 34:**Chemical structures of PO and GTO phytochemicals<sup>32</sup>.

On the other hand, according to the results of GC/MS/MS chromatogram of GTO which are represented in **appendix II**, 4-chromanol is the most abundant compound (54.8%) in GTO which is composed of a characteristic ring in the structure of phenolic flavonoids in *Theaceae*

herbs family specially green tea as represented in **Figure (34)**<sup>104</sup>. Furthermore, fatty alcohol such as oleic alcohol were identified in the MS chart of GTO that is characteristic in green tea herbs<sup>105</sup>. These

findings were found to be similar to the findings of (Packer, 2001)<sup>104</sup> who reported that the 4-chromanol ring is a fundamental component of tea flavonoids such as Quercetin and Epicatechin. In this regard, the results of GC/MS/MS chromatogram for both EOs agree to a large extent with previously published reports and confirm the identity and characteristic components for both PO and GTO and shed light on the clear difference in the origin and composition of the both EOs.

### **3.3.A. Impact of homogenization parameters on the average size and zeta potential of CS/PO NPs.**

As reported previously, homogenization parameters such as speed and duration had crucial role in reducing the average size of different NPs by increasing the rotor stator homogenizer speed and duration<sup>106,107</sup>. CS/PO NPs were prepared by using a ratio of CS to PO (1:1) with fixed TPP concentration at 0.5%w/v. Different homogenization speeds (12000, 13000 and 14000 rpm) at different homogenization times (5, 10 and 15 min) were used.

As shown in **Figure(35a)**, homogenization speed had a significant impact on particle size diameter. Increasing the homogenization speed was identified to significantly reduce the NPs diameter. For instance, at 10 min homogenization, the average diameter of the NPs at 12000, 13000 and 14000 rpm were  $549.9 \pm 11.08$ ,  $420.1 \pm 9.77$  and  $404.8 \pm 5.45$  nm, respectively. On the other hand, homogenization time also had an impact on the NPs diameter. So, homogenization for 10 min showed significant lower NPs average diameter at all

homogenization speeds. It should be noted that, at 5 min homogenization, incomplete homogenization was noticed specifically at 12000 rpm. Based on the previous results, homogenization at 14000 rpm that represent the higher speed with duration of 10 min showed the lowest NPs diameter.

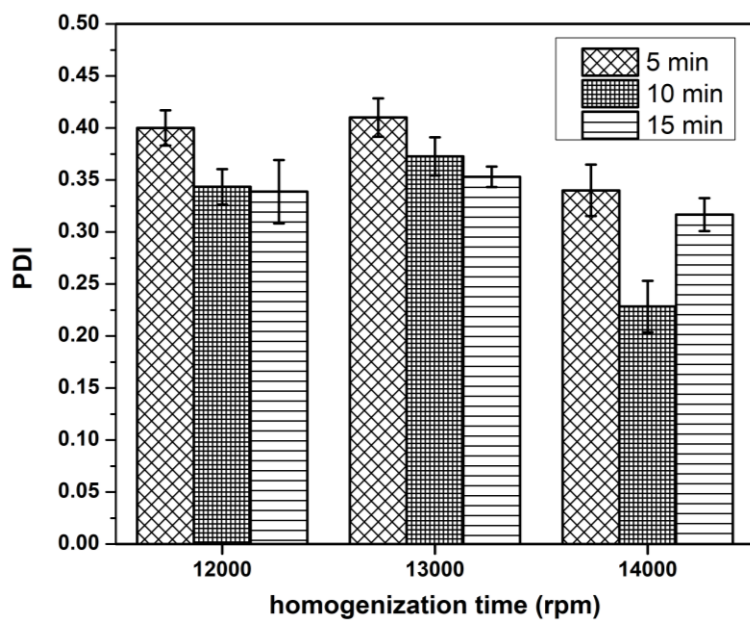
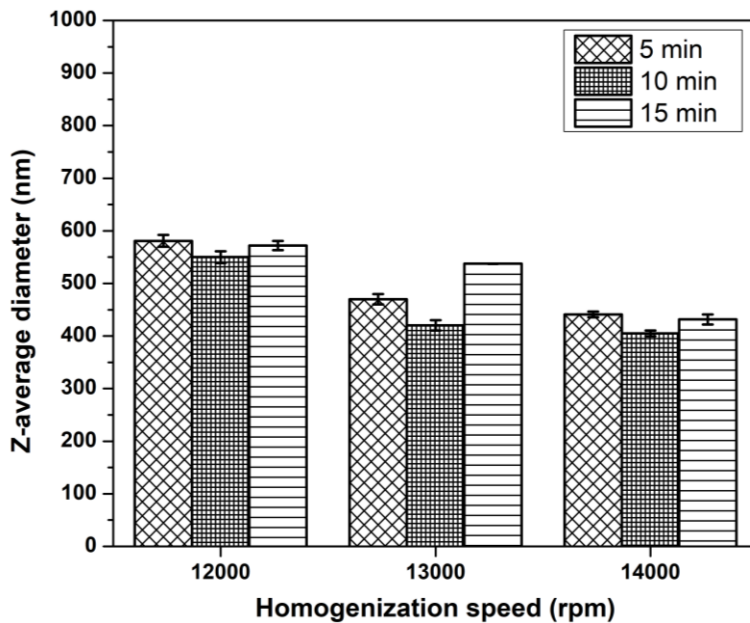


**Figure 35:** Impact of homogenization parameters on (a) the average NPs diameter and (b) size distribution of CS/PO NPs.

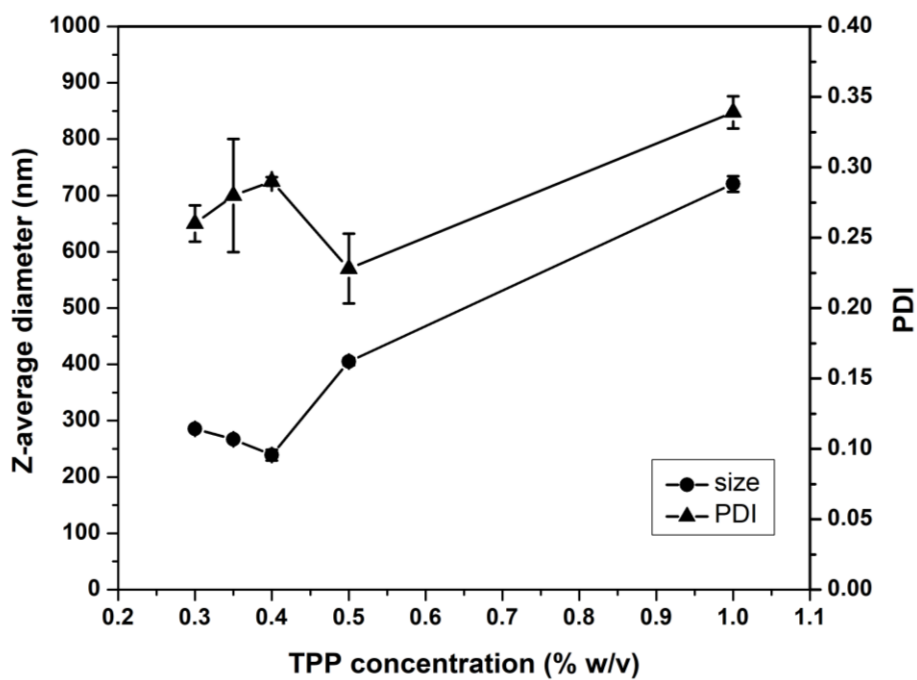
As shown in **Figure (35b)**, homogenization speed had a significant impact on the NPs size distribution. The highest NPs size mono-dispersity (lowest PDI) was identified at homogenization speed of 14000 rpm at all homogenization times while homogenization speed of 13000 rpm showed the lowest NPs size mono-dispersity (highest PDI) at all homogenization times as well. For instance, at 10 min homogenization, the PDI value at 12000, 13000 and 14000 rpm were  $0.34 \pm 0.01$ ,  $0.37 \pm 0.01$  and  $0.22 \pm 0.02$ , respectively. On the other hand, homogenization time also had an impact on the NPs diameter. So, homogenization for 5 min showed the highest PDI value at all homogenization speeds, while, homogenization for 10 min at 14000 rpm showed the lowest PDI value. Based on both average NPs size and PDI results, homogenization at 14000 rpm for 10 min showed the ideal homogenization parameters.

Surprisingly, previous reports agree with our findings and recommended a 10min homogenization at 14000 rpm as an optimum homogenization condition in encapsulation of Oregano, Carum copticum and Carvacrol in CS-TPP system<sup>61,76,108</sup>. It should be pointed out that any further increase in homogenization speed was not favorable, because of the high energy provided to the medium which led to volatilization of EO, particle aggregation and enlargement rather than particle size reduction<sup>106</sup>.

### **3.3.B. Impact of TPP concentration on the average size and zeta potential of CS/PO NPs**

Based on the homogenization parameters studies, new batches were prepared using homogenization speed of 1400 rpm in a duration of 10 min to study the impact of TPP concentrations on the NPs size, size distribution and zeta potential. Different TPP concentrations

were used ranging from 0.3-1% w/v. According to **Figure (36a)**, the NPs size first gradually decreased from  $300 \pm 7.52$  nm to  $238.9 \pm 9.56$  nm at TPP concentration of 0.4 %w/v and then increased dramatically to  $720.3 \pm 13.8$  nm at TPP concentration of 1% w/v. Based on these results, the TPP concentration of 0.4%w/v showed the lowest NPs size.



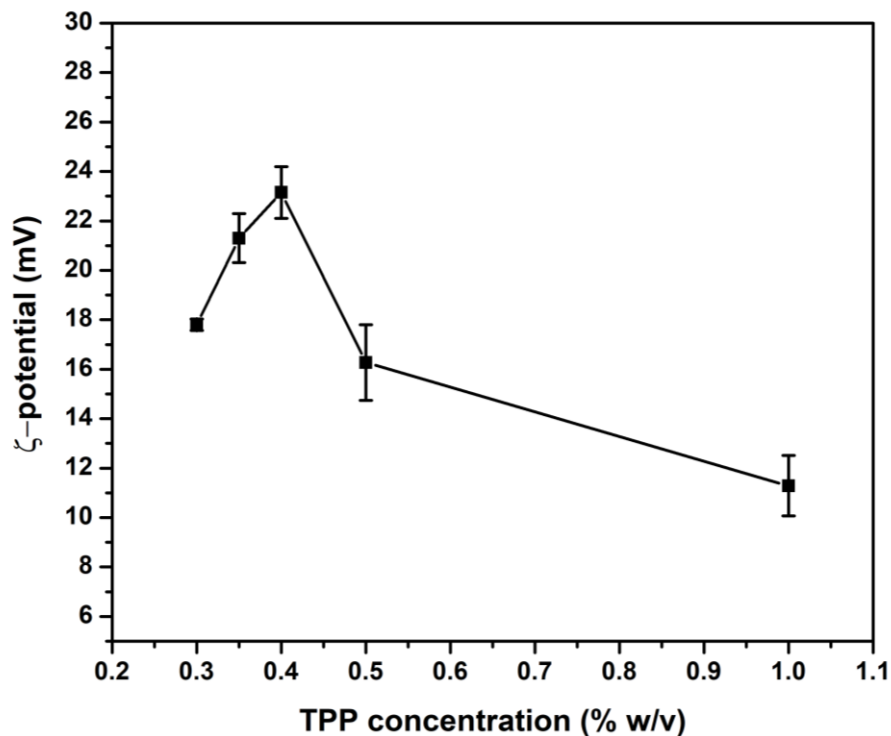


**Figure 36:** Impact of TPP concentrations on (a) the NPs size and size distribution (b) the zeta potential of CS/PO NPs.

According to NPs mono-dispersity, as shown in **Figure** (36a), increasing the concentration of TPP showed a statistically no change in PDI value reaching  $0.29 \pm 0.003$  nm at TPP concentration of 0.4% w/v, then a significant increase in PDI value reaching  $0.339 \pm 0.01$  nm that appeared at TPP concentration of 1%w/v. Based on these results, the TPP concentration of 0.3 to 0.4%w/v showed statistically no change in mono-dispersity of the NP size.

As shown in **Figure** (36b), increasing the concentration of TPP showed a significant increase in zeta potential (ZP) value reaching  $23.15 \pm 1.05$  mV at TPP (0.4% w/v). The reason behind this elevation in ZP value at the concentration of TPP below (0.4 % w/v) might be due to the formation of more tightly compacted NPs. TPP is a cross-linker with negative charge that minimizes the electrostatic repulsion between CS molecules and thus enhances the aggregation

and NP formation<sup>76</sup>. As the NP forms, additional incorporation of TPP is suggested to increase the internal cross-linking between CS chains within the NP, leading to the formation of more tightly bound CS chains that increase the surface area per unit volume of the particle thus increasing the exposed charges on NPs surface. On the other hand, increasing the concentration of TPP more than 0.4% w/v results in dramatical decrease in ZP value to  $11.29 \pm 1.21$  mV that appeared at TPP concentration of 1%w/v. The reason behind that is might be due to the neutralization of the majority of the CS protonated amino groups by TPP anions that enhance hydrogen bonding interactions between the formed NPs and that might be a reason for the dramatic size enlargement of the NPs<sup>109,110,111</sup>. Based on these results, the TPP concentration of 0.4%w/v showed the most significant stable NPs.

Based on the previous experiments, the ideal conditions for the preparation of the CS/PO NPs were homogenization speed of 1400 rpm for 10 min with TPP concentration of 0.4%. After establishing the optimum preparation conditions, different ratios of CS to PO and GTO were used (1:0.25, 1:0.50, 1:0.75 and 1:1.00 w/w) followed by NPs characterization, encapsulation efficiency determination, *in-vitro* release and stability of phenolic contents in the NPs as will be described in the following sections.

### **3.4. Characterization of nanoparticles formulations of EOs.**

#### **3.4.A. Nanoparticles hydrodynamic size**

Nanoparticles hydrodynamic size were studied using dynamic light scattering (DLS) technique (Zetasizer). As represented in **Figure (37)**, chitosan nanoparticles (CS NPs) possessed an average diameter of  $217.2 \pm 6.42$  nm. On the other hand, CS/PO NPs with CS to PO ratio of (1:0.25, 1:0.50, 1:0.75 and 1:1.00 w/w) showed an average diameter of  $231.4 \pm 12.72$ ,  $249.7$

$\pm 2.78$ ,  $252.6 \pm 3.48$  and  $238.9 \pm 9.56$  nm, respectively. Results revealed that the mean particle size increased significantly as initial PO content increased until  $252.6 \pm 3.48$  nm at CS/PO ratio of 1:0.75 w/w. Finally, the size tended to decrease at CS/PO ratio of (1:1.00 w/w) samples to  $238.9 \pm 9.56$  nm.

GTO-loaded CS NPs (CS/GTO NPs) with CS to GTO ratio of (1:0.25, 1:0.50, 1:0.75 and 1:1.00 w/w) showed an average diameter of ( $226.3 \pm 4.9$ ,  $240.9 \pm 7.33$ ,  $249.7 \pm 28.75$  and  $237.5 \pm 15.69$  nm, respectively as represented in **Figure (37)**. In contrast to PO, the mean particle size showed statistically no change with increased initial GTO content until  $249.7 \pm 28.75$  nm at CS/GTO ratio of (1:0.75 w/w).

Both EOs showed a maximum NPs size at a ratio of CS/EO (1:0.75 w/w). The previous results showed statistically no change in sizes between the two EOs with different concentrations revealing the independency of CS NP hydrodynamic diameter on the type of EO.

These results are agreed with the (Hosseini et al., 2013)<sup>108</sup> findings who found that the average diameter of the NPs increased from 281 nm to 402 nm after encapsulation of Oregano in CS-TPP system. Furthermore, (Yoksan et al., 2011)<sup>76</sup> revealed the size increase of NPs from 518 nm to 716 nm after encapsulation of Carvacrol in CS-TPP system. However, these findings contradict the results of (Feyzioglu et al., 2016)<sup>63</sup> who found a reduction in the NPs size from 237 nm to 140 nm after encapsulation of summer savory in CS-TPP system. So, in our work, a possible reason behind the size increase of the NPs diameters in both EOs might be due to the swelling and aggregation of CS polymer while dispersed in water<sup>76</sup>.

According to the size distribution of both CS/PO NPs and CS/GTO NPs with their different concentrations, The PDI values ranged from 0.22 – 0.25 and from 0.24 – 0.25 in CS/PO NPs and CS/GTO NPs, respectively. Increasing the PO and GTO content had a non-significant impact on the PDI value. Furthermore, the previous results showed statistically no change in PDI between both PO and GTO revealing the independency of CS NP size distribution on the type of EO. The above data are represented in **appendix III**.

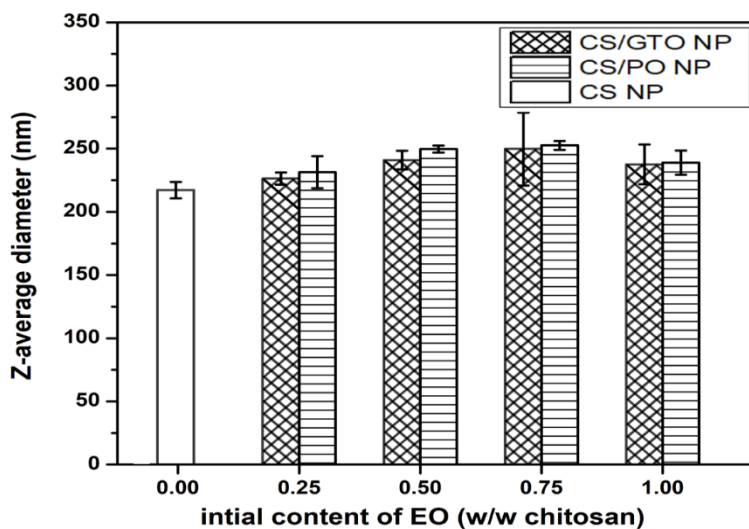


**Figure 37:** Z-average diameter of nanoparticles as a function of initial PO and GTO content.

### 3.4.B. Zeta potential of nanoparticles.

Zeta potential (ZP) studies were performed to show the impact of EOs loading on the surface charge and stability of the prepared NPs. As represented in **Figure (38)**, CS NPs gave a ZP value of  $+24.9 \pm 0.95$  mV. On the other hand, CS/PO NPs showed ZP values of  $(20.95 \pm 0.66, 20.9 \pm 0.23, 21.2 \pm 0.98$  and  $23.15 \pm 1.05$  mV for CS/PO ratio of (1:0.25, 1:0.50, 1:0.75 and 1:1.00 w/w) respectively. Results indicated that increasing the PO content reduced significantly the value of ZP. The higher ZP value of PO loaded CS NP that showed the highest stability occurred with CS/PO ratio (1:1.00 w/w).

On the other hand, CS/GTO NPs showed ZP values of ( $24.2 \pm 0.3$ ,  $21.3 \pm 0.4$ ,  $24.5 \pm 1.64$  and  $17.8 \pm 0.4$  mV) for CS/GTO ratio of (1:0.25, 1:0.50, 1:0.75 and 1:1.00 w/w) respectively, as represented in **Figure** (38). Results indicated that increasing the GTO content reduced significantly the value of ZP. CS/GTO ratio (1:0.75 w/w) showed the highest stability. Based on previous results, statistically no change in ZP between the two EOs with different concentrations revealing the independency of CS NPs surface charge on the type of EO.

These results were found to be in agreement with the findings of (Haider et al., 2017)<sup>56</sup> in the encapsulation of krill oil in CS-TPP system who found a reduction of ZP from +35 mV to +24 mV. Moreover, the encapsulation of eugenol in CS-TPP system (Woranuch et al., 2013)<sup>53</sup> showed a decrease in ZP value from +37 mV to +16 mV. So, in our case, a possible reason behind the reduction in ZP in both EOs might be due to a shielding effect and the coating of protonated  $\text{NH}_2$  group by PO and GTO on the CS NPs<sup>76</sup>. The decrease in ZP value enhances the attractions between the formed NPs that might be a possible reason behind the increase in the average diameter in comparison with the CS NPs with increasing PO<sup>63</sup>.

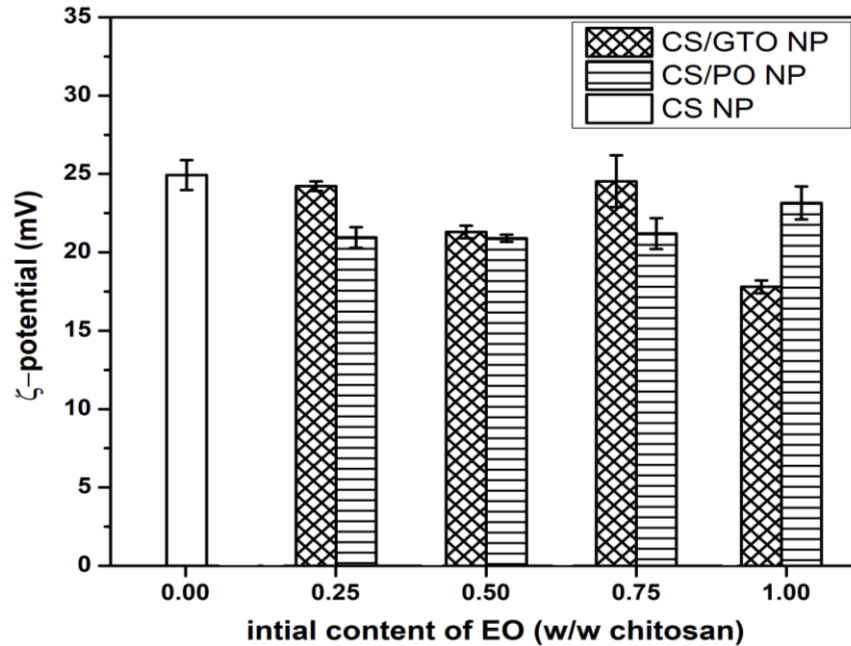


**Figure 38:** Zeta potential of CS NPs as a function of initial PO and GTO content.

### 3.4.C. Morphology of nanoparticles.

The size and morphology of the NPs was examined by transmission electron microscope (TEM). CS NPs, CS/PO NPs (1:1 w/w) and CS/GTO NPs (1:1 w/w) appeared as spherical shapes as shown in **Figure (39)**. The difference in shape between the nanoparticles were insignificant revealing the independency of CS NPs shape and morphology on the type of EO. This was found to be in agreement with the findings of (Yoksan et al., 2011)<sup>76</sup> in the encapsulation of carvacrol.

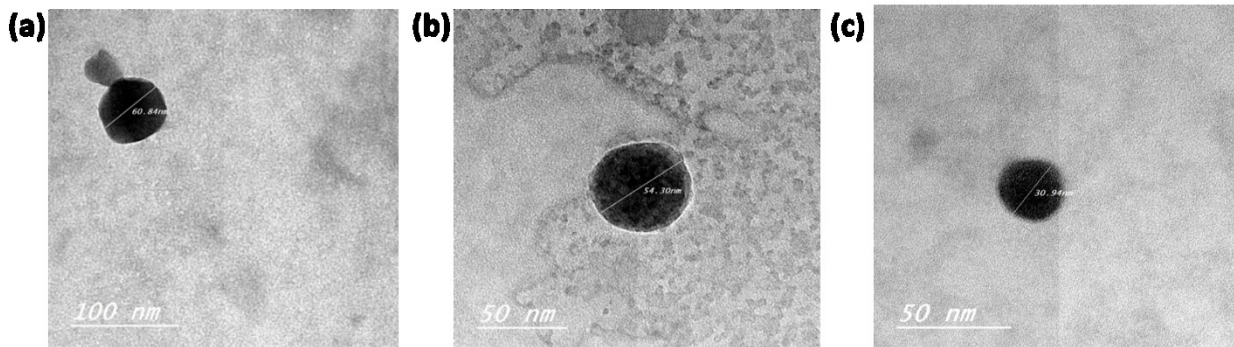


**Figure 39:** TEM of spherical nanoparticle, CS NP (a), CS/PO NP (1:1) (b) and CS/GTO NP (1:1) (c).

As represented in the size distribution histograms (**Figure 40**), the size range of CS NPs, CS/PO NPs and CS/GTO NPs were between 10-90 nm, 20-90 nm and 10-70nm, respectively. Furthermore, the estimated average size for CS NPs, CS/PO NPs and CS/GTO NPs were 36.1 nm, 43.5 nm, and 30.7 nm, respectively. The encapsulation of PO increased significantly the size of the CS/PO NPs compared with CS NPs while the encapsulation of GTO reduces significantly the size of the CS/GTO NPs compared with CS NPs.

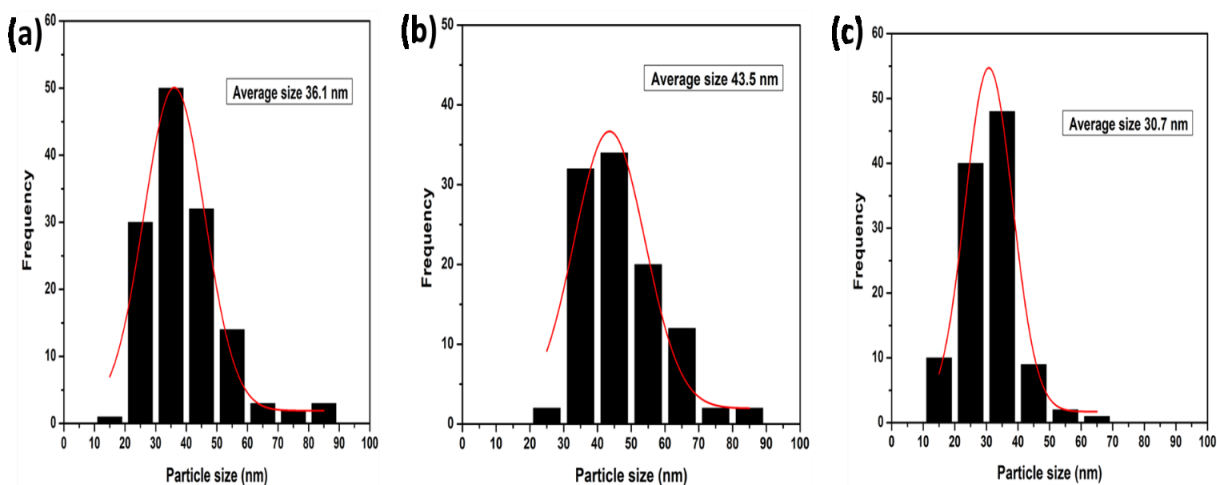


**Figure 40:** Size distribution histograms of the prepared nanoparticles, CS NP (a), CS/PO NP (1:1) (b) and CS/GTO NP (1:1) (c).

However, most of our NPs (CS NPs, CS/PO NPs and CS/GTO NPs) were aggregated as shown in **Figure (41)** that might be due to be a fusion and combination of the CS/PO NPs and CS/GTO NPs with each other as well as PO and GTO content on the surface of the particle similar to what was previously reported by (Yoksan et al., 2010)<sup>112</sup> as represented in **Figure (42)** after encapsulation of carvacrol in CS NPs .

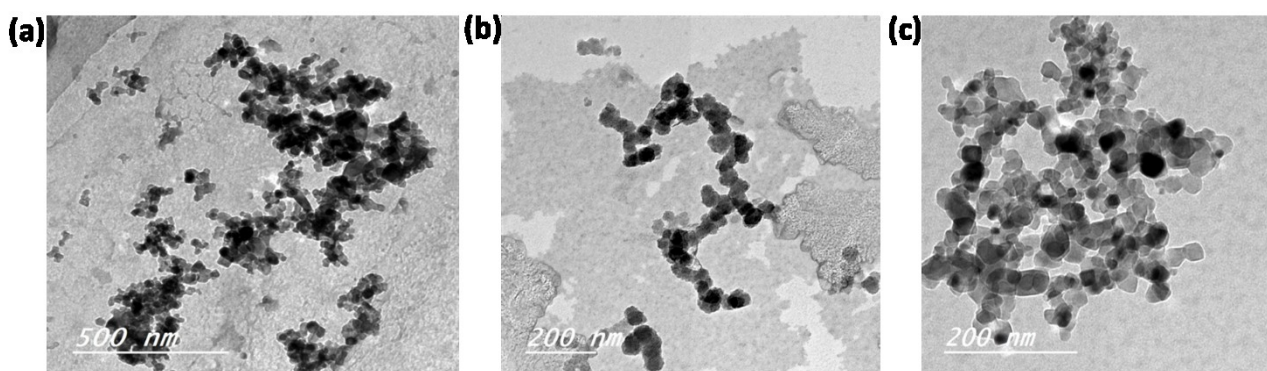


**Figure 41:**TEM of aggregated nanoparticle, CS NP (a), CS/PO NP (1:1) (b) and CS/GTO NP (1:1) (c).

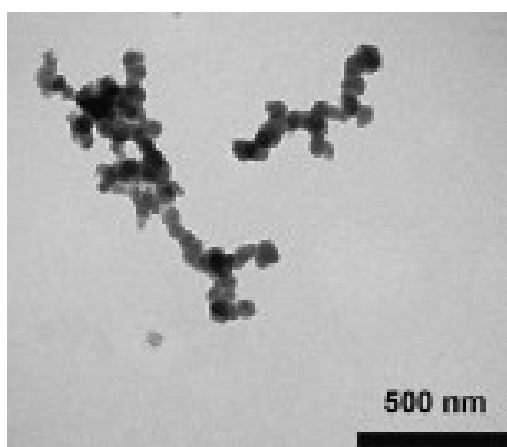


**Figure 42:**TEM of aggregated CS/ Carvacrol nanoparticle<sup>76</sup>.

It should be figure out that the mean average size of all nanoparticles that estimated by zetasizer was greater than that detected by TEM. This is mainly because the size that is determined by zetasizer is a hydrodynamic size where the NPs are suspended in solutions that enhances the aggregation of the NPs as mentioned before<sup>76</sup>.

#### **3.4.D. Fourier transform infra-red (FT-IR) spectroscopy analysis of CS, EOs and NPs**

Fourier transform infra-red (FTIR) spectroscopy analysis was used to study the chemical characteristics of pure PO, CS NPs and CS/PO NPs (with ratios of 1:0.25, 1:0.5, 1:0.75 and 1:1.00 w/w). FTIR spectra of CS NP (**Figure 43a**) showed characteristic peaks at  $3433\text{ cm}^{-1}$  due to hydroxyl group and primary amine stretching.  $Sp^3$  C-H stretching appeared at  $2933\text{ cm}^{-1}$  while amide stretching peaks appeared at  $1642$  and  $1550\text{ cm}^{-1}$ . In addition, pure PO spectra (**Figure 43b**) showed sharp characteristic peaks at  $2929\text{ cm}^{-1}$  due to  $Sp^3$  C-H stretching and at  $1710\text{ cm}^{-1}$  due to carbonyl stretching. All the characteristic peaks of both CS NP and pure PO were appeared in the spectra of CS/PO NPs (**Figure 43c, d, e and f**) with carbonyl stretching peak that increased with increasing PO content and all peaks were shifted from  $1710\text{ cm}^{-1}$  to  $1731\text{ cm}^{-1}$ . The results of FTIR identify the incorporation of PO in the CS-TPP system.

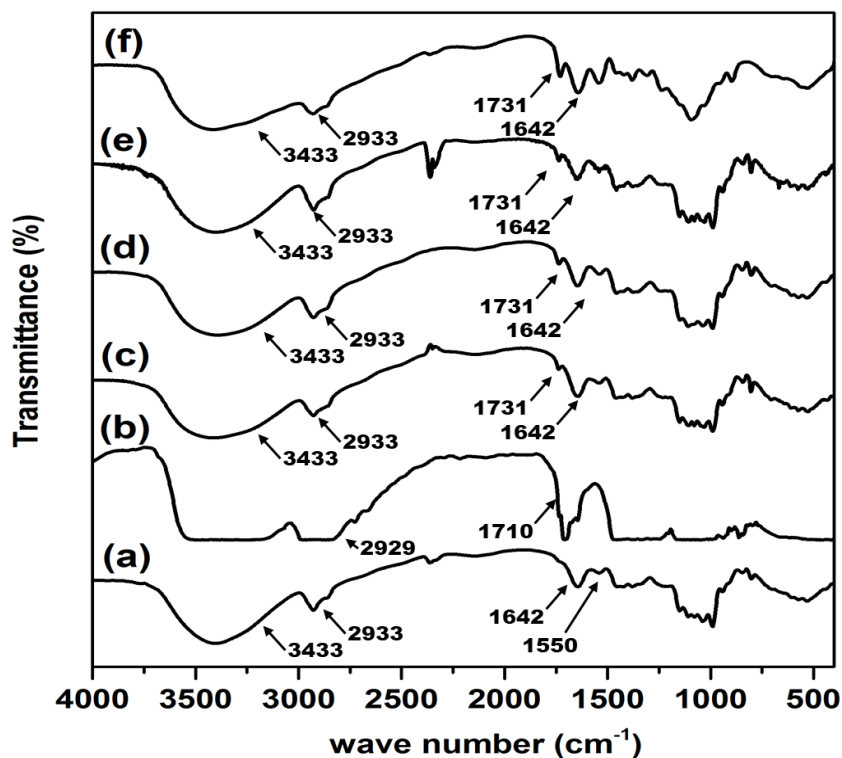


**Figure 43:** FT-IR of CS NP(a), pure PO (b) and CS/PO NP (c-f) with different ratios of CS: PO 1:0.25 (c), 1:0.50 (d), 1:0.75 (e) and 1:1.00 w/w (f).

In the case of CS NPs loaded with GTO, pure GTO spectra (**Figure 44b**) showed sharp characteristic peaks at  $2929\text{ cm}^{-1}$  due to  $Sp^3$  C-H stretching and at  $1731\text{ cm}^{-1}$  due to carbonyl stretching. All the characteristic peaks of both CS NP and pure PO were appeared in the spectra of CS/GTO NPs (**Figure 44c, d, e and f**) with carbonyl stretching peak that increased with increasing GTO content at the same wave number. The results of FT-IR identify the encapsulation of GTO in the CS-TPP system.

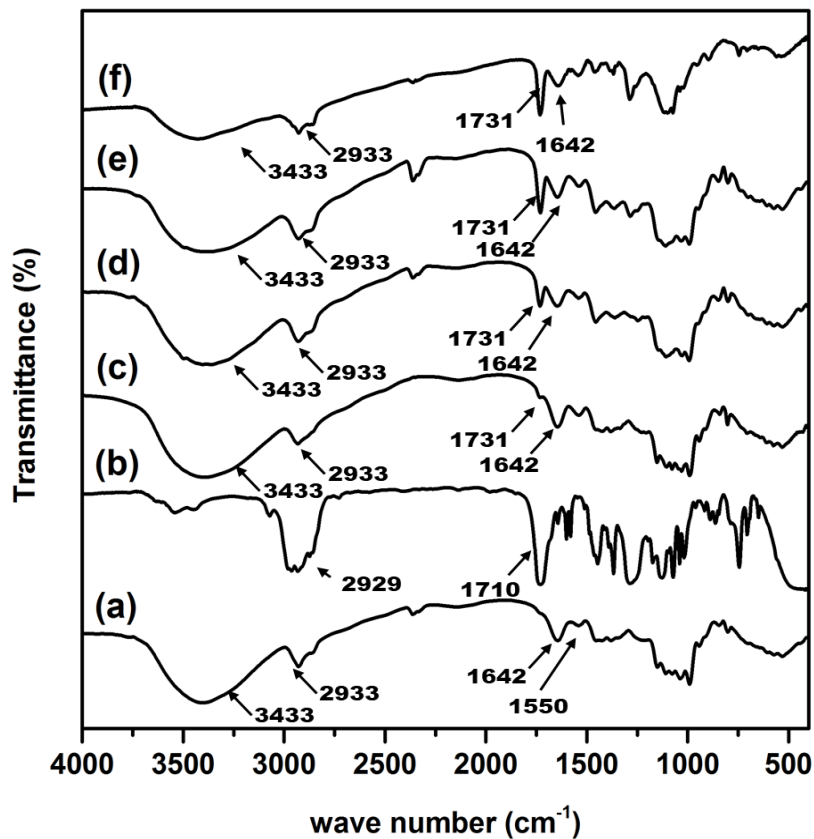


**Figure 44:** FT-IR of CS NP(a), pure GTO (b) and CS/GTO NP (c-f) with different ratios of CS: GTO: 1:0.25 (c), 1:0.50 (d), 1:0.75 (e) and 1:1.00 w/w (f).

### 3.4.E. Thermal gravimetric analysis (TGA) of CS, EOs and NPs

TGA analysis was performed as represented by **Figure (45)** to study the thermal stability of both essential oil and nanoparticles.

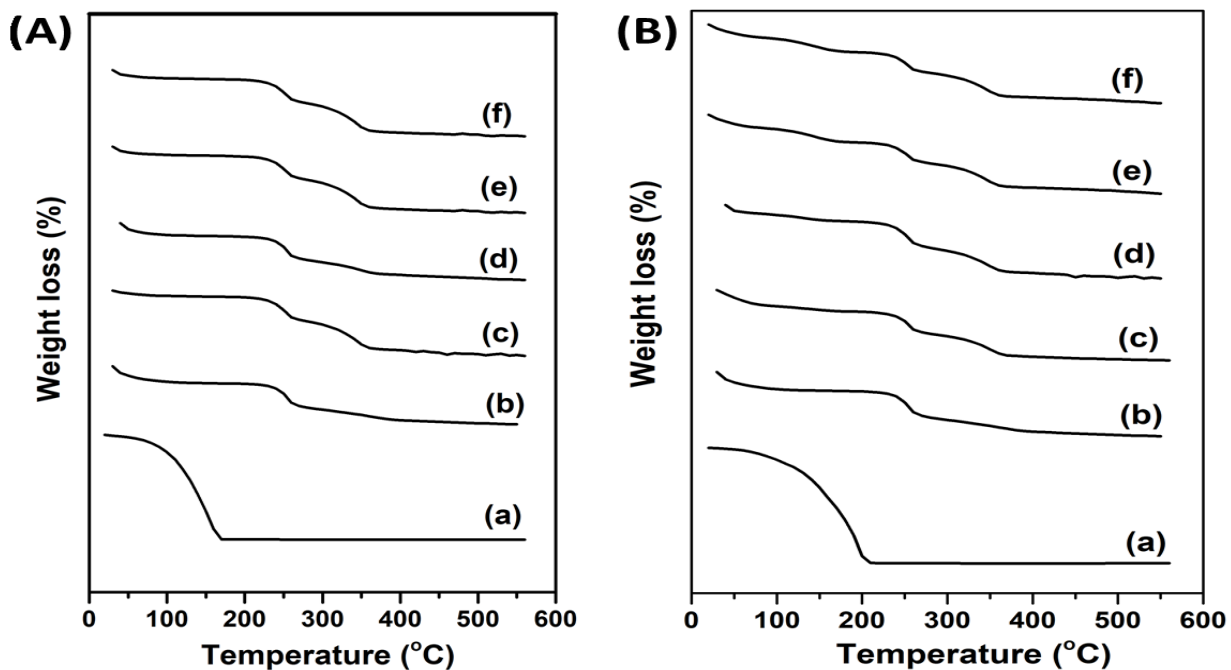


**Figure 45:** TGA thermogram of CS/PO NP (A) and CS/GTO NP (B): pure EO (a), CS NP (b) and CS/EO NP (c-f) with different ratios of CS: EO 1:0.25 (c), 1:0.50 (d), 1:0.75 (e) and 1:1.00 w/w (f).

The temperature at which material subjected to a highest rate of weight loss is called degradation temperatures ( $T_d$ ) that is identified from estimating the first derivative of the TGA curve at the higher significant weight change which is called derivative thermogravimetry (DTG) thermogram **Figure (46)**.

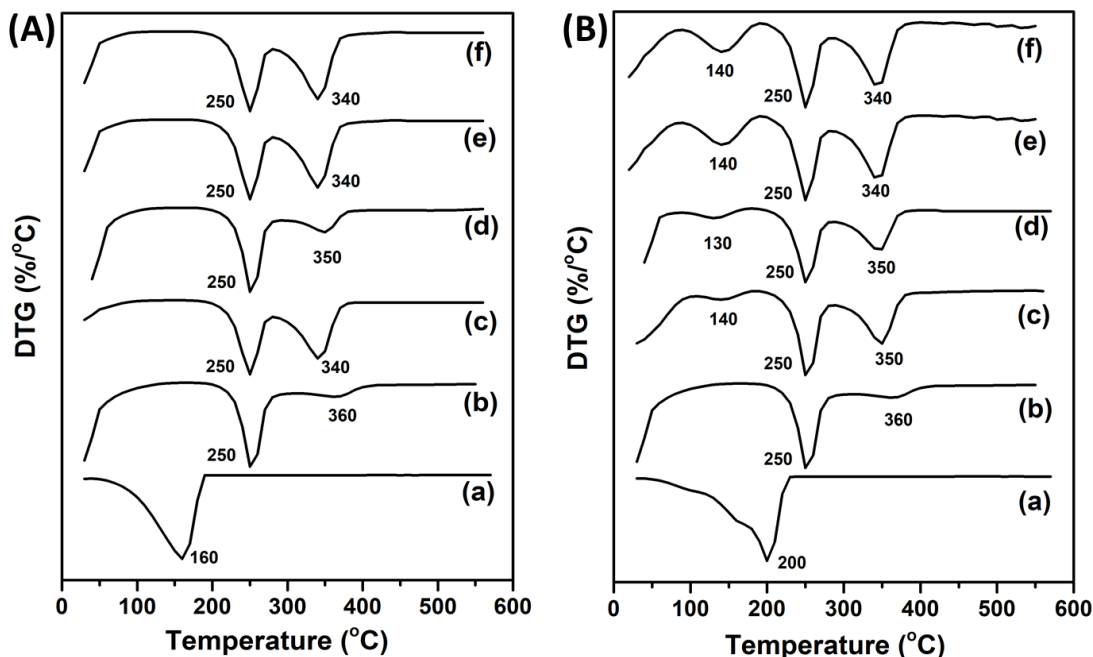


**Figure 46:**DTG thermogram of CS/PO NP (A) and CS/GTO NP (B): pure EO (a), CS NP (b) and CS/EO NP (c-f) with different ratios of CS: EO 1:0.25 (c), 1:0.50 (d), 1:0.75 (e) and 1:1.00 w/w (f).

TGA thermogram of pure PO and GTO showed one mass loss step started at 50 °C (**Figure 45A-a** and **45 B-a**) respectively. The degradation temperatures ( $T_d$ ) of pure PO and pure GTO were 160 °C and 200 °C as shown in **Figure (46 A-a)** and **Figure (46 B-a)**. The previous results indicate the lower thermal stability of both EO.

On the other hand, CS NPs exhibited two-step mass loss (**Figure 45 A-b**) at 90 °C due to the evaporation of moisture and at 250 °C (**Figure 46A – b**) assigned to dehydration and decomposition of the CS<sup>56,108,113</sup>.

CS/GTO NPs exhibited a new step mass from 90-180 °C ( $T_d$  of 140 °C) due to decomposition of free GTO that might be adsorbed on the surface of NPs, which was found to be in agreement

with the finding of (Yoksan et al., 2011)<sup>76</sup> who found that the free carvacrol that adsorb on the surface of CS NPs had a Td of 185°C<sup>62</sup>.

Surprisingly, both CS/PO NPs and CS/GTO NPs with different concentrations exhibited new step mass loss from 280 to 380 °C (**Figure 45 A and B (c-f)**) with a degradation temperature (Td) of (340-350 °C) for both NPs as represented in **Figure (46 A and B (c-f))**. The new step mass loss may reflect the encapsulated PO and GTO which degraded at higher temperature.

These results are in a good agreement with the findings of (Hosseini et al., 2013)<sup>108</sup>, (Yoksan et al., 2011)<sup>62</sup> and (Wu et al., 2005)<sup>114</sup>. All these previous reports showed a degradation temperature ranged between 320 to 340 °C after encapsulation of oregano and ammonium glycyrrhizinate in CS-TPP nanoparticles.

Encapsulated PO and GTO decomposed at 350 °C than free PO and GTO that were decomposed at 160 °C and 200 °C, respectively reflecting the significant improvement of the thermal stability

#### **3.4.F. Powder X-ray Diffraction (XRD) analysis of CS, and NPs**

The crystallographic structure of CS powder, CS NPS, CS/PO NPs and CS/GTO NPs were determined by XRD as shown in **Figure (47)**. CS powder exhibits two characteristic peaks: first peak at  $2\theta$  of 10° and second peak at 20° indicating a higher degree of crystallinity which is similar to what was previously reported by (Yoksan et al., 2011)<sup>62</sup> and (Hosseini et al., 2013)<sup>108</sup>. However, no peak is found in case of CS NPs after TPP cross linking indicating destruction of native crystalline packing structure of CS powder after preparation of CS NPs which was found to be similar to what was previously reported by (Yoksan et al., 2010)<sup>113</sup>, (Jingou et al., 2010)<sup>115</sup> and (Hosseini et al., 2013)<sup>108</sup>. Diffraction pattern of CS/PO NPs and CS/GTO NPs (1:1.00) shows an observed broad peak at  $2\theta$  ranged between 15°-24° more than that in CS NPs

confirming encapsulation of PO in CS NPs which is agreed to the findings of (Hosseini et al., 2013)<sup>108</sup>.

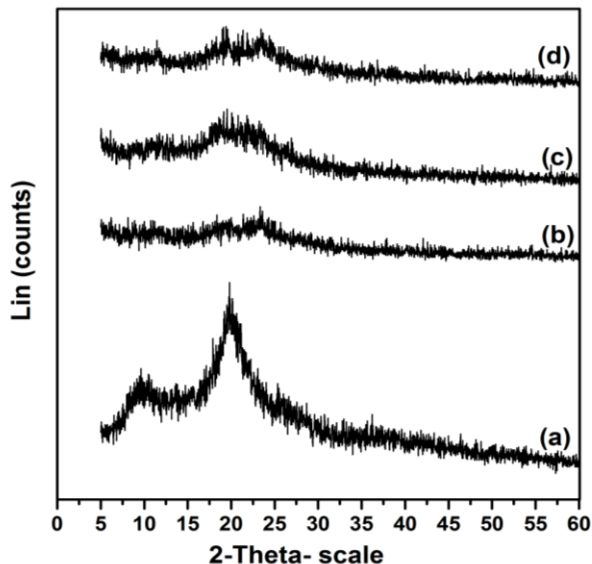


**Figure 47:** XRD pattern of CS powder (a), CS NPs (b), CS/GTO NPs (1:1 w/w) (c) and CS/PO NPs (1:1 w/w) (d).

### 3.5. Determination of the Encapsulation Efficiency (EE%) and loading capacity (LC%) of NPs.

For estimating the amount of both GTO and PO that encapsulated in NPs, UV–Vis spectrophotometry were used. The amount of encapsulated PO was estimated from measuring of the absorbance PO at the wavelength of (227 nm) according to (Deka et al., 2016)<sup>77</sup> as represented in **Figure (48 A)**.

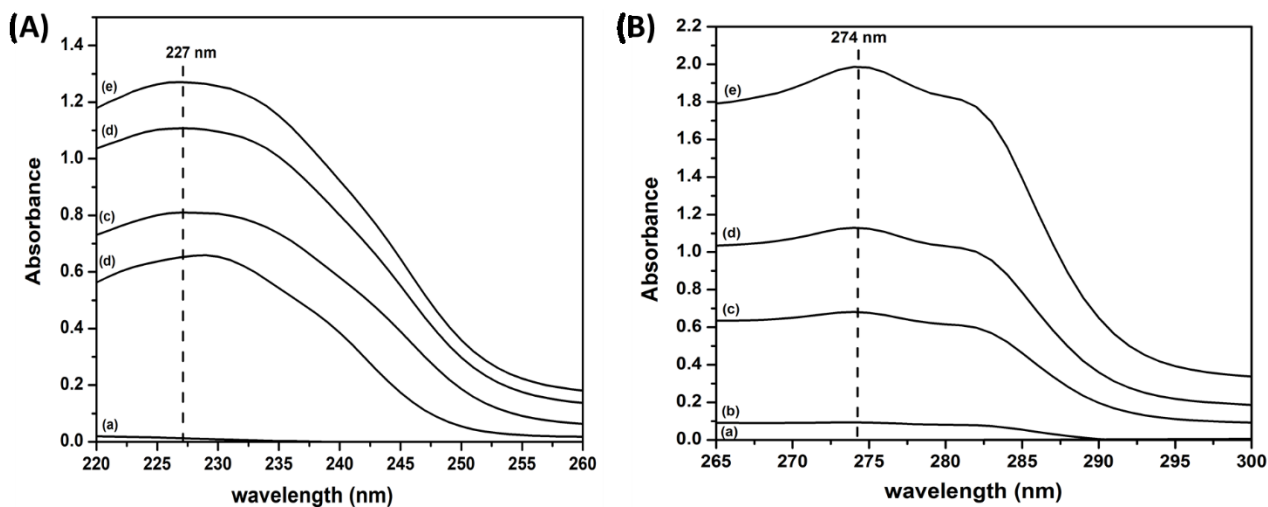


**Figure 48:** UV-Vis spectra of CS/PO NP (A) and CS/GTO NP (B): CS NPs (a) and CS/EO NPs (b-e) with different ratios of CS: EO 1:0.25 (c), 1:0.50 (d), 1:0.75 (e) and 1:1.00 w/w (f).

Standard calibration curve of PO in concentration between (0.1 to 0.7 mg/mL) in ethanol was prepared and a regression line with  $R^2$  of 0.999 was achieved as shown in **Figure (49 A)**.

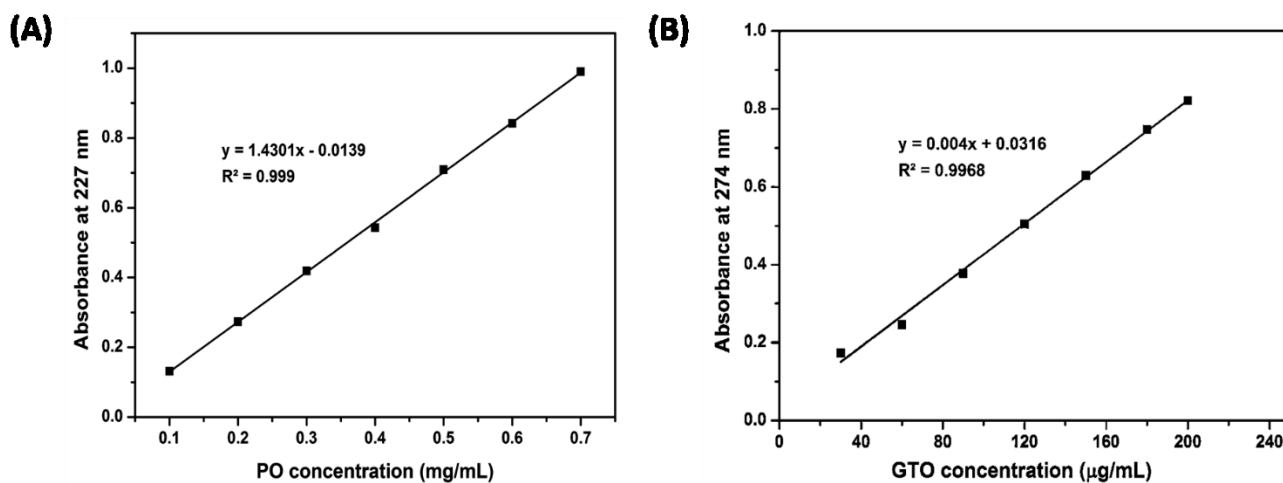


**Figure 49:** Calibration curve of (A) PO in ethanol and (B) GTO in ethanol.

Encapsulation efficiency (EE%), which is the ratio of encapsulated PO to total PO<sup>108</sup>, in CS/PO NPs with PO concentration of 0.25, 0.50, 0.75 and 1.00 (w/w CS) showed an EE% of  $(82.1 \pm$

7.55,  $79.4 \pm 4.1$ ,  $76.7 \pm 1.3$  and  $78.4 \pm 1.95$  %). The EE% results (**Figure 50A**) showed that statistically no change in EE% with increasing the PO content. On the other hand, the loading capacity (LC%), which is the ratio of encapsulated PO to the total weight of NPs<sup>108</sup>, in CS/PO NPs with PO concentration of 0.25, 0.50, 0.75 and 1.00 (w/w CS) showed an LC% of ( $8.15 \pm 0.75$ ,  $13.1 \pm 0.74$ ,  $17.6 \pm 0.5$  and  $22.2 \pm 0.55$  %) as represented in **Figure (50A)**. The results indicated that LC% enhanced with increasing the initial PO content. Maximum EE% identified at CS/PO ratio of 1:0.25 w/w while maximum LC% appeared at ratio of 1:1 w/w.

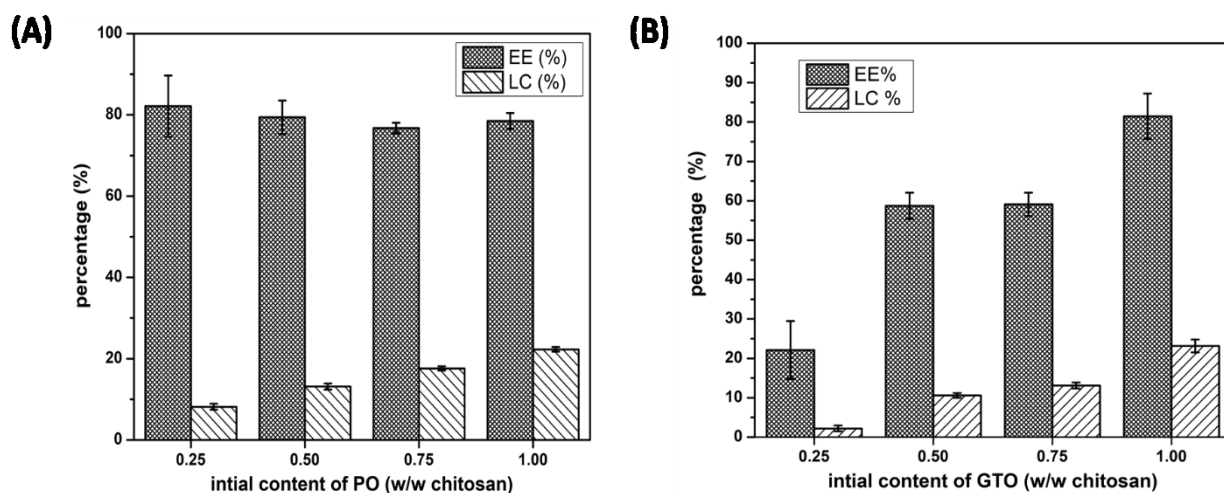


**Figure 50:** EE% and LC% of (A) CS/PO as a function of initial PO content and (B) CS/GTO as a function of initial GTO content

The amount of encapsulated GTO was estimated from the absorbance at the wavelength of (274 nm) according to (Pan et al., 2016)<sup>116</sup> as represented in **Figure (48 B)**. Standard calibration curve of GTO in concentration between (30- 200  $\mu\text{g/mL}$ ) in ethanol was prepared and a regression line with  $R^2$  of 0.996 was achieved as shown in **Figure (49 B)**. The EE% in CS/GTO NPs with GTO concentration of 0.25, 0.50, 0.75 and 1.00 (w/w CS) showed an EE% of ( $22.13 \pm 7.36$ ,  $58.72 \pm 3.32$ ,  $59.12 \pm 2.96$  and  $81.46 \pm 5.76$ ). The EE% results showed that increasing the GTO content

up to the ratio of (1:1 w/w) led to an increase in EE% as shown in **Figure (50B)**. On the other hand, the LC% in CS/GTO NPs with GTO concentration of 0.25, 0.50, 0.75 and 1.00 (w/w CS) showed an LC% of ( $2.2 \pm 0.72$ ,  $10.6 \pm 0.6$ ,  $13.08 \pm 0.75$  and  $23.14 \pm 1.63$  %) as represented in **Figure (50B)**. The results indicated that LC% increased with increasing in GTO content. Maximum EE% and LC% identified at CS/GTO ratio of 1:1.

EE% results showed that increasing the PO content up to the ratio of (1:0.75 w/w) led to a decrease in the EE% that might be as a result of the encapsulation limitation of PO in CS-TPP system, which was found to be in agreement with the findings reported on the encapsulation of ascorbyl palmitate (Yoksan et al., 2010)<sup>113</sup> and Oregano (Hosseini et al., 2013)<sup>108</sup>. On the other hand, EE% results showed that increasing the GTO content up (1:1.00 w/w) led to an increase in EE% .Furthermore, the LC% of both GTO and GTO enhanced with increasing the initial PO and GTO content, respectively which is in agreement with the findings reported on the encapsulation of ascorbyl palmitate by (Yoksan et al., 2010)<sup>113</sup> and Oregano (Hosseini et al., 2013)<sup>108</sup>.

### **3.6. *In-vitro* release studies of NPs**

The *in-vitro* release study of PO from CS/PO NPs (1:1.00 w/w) NPs was carried out for 96 hours in different pH media (3 and 7.4) to confirm the successful encapsulation of PO, and to determine the rate of PO releasing from the NPs. Based on the release rate, the release profile of PO showed three different release stages, as represented in **Figure (51)**. The initial burst release was observed for the first 6 hours, PO was released up to  $34.8 \pm 1.63$  % and  $40.7 \pm 0.73$  % in acetate buffer of (pH 3), and phosphate buffer saline (PBS) of (pH 7.4), respectively. A significantly decreased in release rate was observed in the second stage (from 6 hours to 72 hours), PO was released up to  $50.7 \pm 0.24$  % and  $61.3 \pm 4.93$  % in acetate buffer and PBS, respectively. The final stage (from 72 hours to 96 hours) showed the release of PO reaching

plateau at this stage and PO was released up to  $52.7 \pm 0.24\%$  and  $63.3 \pm 3.9 \%$  in acetate buffer and PBS, respectively. The amount of PO released was affected by the pH of the media. At acidic media (pH 3), PO was released from CS NPs rapidly than at higher pH media (pH 7.4).

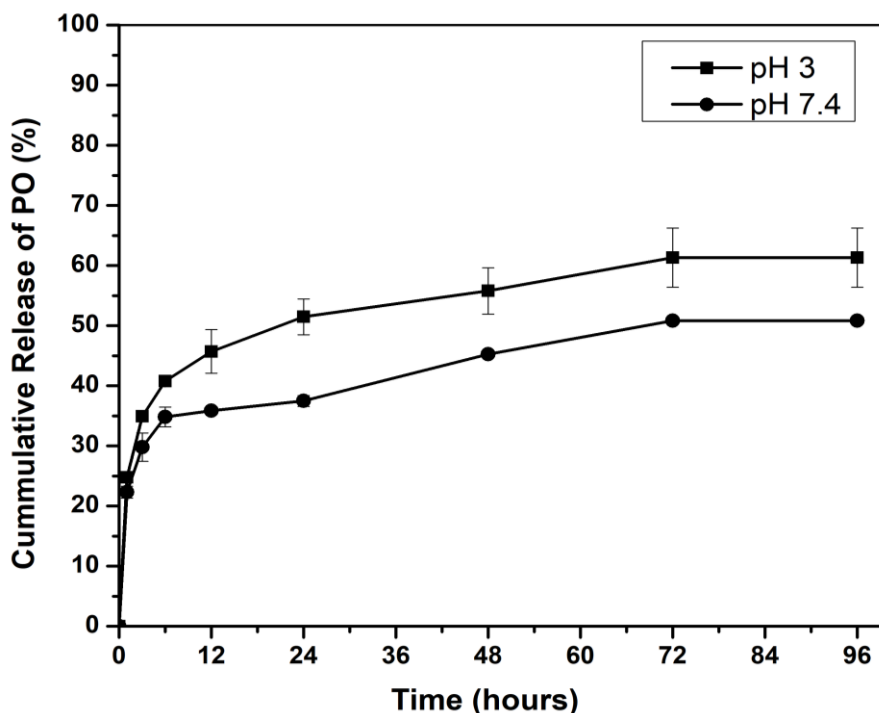


**Figure 51:** *In-vitro* release profiles of PO from CS/PO NPs (1:1) in different pH media: pH 3 and pH 7.4.

The *in-vitro* release study of GTO from CS/GTO NPs (1:1.00 w/w) NPs was carried out for 72 hours in different pH media (3 and 7.4). Based on the release rate, the release profile of GTO showed three different release stages, as represented in **Figure (52)**. The initial release was detected for the first 6 hours, GTO was released up to  $66.7 \pm 11.28 \%$  and  $53.8 \pm 8.89 \%$  in acetate buffer and PBS, respectively. The release rate significantly decreased for the second stage (from 6 to 12 hours), GTO was released up to  $74.5 \pm 12.75$  and  $62.97 \pm 9.17 \%$  in acetate buffer and PBS, respectively. The final stage (from 12 hours to 72 hours) showed the release of

GTO reaching plateau at this stage and GTO was released up to  $74.9 \pm 10$  and  $63.1 \pm 8.83$  % in acetate buffer and PBS, respectively. Similar to PO release profile, the amount of GTO released was affected by the pH of the media. At acidic media (pH 3), GTO was released from CS NPs rapidly higher pH media (pH 7.4).

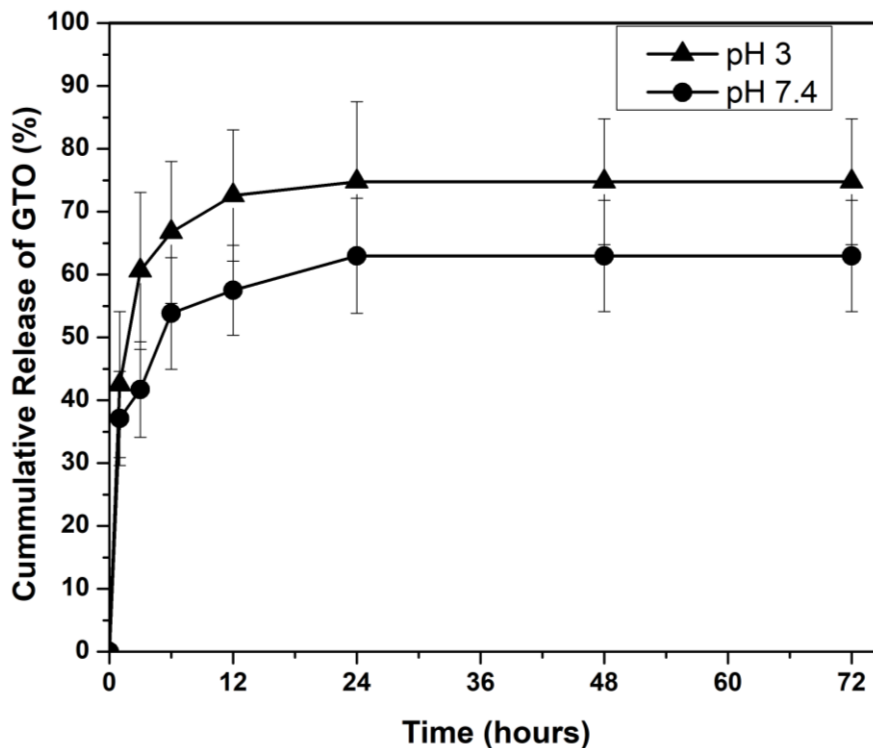


**Figure 52:** *In-vitro* release profiles of GTO from CS/GTO NPs (1:1.00) in different pH media: pH 3 and pH 7.4.

As represented in the previous results, the amount of PO and GTO released was affected by the pH of the media. At acidic media (pH 3), both PO and GTO were released from CS NPs very quickly, and the released PO and GTO contents were significantly higher than that occurs at higher pH media (pH 7.4) which is most probably due to the swelling and partial dissolution of the NPs that are shown in **Figure (53)**<sup>62</sup>.

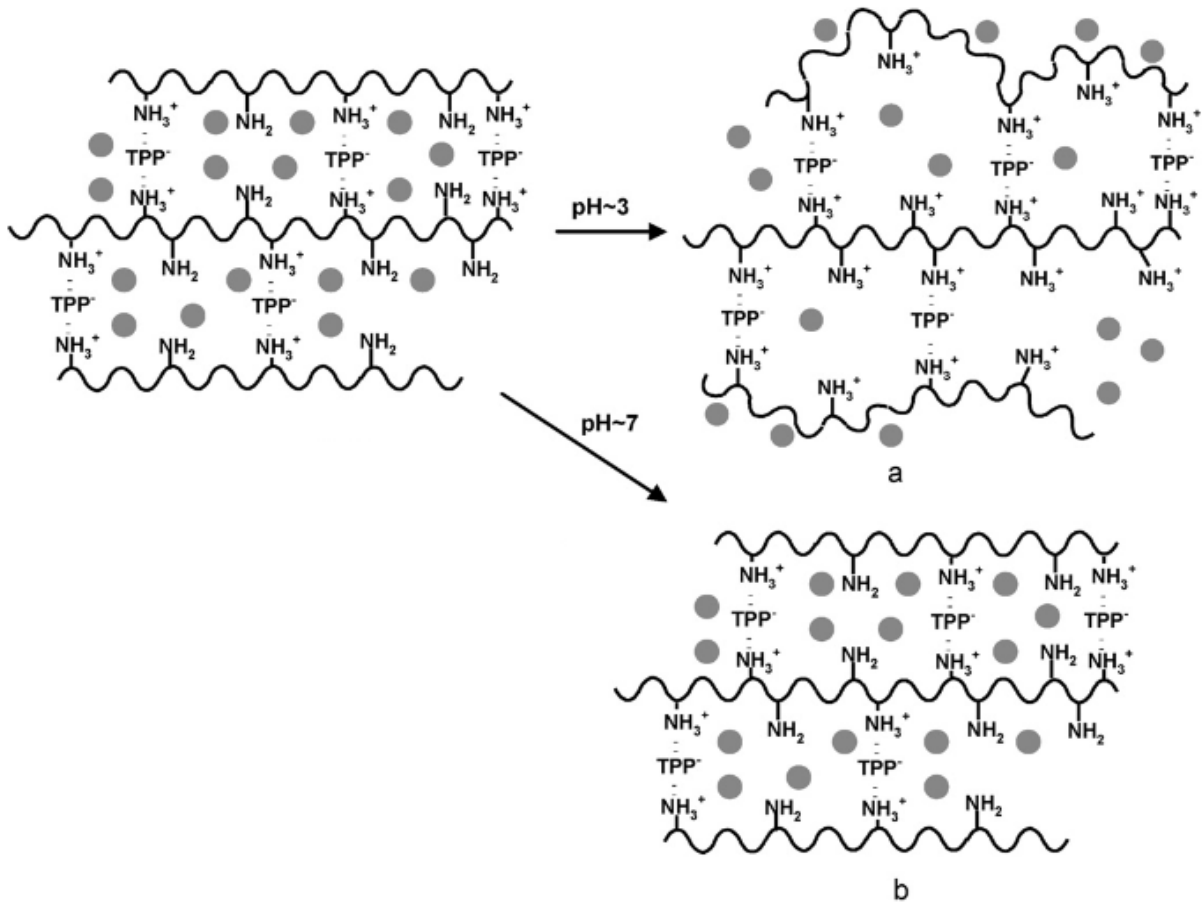


**Figure 53:** Impact of pH of the release media on CS-TPP system<sup>76</sup>.

It should be pointed out that the released PO and GTO were not completely released from NPs because complete release needs complete degradations of CS NPs. The release results agreed to the findings reported on the release of carvacrol from CS-TPP system (Yoksan et al., 2011)<sup>62</sup>.

### 3.7. Stability of phenolic contents in CS NPs

To investigate antioxidant activity of both PO and GTO, electron-transfer reaction including the total phenolic assay using Folin–Ciocalteu reagent was used<sup>61</sup>.

In the case of PO, each gram was equivalent to  $1.15 \pm 0.01$  mg GAE, while, on the other hand, each gram of GTO was equivalent to  $7.15 \pm 0.29$  mg GAE, which is about 6.21 folds increase in TPC, as shown in **Figure** (54). This significantly higher TPC in GTO over PO is basically due to the difference in the origin and composition of both EOs which was also confirmed by the GC/MS/MS findings of both EOs.

To study the ability of CS NPs to maintain the stability of phenolic contents of both PO and GTO; the CS NPs, CS/PO NPs and CS/GTO NPs were assayed for their TPC using Folin–Ciocalteu reagent for 6 hours. As shown in **Figure** (54). CS NPs, CS/PO NPs and CS/GTO NPs has TPC of  $0.06 \pm 0.01$ ,  $1.08 \pm 0.01$  and  $7.39 \pm 0.29$  mg gallic acid, respectively.

TP content that arise for CS NPs might be explained by chromogenes that formed after the reaction between CS and Folin–Ciocalteu reagent as previously reported by (Esmaeili et al., 2015)<sup>117</sup>, (Moradi et al., 2012)<sup>118</sup> and (Ruiz-Navajas et al., 2013)<sup>119</sup>.

Both CS/PO NPs and CS/GTO NPs have significantly higher TPC than CS NPs. On the other hand, the TPC that identified for encapsulated PO is significantly lower than free PO that might be due to slow release profile of PO as mentioned in the *in vitro* analysis section which agree with the findings of (Esmaeili et al., 2015)<sup>117</sup>. On the other hand, for encapsulated GTO showed statistically no change in the TPC than free GTO. Based on these results, CS NPs can maintain the stability of TPC.

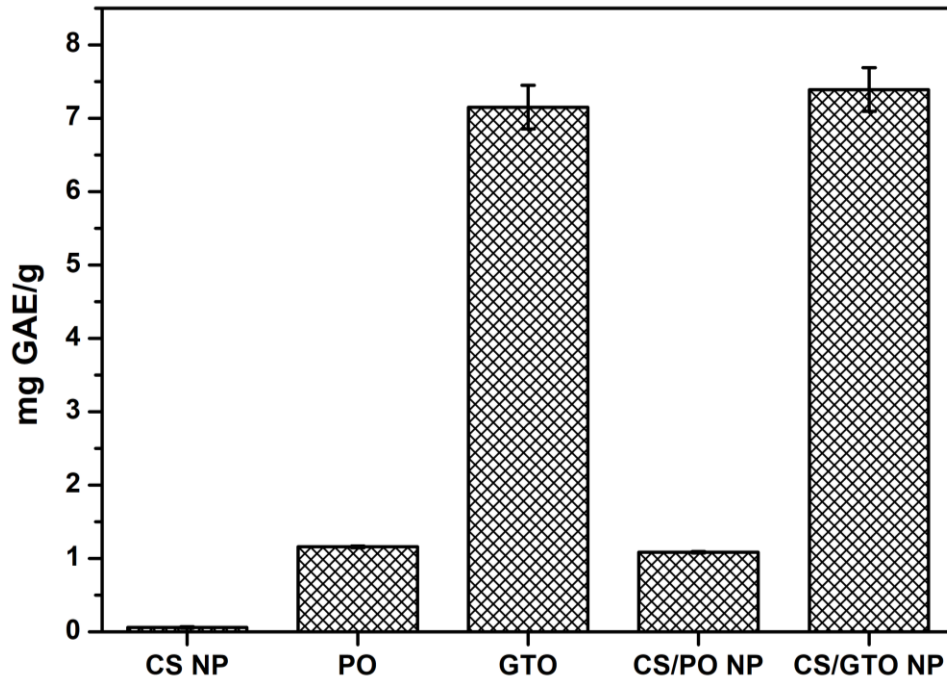


**Figure 54:**TPC of CS NPs, PO, GTO, CS/GTO NPs and CS/PO NPs expressed in (mg GAE/g oil).

# **Chapter 4**

## **Antioxidant and antibacterial activities of Chitosan/ (Peppermint and Green Tea Oil) Nanoparticles**

## Chapter 4: Antioxidant and antibacterial activities of Chitosan/ (Peppermint and Green Tea Oil) Nanoparticle

### 4.1. Evaluation of antioxidant activity of EOs NPs

DPPH assay was one of the suitable methods to determine the antioxidant activity of the EO and their CS NPs counterparts in an *in-vitro* condition. DPPH molecule (**Figure 55**) has the capability to oxidize molecules by acting as hydrogen ion acceptor. Thus, this assay was used to estimate the antioxidant activity of many EOs formulations<sup>117,120</sup>.

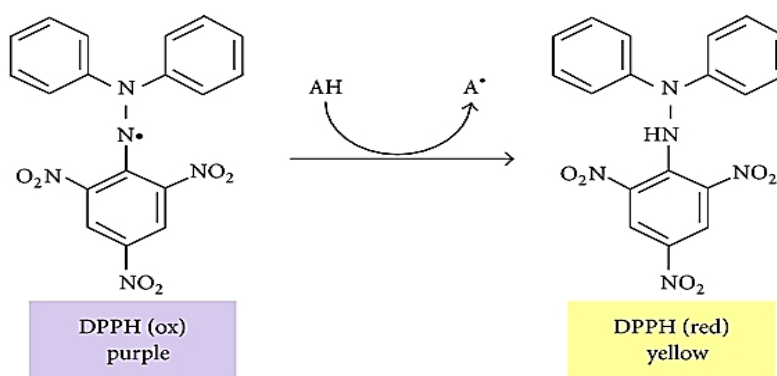


**Figure 55:** Mechanism of DPPH oxidation<sup>120</sup>.

According to **Figure (56)**, DPPH radical scavenging ability was identified for predetermined CS/PO NPs and corresponding PO and CS NPs amounts. CS NPs have antioxidant activity that ranges between 9.3 to 21.13% for concentration ranges between 6 to 48 mg/mL respectively. On the other hand, both CS/PO NPs and corresponding amounts of pure PO (range between 0.4 – 3.5 mg/mL) show a concentration-dependent antioxidant activity (**Figure 56**) and were in the range of 24.4 - 71.4 and 13 to 52.3%, respectively.

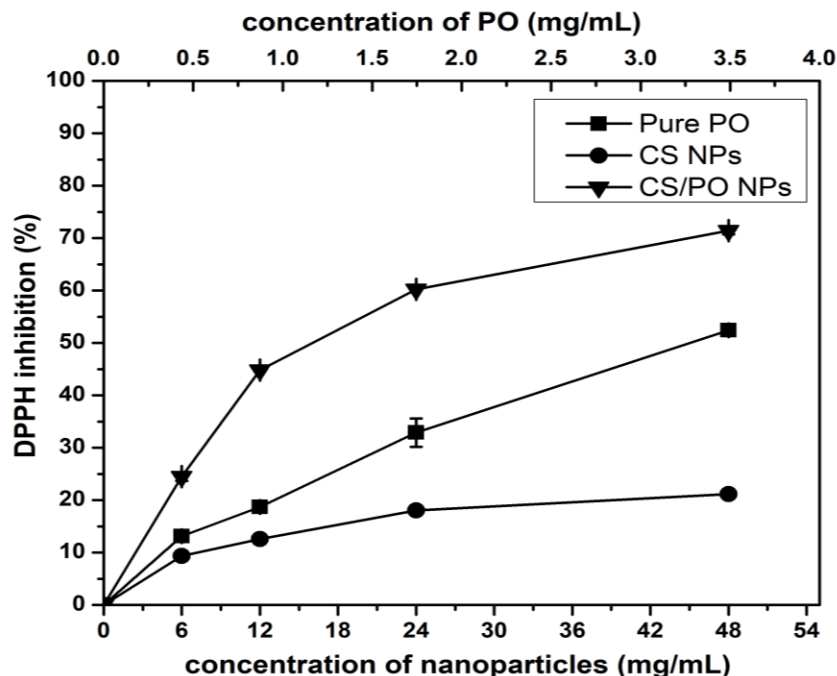


**Figure 56:** DPPH inhibition (%) of pure PO, CS NPs and CS/PO NPs.

Furthermore, DPPH radical scavenging ability was identified for predetermined CS/GTO NPs and corresponding GTO and CS NPs amounts. CS NPs have antioxidant activity that ranges between 5 to 18 % for concentration ranges between 2.5 to 20.1 mg/mL respectively that shows a limited antioxidant activity as mentioned above. It should be pointed out that the difference in CS NPs % DPPH inhibition between CS/PO system and CS/GTO system is due to using different concentration range of CS NPs due to the difference in % DPPH inhibition of pure PO and GTO. On the other hand, both CS/GTO NPs and corresponding amounts of pure GTO (range between 0.19 – 1.58 mg/mL) show a concentration-dependent antioxidant activity (**Figure 57**) and were in the range of 45.9 – 94.2 and 26.9 to 73.1%, respectively.

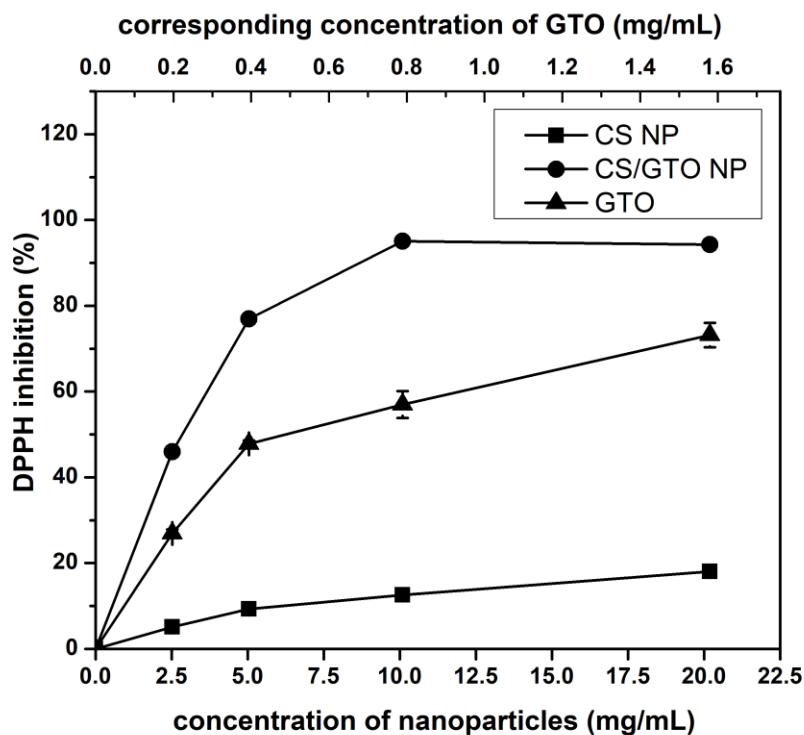


**Figure 57:** DPPH inhibition (%) of pure GTO, CS NPs and CS/GTO NPs.

Based on the previous results, the  $IC_{50}$  (concentration required to scavenge DPPH radicals by 50%) was calculated for PO, GTO, CS, CS/PO NPs and CS/GTO NPs as shown in **Table (9)**.

**Table 8:**  $IC_{50}$  of antioxidant activities of PO, GTO, CS NPs, CS/PO NPs and CS/GTO NPs.

Sample	$IC_{50}$ (mg/mL)
<b>PO</b>	3.25
<b>GTO</b>	0.81
<b>CS NPs</b>	116.07
<b>CS/PO NPs</b>	22.20 (1.61 mg/mL for corresponding PO)
<b>CS/GTO NPs</b>	4.40 (0.34 mg/mL for corresponding GTO)

As represented in (**Table 8**), CS/NPs showed a limited antioxidant activity ( $IC_{50}$ ) of 116.07 mg/mL that agrees to the findings of (Chen et al., 2009)<sup>78</sup> and (Esmaeili et al., 2015)<sup>117</sup>. The reason behind that might be related to the CS, TPP crosslinking which masks the CS amino groups responsible for the reaction with DPPH molecules as was mentioned by (Xie et al., 2001)<sup>121</sup>, (Chen et al., 2009)<sup>78</sup>, (Barzegar et al., 2016)<sup>122</sup> and (Esmaeili et al., 2015)<sup>139</sup>. On the other hand, bulk PO and GTO showed antioxidant activities ( $IC_{50}$ ) of 3.25 mg/mL and 0.81 mg/mL. It should be noted that the antioxidant activity of pure GTO was significantly higher than PO by about 4 folds. The reason behind that might be due to the impact of phenolic contents that are found in higher amount in GTO than PO as mentioned in chapter 4. To enhance the antioxidant activity of both bulk EOs, nano-encapsulated EOs were tested against DPPH.

Surprisingly, the antioxidant activity of encapsulated PO was significantly higher than free PO by 2 folds. However, the antioxidant activity of PO was not significantly higher than CS NPs. Similarly, the antioxidant activity of encapsulated GTO was improved significantly than free GTO and by ~2.4 folds. The antioxidant activity findings of both EOs agree with the findings of (Barzegar et al., 2016)<sup>122</sup> in enhancement of the antioxidant activity of encapsulated thyme oil in CS NPs by 24.45%, and (Woranuch et al., 2013)<sup>53</sup> in the improvement of scavenging activity of loaded eugenol in CS NPs by 2.7 fold, in addition to (Lee et al., 2011) in an increase of DPPH inhibition of astaxanthin in calcium alginate gel beads. The reason behind this improvements in case of PO and GTO NPs might be due to the protective effect of encapsulation that decreases evaporation rate via controlled release of PO and GTO during the assay that was identified by (Barzegar et al., 2016)<sup>122</sup> in the encapsulation of thyme oil in CS NPs.

Based on these results, encapsulation of GTO and PO in CS NPs enhanced the antioxidant activity of free GTO and PO, respectively. Furthermore, CS/GTO NPs showed a significant higher antioxidant activity than CS/PO NPs by about 4.7 folds.

## **5.2. Evaluation of the antibacterial activity of EOs NPs**

Agar dilution and colony counting methods were used to investigate the impact of encapsulation of PO and GTO on the antibacterial activity against both *Staphylococcus aureus* (*S. aureus*) and *Escherichia coli* (*E.coli*) as examples for Gram positive and Gram negative bacteria, respectively in LB agar media (Wei et al., 2009)<sup>79</sup>. The antibacterial activity was estimated through the reduction in numbers of the bacterial colonies after introducing the sample compared to the positive control (LB media with bacteria only).

### **5.2.1. Evaluation of antibacterial activity of EOs NPs against *S. aureus***

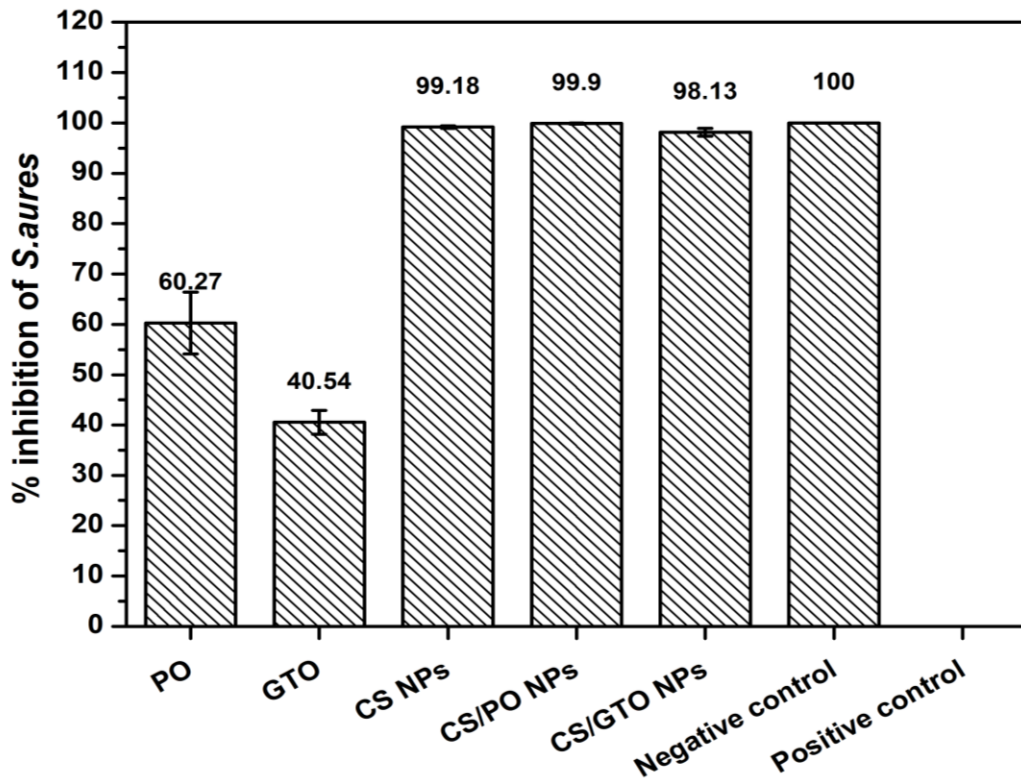
As represented in **Figure** (58A, B), positive control shows a large number of colonies indicating a good growth of *S. aureus* while the negative control shows no colonies representing the sterility of the agar medium<sup>79</sup>. Bulk PO and GTO showed antibacterial activities of  $60.2 \pm 6.12\%$  and  $40.54 \pm 2.36$ , respectively. Bulk PO and GTO antibacterial activities rely on the penetration of phytochemical components through the phospholipid of cell membrane and the damage of proteins and lipids<sup>39,123,124</sup>. It should be noted that the antibacterial activity of bulk PO was significantly higher than GTO by about 19.7% which agrees with the findings of (OSAWA et al., 1999)<sup>125</sup>. The reason behind that might be due to the presence of proteins in LB agar media that might hinder the antibacterial activity of GTO as its polyphenols bactericidal potential relies on the destruction of cell membranes proteins<sup>125</sup>. However, both bulk EOs still showed lower

antimicrobial activity. As a trial to enhance the bactericidal activity of both bulk EOs, nano-encapsulated EOs were tested against *S. aureus*.

Surprisingly, encapsulated PO showed a significant enhancement of bactericidal activity by about 39.63% over bulk PO. In the same way, a significant enhancement of the antibacterial activity was revealed for encapsulated GTO against *S. aureus* by about 57.5%. It should be noted that the maximum antibacterial activity was found in CS/PO NPs ( $99.9 \pm 0.1\%$ ). Therefore, the nano-encapsulation of both bulk EOs was a magical solution for enhancing the antimicrobial potential.

These results agree with the findings of (Esmaeili et al., 2015)<sup>117</sup> that showed an enhancement of the antibacterial activity of encapsulated *Carum copticum* essential oil (CEO) over pure CEO by 1.16 folds. On the other hand, (Yoksan et al., 2011)<sup>62</sup> showed an antibacterial activity of encapsulated carvacrol in CS NPs that was very close to free carvacrol. The reason behind the enhancement of bactericidal activity of encapsulated oils might be related to the antibacterial activity of CS NPs themselves that showed bactericidal activity against *S. aureus* by about  $99.1 \pm 0.23\%$ . CS NPs antimicrobial activity might be due to ionic interaction between the positive charge on CS and the anionic surface of bacteria.

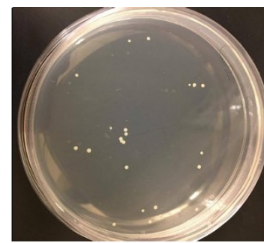
It should be noted that CS NPs, CS/PO NPS and CS/GTO NPs showed statistically no change in antibacterial activities. Based on these results, encapsulated PO showed a maximum antibacterial activity against *S. aureus*. Nevertheless, both CS/PO NPs and CS/GTO NPs could be used as an antimicrobial agent against *S. aureus*.



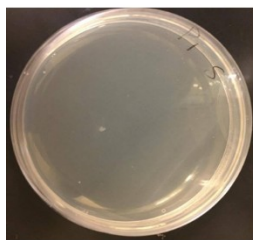
**Pure PO**



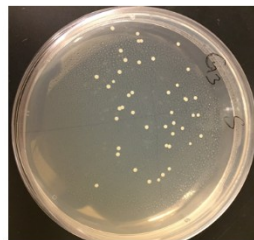
**Pure GTO**



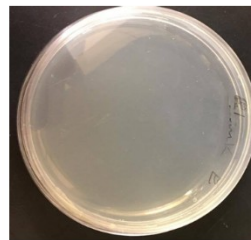
**CS NPs**



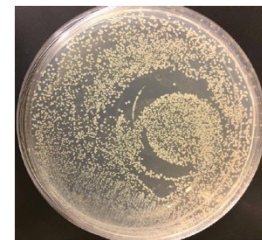
**CS/PO NPs**



**CS/GTO NPs**



**Negative control  
(LB media only)**



**Positive control  
(LB media + *S.aures*)**

**Figure 58:**(A) % Inhibition of *S. aureus* and, (B) representative photographs of the bactericidal activity toward *S. aureus* by PO, GTO, CS NPs, CS/PO NPs, CS/GTO NPs, negative and

positive control.

### 5.2.2. Evaluation of antibacterial activity of EOs NPs against *E.coli*

As represented in **Figure** (59A, B), positive control shows a good growth of *E.coli* while the negative control shows the sterility of the LB agar medium as shown with *S.aureus*<sup>79</sup>. Bulk PO and GTO showed antibacterial activities of  $94.53 \pm 0.53\%$  and  $97.3 \pm 0.34\%$ , respectively. Bulk PO and GTO antibacterial activities rely on the interaction of lipophilic oil and the phospholipid membrane that induce passive permeability<sup>126</sup>. It should be noted that the antibacterial activity of pure GTO was significantly higher than PO by about 2.77 %. The reason behind that might due to the higher GTO polyphenols and their hydrophobicity which enhances their penetration ability through cell phospholipid membranes<sup>127</sup>. In spite of the higher antibacterial activities of both bulk EOs, a further enhancement of the bactericidal activity via nano-encapsulation was tested against *E.coli*.

Similar to the antibacterial results observed with *S. aureus*, the encapsulated PO showed a statistical significant enhancement of bactericidal activity by about 3.01% over bulk PO. Similarly, a significant enhancement of the antibacterial activity was revealed for the encapsulated GTO against *E.coli* by about 1.88%. Both encapsulated GTO and PO showed antibacterial activities against *E.coli* that are very close to their bulk EOs. The reason behind that might be related to the controlled release of oils as well as the antibacterial activity of CS NPs themselves that showed bactericidal activity against *E.coli* by about  $99.2 \pm 0.68\%$  due to ionic reaction between the positive charge on CS and the anionic surface of bacteria. These results agree with the findings of (Esmaeili et al., 2015)<sup>117</sup> that showed an 1.28 folds enhancement of the antibacterial activity of encapsulated CEO over pure CEO.

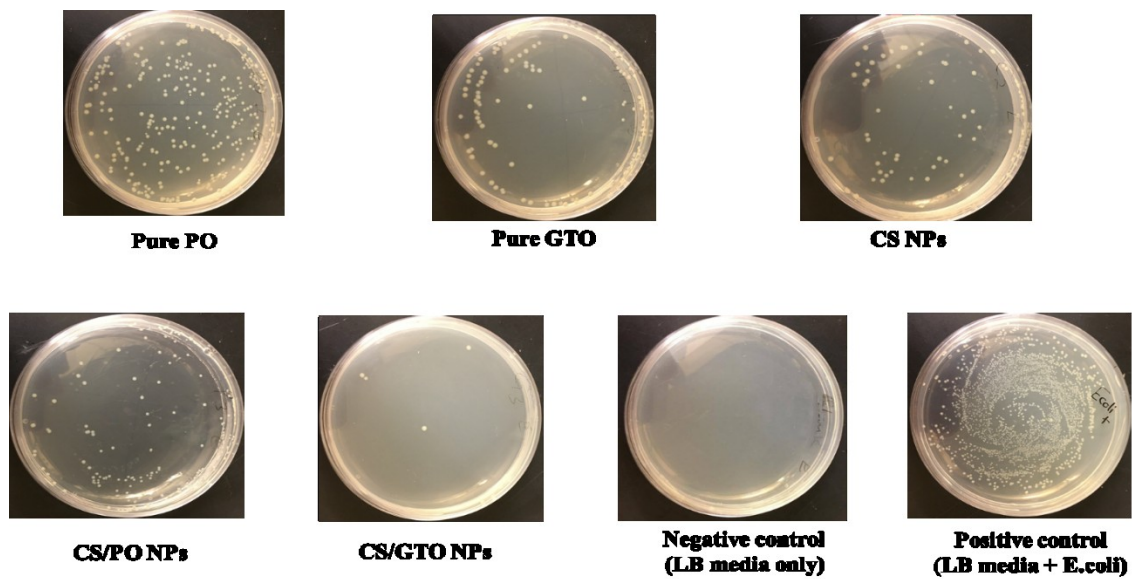
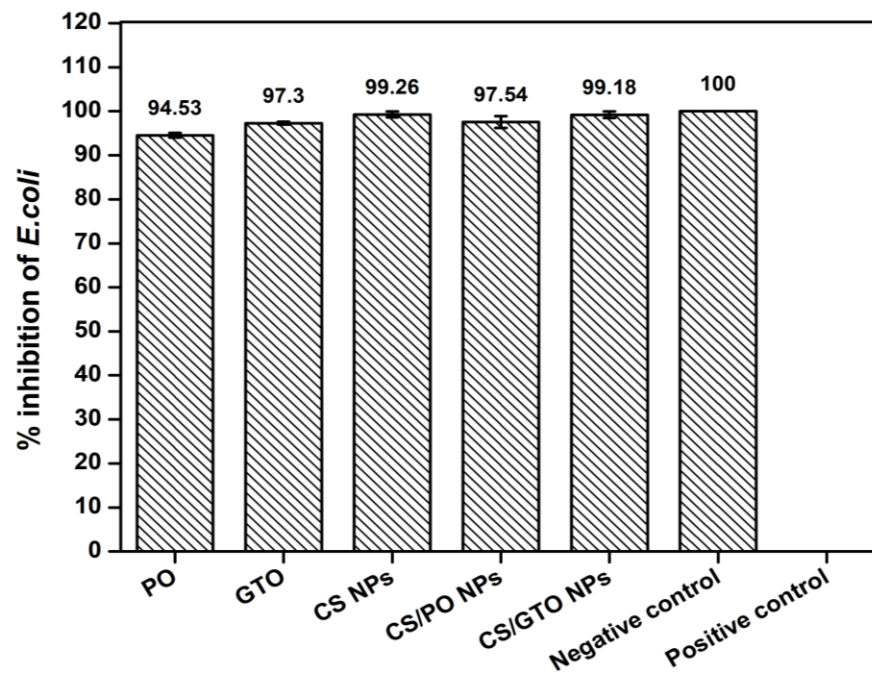


**Figure 59:** (A) % Inhibition of *E. coli* and, (B) representative photographs of the bactericidal activity toward *E. coli* by PO, GTO, CS NPs, CS/PO NPs, CS/GTO NPs, negative and positive control.

It should be noted that CS NPs, CS/PO NPS and CS/GTO NPs showed statistically no change in antibacterial activities. Based on these results, both CS/PO NPs and CS/GTO NPs could be used as an antibacterial agent against *E.coli*. Furthermore, the improvement of antibacterial activity after encapsulation of both PO and GTO in CS NPs against *S. aureus* is significantly higher than that against *E.coli*. In other words, encapsulation of PO enhanced the antimicrobial activity against *S. aureus* more than *E.coli* by 13.1 folds. Whereas, the encapsulation of GTO enhanced the antibacterial activity against *S. aureus* more than *E.coli* by 30.6 folds. The reason behind that might be due to the limited penetration of these hydrophobic EOs through hydrophilic peptidoglycan of bacterial cell wall that is normally found in Gram positive bacteria<sup>62,117,128</sup>.

# **Chapter 5**

## **Conclusion and Future Perspectives**

## Chapter 5: Conclusion and Future perspectives

In this study, two EOs namely; PO and GTO were encapsulated in CS NPs. Two-steps method was used for the encapsulation of EOs in CS NPs which is oil-in-water emulsification followed by cross-linking of CS polymer with sodium tripolyphosphate (TPP) in a process called ionic gelation. To characterize the encapsulated EOs, different characterization techniques were used such as; Fourier transform infrared (FT-IR) spectroscopy, powder X-ray diffraction (XRD), thermogravimetric analysis (TGA) and UV–vis spectrophotometry. Both NPs formulations (CS/PO NPs and CS/GTO NPs) showed a spherical shape with size range of 20-90 nm as detected by Transmission electron microscopy (TEM). As determined by UV–vis spectrophotometry, the EE% of CS/PO NPs and CS/GTO NPs were about 82-78% and 22-81%, respectively, when the initial EO amount was 0.25–1 w/w CS. whereas, the LC% of CS/PO NPs and CS/GTO NPs were about 8-22% and 2.2-23%, respectively for the initial EO amount was 0.25–1 w/w. Furthermore, *in-vitro* release studies of both EOs showed an initial burst effect and followed by a slow release at two different pH conditions: acidic pH (acetate buffer) and neutral pH (phosphate buffer saline). Release rate of both PO and GTO from CS NPs was higher in acetate buffer than phosphate buffer saline. PO was released over 92 hrs reaching of 63% in acetate buffer and 62% in case of phosphate buffer saline. Both PO and GTO showed a thermal stability after encapsulation in CS NPs that reach 350°C. The antioxidant activity of both pure and encapsulated PO and GTO was evaluated by 2,2-diphenyl-1-picrylhydrazyl radical (DPPH). The antioxidant activities of CS/PO NPs and CS/GTO NPs were improved by about 2 and 2.4 folds, respectively. Moreover, to study the stability of total phenolic contents (TPC), Folin–Ciocalteu was used and the results showed the ability of CS-TPP system to preserve the TPC. Finally, agar dilution and colony counting method used to study the antibacterial activity of pure

and encapsulated PO and GTO against Gram positive (*S. aureus*) and Gram negative (*E.coli*) bacteria. Against (*S. aureus*), encapsulated PO showed an enhanced antibacterial activity by about 39.63%, while encapsulated GTO showed an improvement in antibacterial activity by about 57.5% on the other hand, against Gram negative bacteria, encapsulated PO showed an enhanced antibacterial activity by about 3%, while encapsulated GTO showed an improvement in antibacterial activity by about 1.8%.

The study showed that the encapsulation of PO and GTO in CS NPs could protect phenolic contents of PO and GTO, enhance the thermal stability of EOs, improve the antioxidant activity, and improve the antimicrobial activity. Based on these results, the encapsulating of PO and GTO in CS NPs are promising candidates to be used in nutraceutical, cosmetic and pharmaceutical applications.

Further research might be necessary to determine the stability of the EOs properties after encapsulation process with CS NPs under different conditions. For examples, other EOs could be used following the same protocols. In addition, different strains of bacteria could also be investigated. Moreover, different forms of EOs such as nanofibers instead of NPs forms could be fabricated to investigate the influence of the nanostructures on the final antioxidant and antibacterial activities.

# Chapter 6

## Appendices

Chapter 6: Appendices

Appendix I: GC/MS/MS analysis of PO.

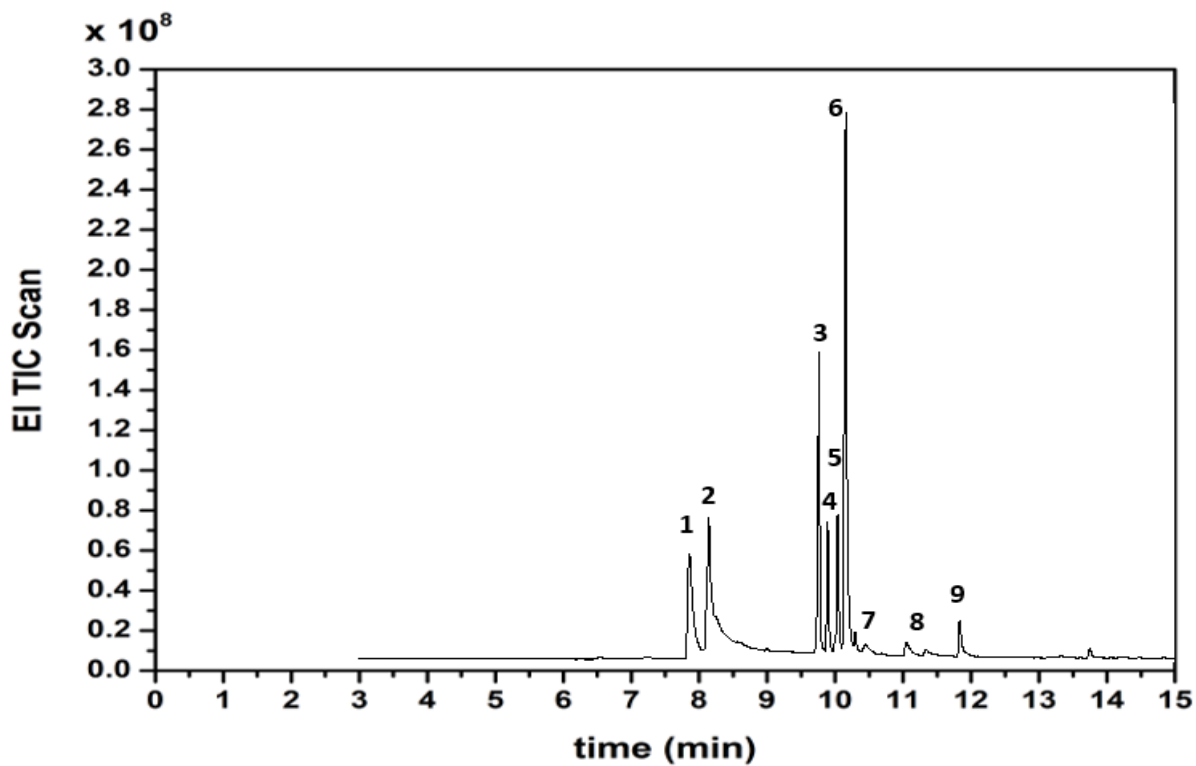


Figure 60: GC/MS/MS chromatogram of PO.

Table 9: Chemical composition of PO.

Peak number	Retention time	Chemical constituent	Relative concentration (%)
1	8.02	Glycerol trimethyl ether	14.62
2	8.289	Hexylene glycol	14.96
3	9.877	l-Menthone	14.55
4	10.012	Tetrahydrocarvone	6.55
5	10.142	Menthol	6.61
6	10.268	Citronellol	36.21
7	10.549	$\alpha$ -Terpineol	1.82
8	11.14	Pulegone	1.87
9	11.914	Levomenthol	2.8

Appendix II: GC/MS/MS analysis of GTO.

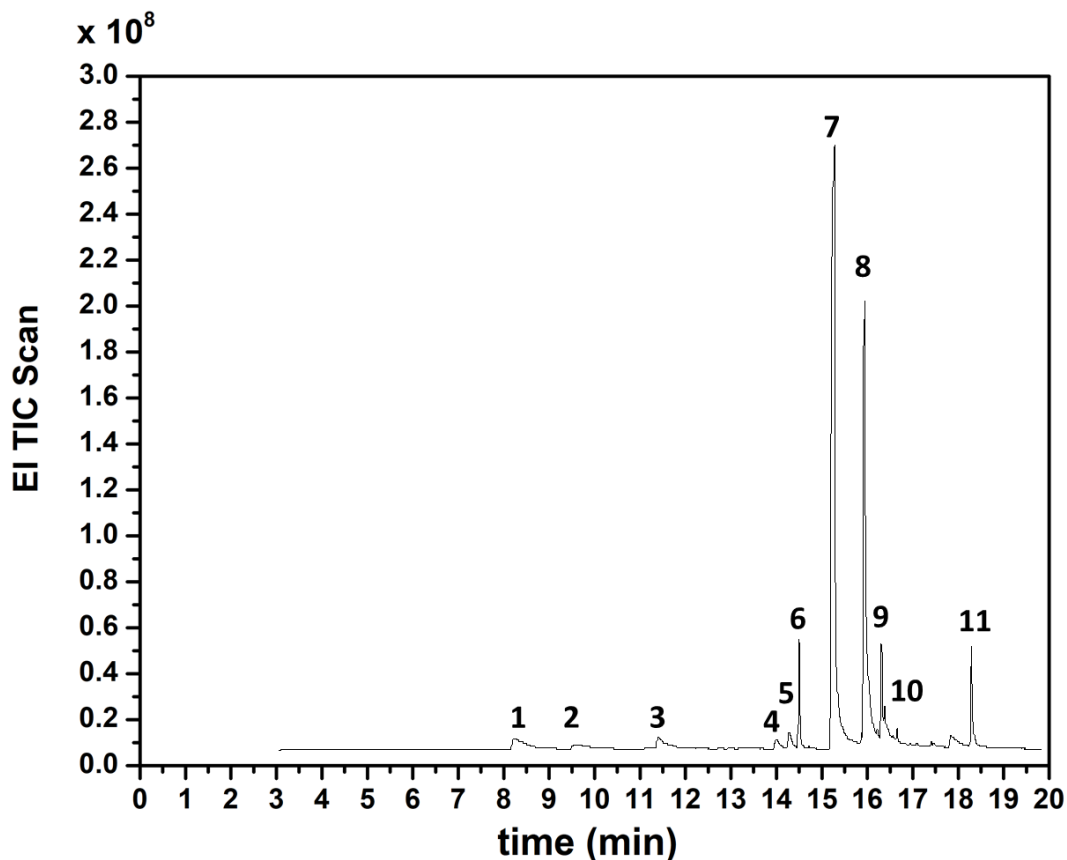


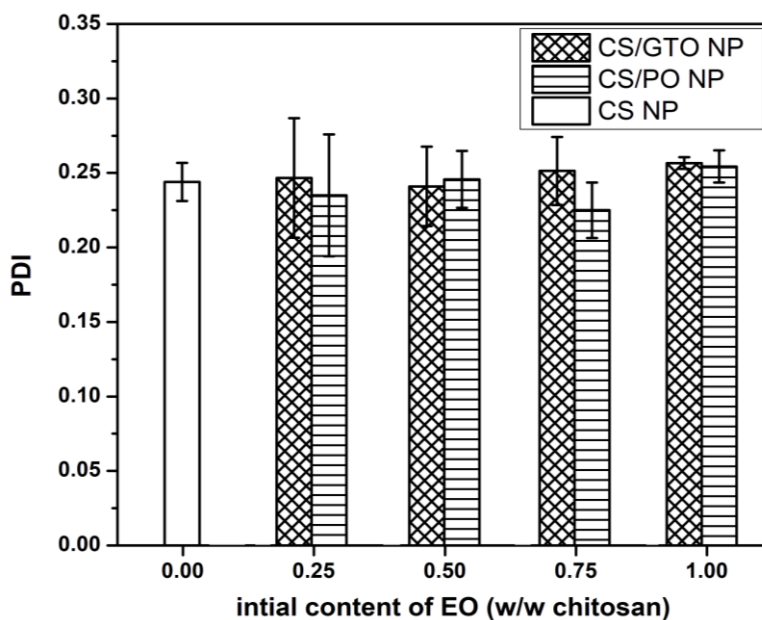
Figure 61: GC/MS/MS chromatogram of GTO.

Table 10: Chemical composition of GTO.

Peak number	Retention time	Chemical constituent	Relative concentration (%)
1	8.285	D-Limonene	2.9
2	9.637	Camphene	1.99
3	11.499	Linalyl acetate	2.91
4	14.122	Caryophyllene	0.89
5	14.415	Vitamin A aldehyde	0.77
6	14.631	$\alpha$ -Vetivol	3.57
7	15.421	4-Chromanol	54.89
8	16.089	Oleic alcohol	25.08
9	16.472	Curcumenol	2.02
10	16.819	$\beta$ -Irone	1.1
11	18.472	Galaxolide 1	3.9

### Appendix III: Polydispersity of nanoparticles

To study the size distribution of NPs, the PDI was studied using DLS technique (zetaser). As shown in Figure (62), CS NP showed PDI of 0.24. Upon introducing PO to CS-TPP system in different concentrations (0.25, 0.50, 0.75 and 1.00 (w/w CS)), results showed PDI values of (0.23, 0.24, 0.22, 0.23 and 0.25) respectively, indicating that increasing the PO content had a non-significant impact on the PDI value. The lowest PDI was that showing a higher monodispersity in dispersion which occurred with CS/PO (1:0.75 w/w). On the other hand, addition of GTO to CS-TPP system resulted in PDI values of (0.24, 0.24, 0.25, 0.24 and 0.25) in concentrations of (0.25, 0.50, 0.75 and 1.00 (w/w CS) respectively. Similarly, incorporation of GTO to CS NPs had a non-significant impact on the PDI value. The lowest PDI was that showing a higher monodispersity in dispersion that occurred with CS/GTO (1:0.50 w/w). The difference in PDI between both EOs with different concentrations were insignificant revealing the independency of CS NP size distribution on the type of EO.



**Figure 62:** PDI values of nanoparticles as a function of initial PO and GTO content.



# References

## References

- (1) Cohen, M. L. Changing Patterns of Infectious Disease. *Nature* **2000**, *406*, 762–767.
- (2) (US), N. C. for H. S.; Health, U. D. of; Services, H. *Health, United States, 1999: With Health and Aging Chartbook*; National Center for Health Statistics, 1999.
- (3) Garrod, L. P.; Lambert, H. P.; O’Grady, F. Antibiotic and Chemotherapy (Ed 4) Churchill Livingstone. *Edinb. Lond.* **1973**, 52.
- (4) Organization, W. H.; others. Removing Obstacles to Healthy Development: Report on Infectious Diseases. **1999**.
- (5) *The World Health Report 1998: Life in the 21st Century*; World Health Organization, Ed.; WHO: Geneva, 1998.
- (6) Davey, M. E.; O’toole, G. A. Microbial Biofilms: From Ecology to Molecular Genetics. *Microbiol. Mol. Biol. Rev.* **2000**, *64*, 847–867.
- (7) Watnick, P.; Kolter, R. Biofilm, City of Microbes. *J. Bacteriol.* **2000**, *182*, 2675–2679.
- (8) Costerton, J. W.; Stewart, P. S.; Greenberg, E. P. Bacterial Biofilms: A Common Cause of Persistent Infections. *Science* **1999**, *284*, 1318–1322.
- (9) Hall-Stoodley, L.; Costerton, J. W.; Stoodley, P. Bacterial Biofilms: From the Natural Environment to Infectious Diseases. *Nat. Rev. Microbiol.* **2004**, *2*, 95–108.
- (10) Flynn, W. T. The Judicious Use of Medically Important Antimicrobial Drugs in Food-Producing Animals. *Cent. Vet. Med. HFV-1 Food Drug Adm. US Dep. Health Hum. Serv.* **2012**.
- (11) Brunton, L. L.; Chabner, B. A.; Knollmann, B. C. *Chemotherapy of Microbial Diseases: Goodman & Gilman’s the Pharmacological Basis of Therapeutics, 12e*; McGraw-Hill Global Education Holdings, LLC, Section VII. <http://accessmedicine.com/resourceTOC.aspx>, 2013.
- (12) Wu, H.; Moser, C.; Wang, H.-Z.; Høiby, N.; Song, Z.-J. Strategies for Combating Bacterial Biofilm Infections. *Int. J. Oral Sci.* **2015**, *7*, 1–7.
- (13) Bbosa, G. S.; Mwebaza, N.; Odda, J.; Kyegombe, D. B.; Ntale, M. Antibiotics/Antibacterial Drug Use, Their Marketing and Promotion during the Post-Antibiotic Golden Age and Their Role in Emergence of Bacterial Resistance. *Health (N. Y.)* **2014**, *2014*.
- (14) LAUB, R.; SCHNEIDER, Y.-J.; TROUET, Andr. Antibiotic Susceptibility of Salmonella Spp. at Different PH Values. *Microbiology* **1989**, *135*, 1407–1416.
- (15) Herrmann, G.; Yang, L.; Wu, H.; Song, Z.; Wang, H.; Høiby, N.; Ulrich, M.; Molin, S.; Riethmüller, J.; Döring, G. Colistin-Tobramycin Combinations Are Superior to Monotherapy Concerning the Killing of Biofilm Pseudomonas Aeruginosa. *J. Infect. Dis.* **2010**, *202*, 1585–1592.
- (16) Pelgrift, R. Y.; Friedman, A. J. Nanotechnology as a Therapeutic Tool to Combat Microbial Resistance. *Adv. Drug Deliv. Rev.* **2013**, *65*, 1803–1815.
- (17) Stewart, P. S. Mechanisms of Antibiotic Resistance in Bacterial Biofilms. *Int. J. Med. Microbiol.* **2002**, *292*, 107–113.
- (18) Piddock, L. J. Understanding the Basis of Antibiotic Resistance: A Platform for Drug Discovery. *Microbiology* **2014**, *160*, 2366–2373.
- (19) Hancock, J. T.; Desikan, R.; Neill, S. J. *Role of Reactive Oxygen Species in Cell Signalling Pathways*; Portland Press Limited, 2001.

- (20) Jones, D. P. [11] Redox Potential of GSH/GSSG Couple: Assay and Biological Significance. *Methods Enzymol.* **2002**, *348*, 93–112.
- (21) Sies, H.; others. Oxidative Stress: Introductory Remarks. *Oxidative Stress* **1985**, 1–8.
- (22) Baser, K. H. C.; Buchbauer, G. *Handbook of Essential Oils: Science, Technology, and Applications*; CRC Press, 2015.
- (23) Tongnuanchan, P.; Benjakul, S. Essential Oils: Extraction, Bioactivities, and Their Uses for Food Preservation: Bioactivities and Applications of Essential Oils.... *J. Food Sci.* **2014**, *79*, R1231–R1249.
- (24) Bilia, A. R.; Guccione, C.; Isacchi, B.; Righeschi, C.; Firenzuoli, F.; Bergonzi, M. C. Essential Oils Loaded in Nanosystems: A Developing Strategy for a Successful Therapeutic Approach. *Evid. Based Complement. Alternat. Med.* **2014**, *2014*, 1–14.
- (25) Perineau, F.; Ganou, L.; Vilarem, G. Studying Production of Lovage Essential Oils in a Hydrodistillation Pilot Unit Equipped with a Cohobation System. *J. Chem. Technol. Biotechnol.* **1992**, *53*, 165–171.
- (26) Babu, K. G. D.; Kaul, V. K. Variation in Essential Oil Composition of Rose-Scented Geranium (*Pelargonium* Sp.) Distilled by Different Distillation Techniques. *Flavour Fragr. J.* **2005**, *20*, 222–231.
- (27) Jiménez-Carmona, M. M.; Ubera, J. L.; Luque de Castro, M. D. Comparison of Continuous Subcritical Water Extraction and Hydrodistillation of Marjoram Essential Oil. *J. Chromatogr. A* **1999**, *855*, 625–632.
- (28) Continuous countercurrent deterpenation of lemon essential oil by means of supercritical carbon dioxide: Experimental data and process modelling  
<http://www.sciencedirect.com.library.aucegypt.edu:2048/science/article/pii/S0009250907007816> (accessed May 8, 2017).
- (29) Comparison of hydrodistillation and supercritical fluid extraction for the determination of essential oils in aromatic plants - ScienceDirect  
<http://www.sciencedirect.com.library.aucegypt.edu:2048/science/article/pii/002196739383017M> (accessed May 8, 2017).
- (30) Señoráns, F. J.; Ibañez, E.; Cavero, S.; Tabera, J.; Reglero, G. Liquid Chromatographic–mass Spectrometric Analysis of Supercritical-Fluid Extracts of Rosemary Plants. *J. Chromatogr. A* **2000**, *870*, 491–499.
- (31) McHugh, M.; Krukons, V. *Supercritical Fluid Extraction: Principles and Practice*; Elsevier, 2013.
- (32) Guenther, E.; others. The Essential Oils, Vol. IV. *Essent. Oils Vol IV* **1950**.
- (33) Guenther, E. *Individual Essential Oils of the Plant Families Ericaceae, Betulaceae, Valerianaceae, Verbenaceae, Cistaceae, Cruciferae, Liliaceae, Iridaceae, Araceae, Palmae, Cyperaceae, Moraceae, Aristolochiaceae, Chenopodiaceae, Ranunculaceae, Euphorbiaceae, Malvaceae, Usneaceae, Podocarpaceae, Pinaceae, Taxodiaceae, and Cupressaceae*; Krieger Pub Co, 1972; Vol. 6.
- (34) Patra, J.; Baek, K.-H. Antibacterial Activity and Action Mechanism of the Essential Oil from *Enteromorpha Linza* L. against Foodborne Pathogenic Bacteria. *Molecules* **2016**, *21*, 388.
- (35) Penalver, P.; Huerta, B.; Borge, C.; Astorga, R.; Romero, R.; Perea, A. Antimicrobial Activity of Five Essential Oils against Origin Strains of the Enterobacteriaceae Family. *Apmis* **2005**, *113*, 1–6.

- (36) Gaysinsky, S.; Davidson, P. M.; Bruce, B. D.; Weiss, J. Growth Inhibition of Escherichia Coli O157: H7 and Listeria Monocytogenes by Carvacrol and Eugenol Encapsulated in Surfactant Micelles. *J. Food Prot.* **2005**, *68*, 2559–2566.
- (37) İşcan, G.; Kirimer, N.; Kürkcüoğlu, M.; Başer, H. C.; DEMİrci, Fati. Antimicrobial Screening of Mentha Piperita Essential Oils. *J. Agric. Food Chem.* **2002**, *50*, 3943–3946.
- (38) Chan, E. W. C.; Soh, E. Y.; Tie, P. P.; Law, Y. P. Antioxidant and Antibacterial Properties of Green, Black, and Herbal Teas of Camellia Sinensis. *Pharmacogn. Res.* **2011**, *3*, 266.
- (39) Pintore, G.; Usai, M.; Bradesi, P.; Juliano, C.; Boatto, G.; Tomi, F.; Chessa, M.; Cerri, R.; Casanova, J. Chemical Composition and Antimicrobial Activity of Rosmarinus Officinalis L. Oils from Sardinia and Corsica. *Flavour Fragr. J.* **2002**, *17*, 15–19.
- (40) Hammer, K. A.; Carson, C. F.; Riley, T. V. Antimicrobial Activity of Essential Oils and Other Plant Extracts. *J. Appl. Microbiol.* **1999**, *86*, 985–990.
- (41) Smith-Palmer, A.; Stewart, J.; Fyfe, L. Antimicrobial Properties of Plant Essential Oils and Essences against Five Important Food-Borne Pathogens. *Lett. Appl. Microbiol.* **1998**, *26*, 118–122.
- (42) Negi, P. S.; Jayaprakasha, G. K.; Jagan Mohan Rao, L.; Sakariah, K. K. Antibacterial Activity of Turmeric Oil: A Byproduct from Curcumin Manufacture. *J. Agric. Food Chem.* **1999**, *47*, 4297–4300.
- (43) Bajpai, V. K.; Baek, K.-H.; Kang, S. C. Control of Salmonella in Foods by Using Essential Oils: A Review. *Food Res. Int.* **2012**, *45*, 722–734.
- (44) Burt, S. Essential Oils: Their Antibacterial Properties and Potential Applications in Foods—a Review. *Int. J. Food Microbiol.* **2004**, *94*, 223–253.
- (45) Nazzaro, F.; Fratianni, F.; De Martino, L.; Coppola, R.; De Feo, V. Effect of Essential Oils on Pathogenic Bacteria. *Pharmaceuticals* **2013**, *6*, 1451–1474.
- (46) Miguel, M. G. Antioxidant and Anti-Inflammatory Activities of Essential Oils: A Short Review. *Molecules* **2010**, *15*, 9252–9287.
- (47) Calo, J. R.; Crandall, P. G.; O’Bryan, C. A.; Ricke, S. C. Essential Oils as Antimicrobials in Food Systems – A Review. *Food Control* **2015**, *54*, 111–119.
- (48) Turek, C.; Stintzing, F. C. Stability of Essential Oils: A Review. *Compr. Rev. Food Sci. Food Saf.* **2013**, *12*, 40–53.
- (49) Sticher, O. Ätherische Öle Und Drogen, Die Ätherisches Öl Enthalten. In *Pharmakognosie—Phytopharmazie*; Springer, 1999; pp. 629–769.
- (50) Li, N.; Taylor, L. S.; Ferruzzi, M. G.; Mauer, L. J. Color and Chemical Stability of Tea Polyphenol (–)-Epigallocatechin-3-Gallate in Solution and Solid States. *Food Res. Int.* **2013**, *53*, 909–921.
- (51) Rossi, M.; Cubadda, F.; Dini, L.; Terranova, M. L.; Aureli, F.; Sorbo, A.; Passeri, D. Scientific Basis of Nanotechnology, Implications for the Food Sector and Future Trends. *Trends Food Sci. Technol.* **2014**, *40*, 127–148.
- (52) nanostructured material <http://eng.thesaurus.rusnano.com/wiki/article1371> (accessed May 18, 2017).
- (53) Schairer, D. O.; Chouake, J. S.; Nosanchuk, J. D.; Friedman, A. J. The Potential of Nitric Oxide Releasing Therapies as Antimicrobial Agents. *Virulence* **2012**, *3*, 271–279.
- (54) Blecher, K.; Nasir, A.; Friedman, A. The Growing Role of Nanotechnology in Combating Infectious Disease. *Virulence* **2011**, *2*, 395–401.

- (55) Friedman, A. J.; Phan, J.; Schairer, D. O.; Champer, J.; Qin, M.; Pirouz, A.; Blecher-Paz, K.; Oren, A.; Liu, P. T.; Modlin, R. L.; *et al.* Antimicrobial and Anti-Inflammatory Activity of Chitosan–alginate Nanoparticles: A Targeted Therapy for Cutaneous Pathogens. *J. Invest. Dermatol.* **2013**, *133*, 1231–1239.
- (56) Huang, L.; Dai, T.; Xuan, Y.; Tegos, G. P.; Hamblin, M. R. Synergistic Combination of Chitosan Acetate with Nanoparticle Silver as a Topical Antimicrobial: Efficacy against Bacterial Burn Infections. *Antimicrob. Agents Chemother.* **2011**, *55*, 3432–3438.
- (57) Brown, A. N.; Smith, K.; Samuels, T. A.; Lu, J.; Obare, S. O.; Scott, M. E. Nanoparticles Functionalized with Ampicillin Destroy Multiple-Antibiotic-Resistant Isolates of *Pseudomonas Aeruginosa* and *Enterobacter Aerogenes* and Methicillin-Resistant *Staphylococcus Aureus*. *Appl. Environ. Microbiol.* **2012**, *78*, 2768–2774.
- (58) Huh, A. J.; Kwon, Y. J. “Nanoantibiotics”: A New Paradigm for Treating Infectious Diseases Using Nanomaterials in the Antibiotics Resistant Era. *J. Controlled Release* **2011**, *156*, 128–145.
- (59) Lellouche, J.; Friedman, A.; Lahmi, R.; Gedanken, A.; Banin, E. Antibiofilm Surface Functionalization of Catheters by Magnesium Fluoride Nanoparticles. *Int J Nanomedicine* **2012**, *7*, 1175–88.
- (60) Liu, Z.; Jiao, Y.; Wang, Y.; Zhou, C.; Zhang, Z. Polysaccharides-Based Nanoparticles as Drug Delivery Systems. *Adv. Drug Deliv. Rev.* **2008**, *60*, 1650–1662.
- (61) Woranuch, S.; Yoksan, R. Eugenol-Loaded Chitosan Nanoparticles: I. Thermal Stability Improvement of Eugenol through Encapsulation. *Carbohydr. Polym.* **2013**, *96*, 578–585.
- (62) Hosseini, S. F.; Zandi, M.; Rezaei, M.; Farahmandghavi, F. Two-Step Method for Encapsulation of Oregano Essential Oil in Chitosan Nanoparticles: Preparation, Characterization and in Vitro Release Study. *Carbohydr. Polym.* **2013**, *95*, 50–56.
- (63) de Oliveira, E. F.; Paula, H. C.; de Paula, R. C. Alginate/Cashew Gum Nanoparticles for Essential Oil Encapsulation. *Colloids Surf. B Biointerfaces* **2014**, *113*, 146–151.
- (64) Haider, J.; Majeed, H.; Williams, P. A.; Safdar, W.; Zhong, F. Formation of Chitosan Nanoparticles to Encapsulate Krill Oil (*Euphausia Superba*) for Application as a Dietary Supplement. *Food Hydrocoll.* **2017**, *63*, 27–34.
- (65) Zhang, Y.; Niu, Y.; Luo, Y.; Ge, M.; Yang, T.; Yu, L. L.; Wang, Q. Fabrication, Characterization and Antimicrobial Activities of Thymol-Loaded Zein Nanoparticles Stabilized by Sodium Caseinate–chitosan Hydrochloride Double Layers. *Food Chem.* **2014**, *142*, 269–275.
- (66) Gomes, C.; Moreira, R. G.; Castell-Perez, E. Poly (DL-Lactide-Co-Glycolide)(PLGA) Nanoparticles with Entrapped Trans-Cinnamaldehyde and Eugenol for Antimicrobial Delivery Applications. *J. Food Sci.* **2011**, *76*, N16–N24.
- (67) Iannitelli, A.; Grande, R.; Stefano, A. D.; Giulio, M. D.; Sozio, P.; Bessa, L. J.; Laserra, S.; Paolini, C.; Protasi, F.; Cellini, L. Potential Antibacterial Activity of Carvacrol-Loaded Poly (DL-Lactide-Co-Glycolide)(PLGA) Nanoparticles against Microbial Biofilm. *Int. J. Mol. Sci.* **2011**, *12*, 5039–5051.
- (68) Wattanasatcha, A.; Rengpipat, S.; Wanichwecharungruang, S. Thymol Nanospheres as an Effective Anti-Bacterial Agent. *Int. J. Pharm.* **2012**, *434*, 360–365.
- (69) Esmaeili, A.; Asgari, A. In Vitro Release and Biological Activities of *Carum Copticum* Essential Oil (CEO) Loaded Chitosan Nanoparticles. *Int. J. Biol. Macromol.* **2015**, *81*, 283–290.

- (70) Keawchaoon, L.; Yoksan, R. Preparation, Characterization and in Vitro Release Study of Carvacrol-Loaded Chitosan Nanoparticles. *Colloids Surf. B Biointerfaces* **2011**, *84*, 163–171.
- (71) Feyzioglu, G. C.; Tornuk, F. Development of Chitosan Nanoparticles Loaded with Summer Savory (*Satureja Hortensis* L.) Essential Oil for Antimicrobial and Antioxidant Delivery Applications. *LWT - Food Sci. Technol.* **2016**, *70*, 104–110.
- (72) Mohammadi, A.; Hashemi, M.; Hosseini, S. M. Nanoencapsulation of Zataria Multiflora Essential Oil Preparation and Characterization with Enhanced Antifungal Activity for Controlling Botrytis Cinerea, the Causal Agent of Gray Mould Disease. *Innov. Food Sci. Emerg. Technol.* **2015**, *28*, 73–80.
- (73) Yingchoncharoen, P.; Kalinowski, D. S.; Richardson, D. R. Lipid-Based Drug Delivery Systems in Cancer Therapy: What Is Available and What Is Yet to Come. *Pharmacol. Rev.* **2016**, *68*, 701–787.
- (74) Donsi, F.; Annunziata, M.; Sessa, M.; Ferrari, G. Nanoencapsulation of Essential Oils to Enhance Their Antimicrobial Activity in Foods. *LWT-Food Sci. Technol.* **2011**, *44*, 1908–1914.
- (75) Zhao, Y.; Wang, C.; Chow, A. H.; Ren, K.; Gong, T.; Zhang, Z.; Zheng, Y. Self-Nanoemulsifying Drug Delivery System (SNEDDS) for Oral Delivery of Zedoary Essential Oil: Formulation and Bioavailability Studies. *Int. J. Pharm.* **2010**, *383*, 170–177.
- (76) Lai, F.; Sinico, C.; De Logu, A.; Zaru, M.; Muller, R. H.; Fadda, A. M. SLN as a Topical Delivery System for Artemisia Arborescens Essential Oil: In Vitro Antiviral Activity and Skin Permeation Study. *Int. J. Nanomedicine* **2007**, *2*, 419.
- (77) Al-Haj, N. A.; Shamsudin, M. N.; Alipiah, N. M.; Zamri, H. F.; Bustamam, A.; Ibrahim, S.; Abdullah, R.; others. Characterization of Nigella Sativa L. Essential Oil-Loaded Solid Lipid Nanoparticles. *Am. J. Pharmacol. Toxicol.* **2010**, *5*, 52–57.
- (78) Moghimipour, E.; Ramezani, Z.; Handali, S. Solid Lipid Nanoparticles as a Delivery System for Zataria Multiflora Essential Oil: Formulation and Characterization. *Curr. Drug Deliv.* **2013**, *10*, 151–157.
- (79) Valenti, D.; De Logu, A.; Loy, G.; Sinico, C.; Bonsignore, L.; Cottiglia, F.; Garau, D.; Fadda, A. M. Liposome-Incorporated Santolina Insularis Essential Oil: Preparation, Characterization and in Vitro Antiviral Activity. *J. Liposome Res.* **2001**, *11*, 73–90.
- (80) Sinico, C.; De Logu, A.; Lai, F.; Valenti, D.; Manconi, M.; Loy, G.; Bonsignore, L.; Fadda, A. M. Liposomal Incorporation of Artemisia Arborescens L. Essential Oil and in Vitro Antiviral Activity. *Eur. J. Pharm. Biopharm.* **2005**, *59*, 161–168.
- (81) Wen, Z.; Liu, B.; Zheng, Z.; You, X.; Pu, Y.; Li, Q. Preparation of Liposomes Entrapping Essential Oil from Atractylodes Macrocephala Koidz by Modified RESS Technique. *Chem. Eng. Res. Des.* **2010**, *88*, 1102–1107.
- (82) Liolios, C. C.; Gortzi, O.; Lalas, S.; Tsaknis, J.; Chinou, I. Liposomal Incorporation of Carvacrol and Thymol Isolated from the Essential Oil of Origanum Dictamnus L. and in Vitro Antimicrobial Activity. *Food Chem.* **2009**, *112*, 77–83.
- (83) Cazaussus, A.; Pes, R.; Sellier, N.; Tabet, J.-C. GC-MS and GC-MS-MS Analysis of a Complex Essential Oil. *Chromatographia* **1988**, *25*, 865–869.
- (84) Keawchaoon, L.; Yoksan, R. Preparation, Characterization and in Vitro Release Study of Carvacrol-Loaded Chitosan Nanoparticles. *Colloids Surf. B Biointerfaces* **2011**, *84*, 163–171.

- (85) Deka, C.; Deka, D.; Bora, M. M.; Jha, D. K.; Kakati, D. K. Synthesis of Peppermint Oil-Loaded Chitosan/Alginate Polyelectrolyte Complexes and Study of Their Antibacterial Activity. *J. Drug Deliv. Sci. Technol.* **2016**, *35*, 314–322.
- (86) Chen, F.; Shi, Z.; Neoh, K. g.; Kang, E. t. Antioxidant and Antibacterial Activities of Eugenol and Carvacrol-Grafted Chitosan Nanoparticles. *Biotechnol. Bioeng.* **2009**, *104*, 30–39.
- (87) Wei, D.; Sun, W.; Qian, W.; Ye, Y.; Ma, X. The Synthesis of Chitosan-Based Silver Nanoparticles and Their Antibacterial Activity. *Carbohydr. Res.* **2009**, *344*, 2375–2382.
- (88) Maa, Y.-F.; Hsu, C. Liquid-Liquid Emulsification by Rotor/Stator Homogenization. *J. Controlled Release* **1996**, *38*, 219–228.
- (89) Dhankhar, P. Homogenization Fundamentals. *IOSR J Eng* **2014**, *4*, 1–8.
- (90) Abdelwahed, W.; Degobert, G.; Stainmesse, S.; Fessi, H. Freeze-Drying of Nanoparticles: Formulation, Process and Storage Considerations. *Adv. Drug Deliv. Rev.* **2006**, *58*, 1688–1713.
- (91) Bhattacharjee, S. DLS and Zeta Potential – What They Are and What They Are Not? *J. Controlled Release* **2016**, *235*, 337–351.
- (92) Bhattacharjee, S. DLS and Zeta Potential – What They Are and What They Are Not? *J. Controlled Release* **2016**, *235*, 337–351.
- (93) Williams, D. B.; Carter, C. B. The Transmission Electron Microscope. In *Transmission electron microscopy*; Springer, 1996; pp. 3–17.
- (94) Griffiths, P. R.; Haseth, J. A. D. *Fourier Transform Infrared Spectrometry*; John Wiley & Sons, 2007.
- (95) Griffiths, P. R.; Haseth, J. A. D. *Fourier Transform Infrared Spectrometry*; John Wiley & Sons, 2007.
- (96) Miao, J.; Charalambous, P.; Kirz, J.; Sayre, D. Extending the Methodology of X-Ray Crystallography to Allow Imaging of Micrometre-Sized Non-Crystalline Specimens. *Nature* **1999**, *400*, 342–344.
- (97) Vyazovkin, S. Thermogravimetric Analysis. In *Characterization of Materials*; John Wiley & Sons, Inc., 2002.
- (98) Ainsworth, E. A.; Gillespie, K. M. Estimation of Total Phenolic Content and Other Oxidation Substrates in Plant Tissues Using Folin–Ciocalteu Reagent. *Nat. Protoc.* **2007**, *2*, 875–877.
- (99) Institute of Medical Research and Medicinal Plants Studies, P.O. Box 6163, Yaoundé, Cameroon; A Agbor, G.; Vinson, J. A.; Department of Chemistry, Loyola Science Center, University of Scranton, 204 Monroe Avenue, Scranton, PA, 18510 USA; Donnelly, P. E.; Department of Chemistry, Loyola Science Center, University of Scranton, 204 Monroe Avenue, Scranton, PA, 18510 USA. Folin-Ciocalteu Reagent for Polyphenolic Assay. *Int. J. Food Sci. Nutr. Diet.* **2014**, 147–156.
- (100) *Current Protocols in Food Analytical Chemistry*.
- (101) Chapuis-Lardy, L.; Contour-Ansel, D.; Bernhard-Reversat, F. High-Performance Liquid Chromatography of Water-Soluble Phenolics in Leaf Litter of Three Eucalyptus Hybrids (Congo). *Plant Sci.* **2002**, *163*, 217–222.
- (102) Peterson, G. L. Review of the Folin Phenol Protein Quantitation Method of Lowry, Rosebrough, Farr and Randall. *Anal. Biochem.* **1979**, *100*, 201–220.
- (103) Owen, T. *Fundamentals of Modern UV-Visible Spectroscopy : A Primer*; Hewlett-Packard, 1996.

- (104) Balouiri, M.; Sadiki, M.; Ibsouda, S. K. Methods for in Vitro Evaluating Antimicrobial Activity: A Review. *J. Pharm. Anal.* **2016**, *6*, 71–79.
- (105) White, D. G.; Acar, J.; Anthony, F.; Franklin, A.; Gupta, R.; Nicholls, T.; Tamura, Y.; Thompson, S.; Threlfall, E. J.; Vose, D. Antimicrobial Resistance: Standardisation and Harmonisation of Laboratory Methodologies for the Detection and Quantification of Antimicrobial Resistance. *Rev. Sci. Tech. Int. Off. Epizoot.* **2001**, *20*, 849–858.
- (106) Mishra, K.; Ojha, H.; Chaudhury, N. K. Estimation of Antiradical Properties of Antioxidants Using DPPH Assay: A Critical Review and Results. *Food Chem.* **2012**, *130*, 1036–1043.
- (107) Găinar, I.; Vîlcu, R.; Mocan, M. Supercritical Fluid Extraction and Fractional Separation of Essential Oils. **2002**.
- (108) Namita, P.; Mukesh, R.; Vijay, K. J. *Camellia Sinensis* (Green Tea): A Review. *Glob. J. Pharmacol.* **2012**, *6*, 52–59.
- (109) Werker, E.; Ravid, U.; Putievsky, E. Structure of Glandular Hairs and Identification of the Main Components of Their Secreted Material in Some Species of the Labiatae. *Isr. J. Bot.* **1985**, *34*, 31–45.
- (110) Davis, E. M.; Ringer, K. L.; McConkey, M. E.; Croteau, R. Monoterpene Metabolism. Cloning, Expression, and Characterization of Menthone Reductases from Peppermint. *Plant Physiol.* **2005**, *137*, 873–881.
- (111) Gharib, F. A.; da Silva, J. T. Composition, Total Phenolic Content and Antioxidant Activity of the Essential Oil of Four Lamiaceae Herbs. *Med. Aromat. Plant Sci. Biotechnol.* **2013**, *7*, 19–27.
- (112) Packer, L. *Handbook of Antioxidants*; CRC Press, 2001.
- (113) Ma, C.; Gong, G.; Liu, Z.; Ma, A.; Chen, Z. Stimulatory Effects of Tea Supplements on the Propagation of *Lactobacillus Casei* in Milk. *Int. Dairy J.* **2015**, *43*, 1–6.
- (114) Dillen, K.; Vandervoort, J.; Van den Mooter, G.; Verheyden, L.; Ludwig, A. Factorial Design, Physicochemical Characterisation and Activity of Ciprofloxacin-PLGA Nanoparticles. *Int. J. Pharm.* **2004**, *275*, 171–187.
- (115) Kwon, H.-Y.; Lee, J.-Y.; Choi, S.-W.; Jang, Y.; Kim, J.-H. Preparation of PLGA Nanoparticles Containing Estrogen by Emulsification–diffusion Method. *Colloids Surf. Physicochem. Eng. Asp.* **2001**, *182*, 123–130.
- (116) Hosseini, S. F.; Zandi, M.; Rezaei, M.; Farahmandghavi, F. Two-Step Method for Encapsulation of Oregano Essential Oil in Chitosan Nanoparticles: Preparation, Characterization and in Vitro Release Study. *Carbohydr. Polym.* **2013**, *95*, 50–56.
- (117) Masarudin, M. J.; Cutts, S. M.; Evison, B. J.; Phillips, D. R.; Pigram, P. J. Factors Determining the Stability, Size Distribution, and Cellular Accumulation of Small, Monodisperse Chitosan Nanoparticles as Candidate Vectors for Anticancer Drug Delivery: Application to the Passive Encapsulation of [<sup>14</sup>C]-Doxorubicin. *Nanotechnol. Sci. Appl.* **2015**, *67*.
- (118) Chen, H.; Ruckenstein, E. Formation of Complex Colloidal Particles: Morphologies and Mechanisms. *Soft Matter* **2012**, *8*, 8911–8916.
- (119) Fan, W.; Yan, W.; Xu, Z.; Ni, H. Formation Mechanism of Monodisperse, Low Molecular Weight Chitosan Nanoparticles by Ionic Gelation Technique. *Colloids Surf. B Biointerfaces* **2012**, *90*, 21–27.

- (120) Yoksan, R.; Jirawutthiwongchai, J.; Arpo, K. Encapsulation of Ascorbyl Palmitate in Chitosan Nanoparticles by Oil-in-Water Emulsion and Ionic Gelation Processes. *Colloids Surf. B Biointerfaces* **2010**, *76*, 292–297.
- (121) Yoksan, R.; Jirawutthiwongchai, J.; Arpo, K. Encapsulation of Ascorbyl Palmitate in Chitosan Nanoparticles by Oil-in-Water Emulsion and Ionic Gelation Processes. *Colloids Surf. B Biointerfaces* **2010**, *76*, 292–297.
- (122) Wu, Y.; Yang, W.; Wang, C.; Hu, J.; Fu, S. Chitosan Nanoparticles as a Novel Delivery System for Ammonium Glycyrrhizinate. *Int. J. Pharm.* **2005**, *295*, 235–245.
- (123) Jingou, J.; Shilei, H.; Weiqi, L.; Danjun, W.; Tengfei, W.; Yi, X. Preparation, Characterization of Hydrophilic and Hydrophobic Drug in Combine Loaded Chitosan/Cyclodextrin Nanoparticles and in Vitro Release Study. *Colloids Surf. B Biointerfaces* **2011**, *83*, 103–107.
- (124) Pan, X.; Niu, G.; Liu, H. Microwave-Assisted Extraction of Tea Polyphenols and Tea Caffeine from Green Tea Leaves. *Chem. Eng. Process. Process Intensif.* **2003**, *42*, 129–133.
- (125) Esmaeili, A.; Asgari, A. In Vitro Release and Biological Activities of Carum Copticum Essential Oil (CEO) Loaded Chitosan Nanoparticles. *Int. J. Biol. Macromol.* **2015**, *81*, 283–290.
- (126) Moradi, M.; Tajik, H.; Razavi Rohani, S. M.; Oromiehie, A. R.; Malekinejad, H.; Aliakbarlu, J.; Hadian, M. Characterization of Antioxidant Chitosan Film Incorporated with Zataria Multiflora Boiss Essential Oil and Grape Seed Extract. *LWT - Food Sci. Technol.* **2012**, *46*, 477–484.
- (127) Ruiz-Navajas, Y.; Viuda-Martos, M.; Sendra, E.; Perez-Alvarez, J. A.; Fernández-López, J. In Vitro Antibacterial and Antioxidant Properties of Chitosan Edible Films Incorporated with Thymus Moroderi or Thymus Piperella Essential Oils. *Food Control* **2013**, *30*, 386–392.
- (128) Kumari, A.; Yadav, S. K.; Pakade, Y. B.; Kumar, V.; Singh, B.; Chaudhary, A.; Yadav, S. C. Nanoencapsulation and Characterization of Albizia Chinensis Isolated Antioxidant Quercitrin on PLA Nanoparticles. *Colloids Surf. B Biointerfaces* **2011**, *82*, 224–232.
- (129) Xie, W.; Xu, P.; Liu, Q. Antioxidant Activity of Water-Soluble Chitosan Derivatives. *Bioorg. Med. Chem. Lett.* **2001**, *11*, 1699–1701.
- (130) Barzegar, M.; Ghaderi Ghahfarokhi, M.; Sahari, M. A.; Azizi, M. H. Enhancement of Thermal Stability and Antioxidant Activity of Thyme Essential Oil by Encapsulation in Chitosan Nanoparticles. *J. Agric. Sci. Technol.* **2016**, *18*, 1781–1792.
- (131) Andoğan, B. C.; Baydar, H.; Kaya, S.; Demirci, M.; Özbaşar, D.; Mumcu, E. Antimicrobial Activity and Chemical Composition of Some Essential Oils. *Arch. Pharm. Res.* **2002**, *25*, 860–864.
- (132) Gallucci, M. N.; Oliva, M.; Casero, C.; Dambolena, J.; Luna, A.; Zygadlo, J.; Demo, M. Antimicrobial Combined Action of Terpenes against the Food-Borne Microorganisms Escherichia Coli, Staphylococcus Aureus and Bacillus Cereus. *Flavour Fragr. J.* **2009**, *24*, 348–354.
- (133) OSAWA, K.; SAEKI, T.; YASUDA, H.; HAMASHIMA, H.; SASATSU, M.; ARAI, T. The Antibacterial Activities of Peppermint Oil and Green Tea Polyphenols, Alone and in Combination, against Enterohemorrhagic Escherichia Coil. *Biocontrol Sci.* **1999**, *4*, 1–7.
- (134) Singh, R.; Shushni, M. A.; Belkheir, A. Antibacterial and Antioxidant Activities of Mentha Piperita L. *Arab. J. Chem.* **2015**, *8*, 322–328.

- (135) Daglia, M. Polyphenols as Antimicrobial Agents. *Curr. Opin. Biotechnol.* **2011**, *23*, 174–181.
- (136) Hessle, C. C.; Andersson, B.; Wold, A. E. Gram-Positive and Gram-Negative Bacteria Elicit Different Patterns of pro-Inflammatory Cytokines in Human Monocytes. *Cytokine* **2005**, *30*, 311–318.